ESTE EXEMPLAR CORRESPONDE A REDAÇÃO FINAL DA TESE DEFENDIDA POR JAIRO FRANCISCO USECHE VIVERO E APROVADA PELA COMISSÃO JULGADORA EM 29 / 11 / 2007

ORIENTADOR

UNIVERSIDADE ESTADUAL DE CAMPINAS

FACULDADE DE ENGENHARIA MECÂNICA

COMISSÃO DE PÓS-GRADUAÇÃO EM ENGENHARIA MECÂNICA

Análise pelo Método dos Elementos de Contorno de Placas de Reissner Trincadas e Reparadas com Compósitos Colados

Autor: **Jairo Francisco Useche Vivero**
Orientador: **Prof. Dr. Paulo Sollero**
Co-orientador: **Prof. Dr. Éder Lima de Albuquerque**

35/08

UNIVERSIDADE ESTADUAL DE CAMPINAS

FACULDADE DE ENGENHARIA MECÂNICA

COMISSÃO DE PÓS-GRADUAÇÃO EM ENGENHARIA MECÂNICA

DEPARTAMENTO DE MECÂNICA COMPUTACIONAL

Análise pelo Método dos Elementos de Contorno de Placas de Reissner Trincadas e Reparadas com Compósitos Colados

Autor: Jairo Francisco Useche Vivero
Orientador: Prof. Dr. Paulo Sollero
Co-orientador: Prof. Dr. Éder Lima de Albuquerque

Curso: Engenharia Mecânica
Área de Concentração: Mecânica dos Sólidos e Projeto Mecânico

Tese de doutorado apresentada à comissaão de Pós Graduação da Faculdade de Engenharia Mecânica, como requisito para a obtenção do título de Doutor em Engenharia Mecânica.

Campinas, 2007
S.P . - Brasil

FICHA CATALOGRÁFICA ELABORADA PELA
BIBLIOTECA DA ÁREA DE ENGENHARIA E ARQUITETURA - BAE - UNICAMP

Useche Vivero, Jairo Francisco
Us2a Análise pelo método dos elementos de contorno de placas de Reissner trincadas e reparadas com compósitos colados / Jairo Francisco Useche Vivero.--Campinas, SP: [s.n.], 2007.

Orientadores: Paulo Sollero, Éder Lima de Albuquerque.
Tese (Doutorado) - Universidade Estadual de Campinas, Faculdade de Engenharia Mecânica.

1. Métodos de elementos de contorno. 2. Placas (Engenharia). 3. Mecânica da fratura. 4. Materiais compostos. 5. Aviões – Manutenção e reparos. I. Sollero, Paulo. II. Albuquerque, Éder Lima de. III. Universidade Estadual de Campinas. Faculdade de Engenharia Mecânica. IV. Título.

Titulo em Inglês: Boundary element analysis of cracked Reissner's plates repaired with adhesively bonded composite patches
Palavras-chave em Inglês: Cracked Reissner's plates, Aeronautic composite repairs, Anisotropic Kirchhoff's plates, Boundary element method, Fracture mechanics
Área de concentração: Mecânica dos sólidos e projeto mecânico
Titulação: Doutor em Engenharia Mecânica
Banca examinadora: Euclides de Mesquita Neto, Leandro Palermo Junior, Ariosto Bretanha Jorge, Sergio Francisco Muller de Almeida
Data da defesa: 29/11/2007
Programa de Pós-Graduação: Engenharia Mecânica

UNIVERSIDADE ESTADUAL DE CAMPINAS

FACULDADE DE ENGENHARIA MECÂNICA

COMISSÃO DE PÓS-GRADUAÇÃO EM ENGENHARIA MECÂNICA

DEPARTAMENTO DE MECÂNICA COMPUTACIONAL

TESE DE DOUTORADO

Análise pelo Método dos Elementos de Contorno de Placas de Reissner Trincadas e Reparadas com Compósitos Colados

Autor: **Jairo Francisco Useche Vivero**
Orientador: **Prof. Dr. Paulo Sollero**
Co-orientador: **Prof. Dr. Éder Lima de Albuquerque**

A Banca Examinadora composta pelos membros abaixo aprovou esta Tese:

Prof. Dr. Paulo Sollero, Presidente
FEM/UNICAMP

Prof. Dr. Euclides de Mesquita Neto
FEM/UNICAMP

Prof. Dr. Leandro Palermo Junior
FEC/UNICAMP

Prof. Dr. Ariosto Bretanha Jorge
UNIFEI/Itajubá

Prof. Dr. Sergio Frascino Muller de Almeida
ITA/São José dos Campos

Campinas, 29 de novembro de 2007

Dedicatória

A minha esposa Johana e meu filho Nicolas... o brasileiro!

Agradecimentos

Gostaria de agradecer às pessoas e instituicões que fizeram possivel o sucesso deste trabalho:

- À Universidad Tecnologica de Bolivar em Cartagena de Indias pelo apoio financeiro durante o desenvolvimento deste trabalho e especialmente aos Professores Alfredo Abuchar e Justo Ramos quem tem me apoiado na procura deste objetivo.

- Ao meu orientador Professor Paulo Sollero pela supervisão e apoio durante estes quatro anos de trabalho juntos.

- Ao Professor Eder de Lima Albuquerque pela sua valiosa colaboração, co-orientação e pela sua amizade neste tempo todo.

- Ao Departamento de Mecânica Computacional da UNICAMP pela infra-estrutura fornecida durante a realização deste trabalho.

Cerrando las puertas detrás de uno se abren ventanas hacia el porvenir
Françoise Sagan

Resumo

Useche Vivero, Jairo Francisco, *Análise pelo Método dos Elementos de Contorno de Placas de Reissner Trincadas e Reparadas com Compósitos Colados*, Campinas,: Faculdade de Engenharia Mecânica, Universidade Estadual de Campinas, 2007. 181 p. Tese (Doutorado).

O objetivo deste projeto é o desenvolvimento de uma ferramenta computacional para á análise e projeto de estruturas aeronáuticas trincadas e reparadas por placas de materiais compositos laminadas coladas. As placas metálicas isotropicas da estrutura aeronáutica serão modeladas pelo método dos elementos de contorno considerando a presença de tensões de cisalhamento nos planos normais à superfície das placas (formulação de Reissner-Mindlin). No modelamento do reparo será usada uma formulação por elementos de contorno para placas anisotrópicas sem considerar a presença de tensões de cisalhamento nos planos normais à superfície da placa (formulação do Kirchhoff-Love). A análise será validada com resultados analíticos, numéricos e experimentais disponiveis na literatura e com modelos desenvolvidos pelo método dos elementos finitos.

Palavras Chave

Placas de Reissner trincadas, Reparos Aeronáuticos em Materiais Compositos, Placas de Kirchhoff Anisotrópicas, Método dos Elementos de Contorno, Mecánica da Fratura

Abstract

Useche Vivero, Jairo Francisco, *Boundary Element Analysis of Cracked Reissner's Plates Repaired with Adhesively Composite Patches*, Campinas,: Faculdade de Engenharia Mecânica, Universidade Estadual de Campinas, 2007. 181 p. Tese (Doutorado).

The objective of this project is the development of a computational tool for the analysis and design of cracked aeronautical structures repaired by adhesively bonded laminated composites. The isotropic metallic plates of the aeronautical structure will be modeled by the boundary element method considering the presence of shear stresses in planes that are normal to the surface of the plates (formulation of Reisner-Mindlin). In order to model the repair, a boundary element formulation for anisotropic plates will be used neglecting the presence of shear stresses in planes that are normal to the surface of the plate (formulation of Kirchhoff-Love). The analysis will be validated with analytical, numerical and experimental results avalilable in the literature and with finite element models.

Keywords

Cracked Reissner's plates, Aeronautic Composite Repairs, Anisotropic Kirchhoff's Plates, Boundary Element Method, Fracture Mechanics

Contents

List of Figures

List of Tables

Símbolos

u_α : Componentes de deslocamentos nas direções x_1 e x_2.

w_α : Componentes de deslocamentos generalizados para problemas de flexão.

t_α : Vetor de tensões.

n_α : Vetor unitário normal.

$G_{\alpha\beta}$: Componentes do vetor de Galerkin.

$U_{\alpha\beta}$: Solucão fundamental para deslocamentos para problemas de tensão plana.

$T_{\alpha\beta}$: Solucão fundamental para tração para problemas de tensão plana.

$C_{\alpha\beta\gamma\rho}$: Tensor de constantes elásticas.

$M_{\alpha\beta}$: Componentes do tensor de momentos fletores resultantes.

Q_α : Componentes de vetor de forças de cisalhamento resultantes.

q : forças de corpo para problemas de flexão.

S_{ijkl} : Tensor de flexibilidade.

E_k : Modulo de Young na diredireção do eixo x_k.

G_{ij} : Modulo de cisalhamento no plano x_i-x_j.

v_{ij} : Coeficientes de Poisson no plano x_i-x_j.

$F(x_1, x_2)$: Função de tensão de Airy.

Q_{ij} : Componentes do tensor de rigidez para materiais ortotrópicos.

h : Espessura da chapa/placa.

f_β : Força de corpo para problemas de tensão plana.

$W_{\alpha\beta}$: Solucão fundamental para deslocamentos generalizados para problemas de flexão.

$P_{\alpha\beta}$: Solucão fundamental para tração generalizada para problemas de flexão.

$K_0(z)$, $K_1(z)$: Funções de Bessel modificadas.

$S_{ijk}(\mathbf{x}', \mathbf{x})$: Solucão fundamental para deslocamentos no plano na equação de tração.

$D_{ijk}(\mathbf{x}', \mathbf{x})$: Solucão fundamental para tensões no plano na equação de tração.

$W^*_{i\beta k}$: Solucão fundamental para flexão na equação de tração.

$P^*_{i\beta k}$: Solucão fundamental para tensões por flexão na equação de tração.

$Q^*_{i\beta}$, : Solucão fundamental para forças de corpo no plano na equação de tração.

K_I, K_II, K_III : Fatores de intensificação de tensões.

E : Modulo de Young para materiais isotrópicos.

G : Modulo de cisalhamento para materiais isotrópicos.

$\chi_{\alpha\beta}$: Tensor de curvatura.

ψ_α : Deformaç ao cortante transversal.

$\sigma_{\alpha\beta}$: Tensor de tensões.

$\varepsilon_{\alpha\beta}$: Tensor de deformações unitárias.

$\eta_{jk,l}$: Coeficientes de influência mútua de primer tipo.

$\eta_{l,jk}$: Coeficientes de influência mútua de segundo tipo.

$\varsigma_{ij,kl}$: Coeficientes de Chentsov

U : Matriz de coeficientes da solucão fundamental para deslocamentos no plano.

T : Matriz de coeficientes da solucão fundamental para tração no plano.

W : Matriz de coeficientes da solucão fundamental para flexão.

P : Matriz de coeficientes da solucão fundamental para momentos e forças cortantes.

J : Matriz Jacobiana.

H : Matriz de influência para deslocamentos.

G : Matriz de influência para trações.

B : Vetor de influência para forças de corpo para problemas de tensão plana.

Q : Vetor de influência para forças de corpo para problemas de flexão.

Chapter 1

Introdução

1.1 Reparos de compósitos colados

As estruturas aeronáuticas são constituídas geralmente por painéis e reforçadores metálicos (figura 1). Um painel trincado é freqüentemente reparado colando, rebitando ou parafusando um remendo metálico na área trincada. A vida em fadiga e as tensões residuais no painel reparado é dependente da eficiência da transferência de carga do painel trincado para o reparo. Os reparos colados têm sido usados na indústria aeronáutica e são aceitos como soluções eficientes para o reparo de danos em paneis metálicos. A principal vantagem quando comparado aos reparos parafusados ou rebitados é que fornecem transferência da carga relativamente uniforme entre os componentes estruturais que são ligados (figura 2). Os furos requeridos no caso de reparos parafusados ourebitados agem como concentradores de tensão o que reduz a vida útil do painel aeronáutico. Adicionalmente, os reparos rebitados são feitos geralmente de placas de alumínio ou do mesmo material que compõe a estrutura reparada. No entanto os reparos colados admitem o uso de materiais mais avançados como são os materiais compósitos.

Entre os materiais usados na engenharia, os compósitos apresentam a menor relação

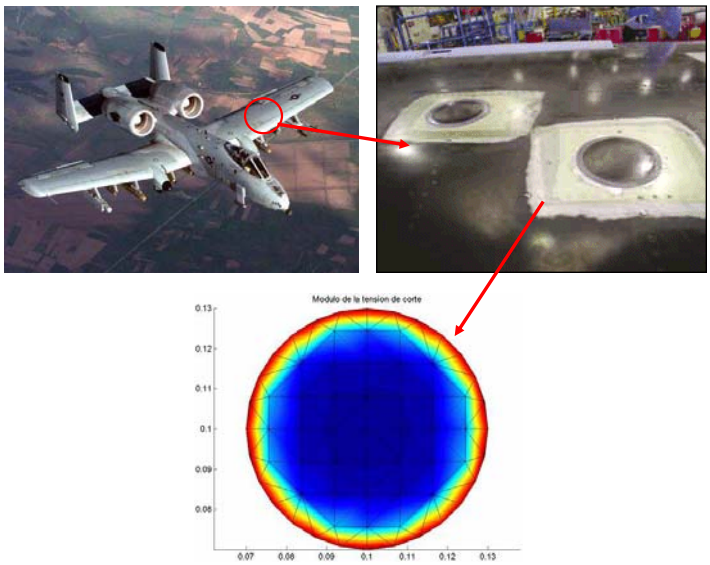

Figure 1.1: Reparo de compósito colado na estrutura do avião. Este tipo de reparo gera um campo de tensões mais uniforme. (Tomado de www.wallpaper.net.au/wallpaperaviation1.php, AFRL Monthy Accomplishment Report, http://www.afrl.af.mil/accomprpt/jan04/accompjan04.htm and Lourenço et al., 2003)

rigidez-densidade, também chamada rigidez específica. Adicionalmente, alguns compósitos apresentam um bom desempenho térmico, alcançando temperaturas similares aos materiais comumente utilizados em projetos de engenharia. Devido à grande variedade das combinações e arranjos das fibras e das matrizes, os engenheiros têm materiais disponíveis para um grande número de projetos que exigem características específicas, tais como: rigidez, resistência, densidade, condutividade térmica ou elétrica ou outras propriedades do material.

O método dos elementos finitos (MEF) foi usado extensivamente para a análise de problemas de fratura em estruturas aeronáuticas, principalmente devido a sua generalidade. No caso de estruturas laminadas o MEF é implementado baseado nas teorias de Kirchhoff ou de Reissner-Mindlin. Entretanto, esta generalidade podería introduzir custos computacionais elevados, principalmente nos problemas que envolvem singularidades no campo de tensões (como aqueles encontrados próximo à ponta de uma trinca) que requer uma discretização mais fina ao redor do ponto de singularidade. O método dos elementos de contorno (MEC)

é uma alternativa numérica atrativa para tratar problemas da mecânica linear da fratura, principalmente devido à sua habilidade para modelar de forma contínua os gradientes elevados do campo de tensões sem a necessidade de discretizar o domínio (desconsiderando forças de corpo). Adicionalmente, os problemas de propagação de trincas podem ser analisados com técnicas simples que requerem unicamente elementos de contorno adicionais na ponta da trinca e algoritmos de solução incrementais. O uso deste método na análise de estruturas aumentou fortemente desde os anos oitenta (Brebbia and Dominguez, 1989). Por sua vez, o comportamento de estruturas laminares trincadas e reparadas com a aplicação de compósitos colados usando o MEC exige ainda muito trabalho de pesquisa.

1.2 Revisão bibliografica

Os primeiros trabalhos que analisaram reparos isotrópicos em estruturas foram apresentados nos anos setenta por Ratawani, 1979, e Erdogan and Arin, 1972. Estes trabalhos apresentam o estudo de reparos colados em chapas infinitas com trincas [1]. Eles usaram soluções analíticas para a deformação e consideraram a compatibilidade dos deslocamentos entre a chapa trincada e o reparo.

Mitchell, Wooley and Chwiruth, 1975, usaram o MEF para estudar o reforço de placas induzido pela aplicação de reparos. Eles usaram uma formulação de elementos finitos bidimensionais com tensões constantes e acoplaram a placa e o reparo através dos nós onde as condições de compatibilidade de deslocamentos foram impostas. Eles analisaram também a presença de uma trinca na placa. Entretanto, o trabalho não considerou a singularidade no campo de tensões na ponta da trinca e também não avaliaram os fatores de intensidade de tensão.

[1] Neste trabalho, o termo chapa (sheet) refere-se a corpos submetidos a carregamento no plano (estado de tensão plana). No entanto o termo placa (plate) refere-se a corpos submetidos a flexão.

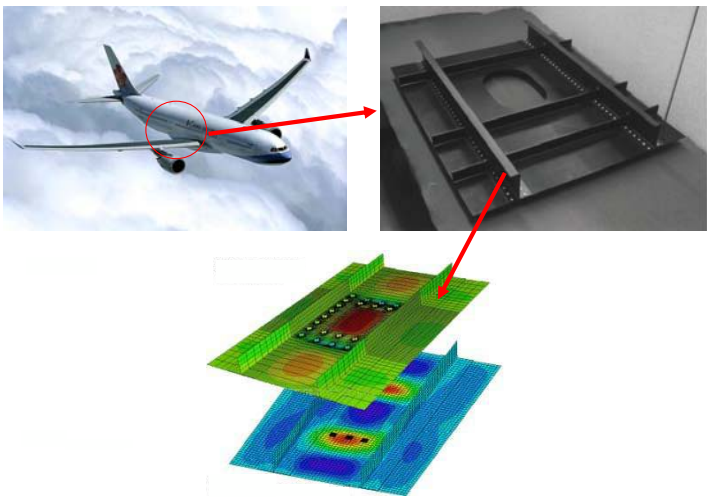

Figure 1.2: Reparo parafusado na estrutura do avião. Este tipo de reparo gera a concentração se tensões nos furos dos parafusos .(Fonte: BOJCAS Project, http://www.smr.ch/bojcas/index.html and Murata Mechinary LTD., http://www.muratec.net)

Nos trabalhos de Jones and Callinan, 1977, Jones and Callinan, 1979 and Jones and Callinan, 1981, usaram o MEF para a análise de placas metálicas reparadas com uma camada de material compósito. Eles desenvolveram uma matriz de rigidez para acoplar a placa, a camada adesiva e o reparo de material compósito. Esta matriz foi acoplada com um modelo do MEF da placa metálica e, na ponta da trinca, eles usaram elementos singulares especiais.

Young et al., 1988 modelaram a chapa trincada e o reparo usando o método dos elementos de contorno. As tensões de cisalhamento na camada adesiva asim como as forças de corpo agindo sobre à placa e o reparo foram modeladas. No trabalho eles usaram uma função de Green especial para modelar domínios com trincas retas, o qual limita a aplicabilidade do modelo.

Tarn and Shek, 1991 estudaram o problema de chapas trincadas reparadas com materiais compósitos colados. Um modelo de mola foi usado para acoplar o modelo da placa trincada com o modelo do reparo. O reparo foi modelado usando o MEF e a trinca usando do MEC.

Young, 1987 modelou a força distribuída de interação entre a chapa e o reparo, discretizando a área de contato entre o reparo e a placa usando celulas internas numa formulação MEC.

Salgado and Aliabadi, 1997 usaram o método dos elementos de contorno dual para modelar chapas metálicas trincadas e o método direto dos elementos do contorno para modelar o reparo. A força distribuída entre a chapa e o reparo foi modelada utilizando o método dos elementos de contorno de reciprocidade dual. Esta formulação foi aplicada por Salgado and Aliabadi, 1998 na análise de chapas finas metálicas reforçadas com reparos isotrópicos colados. A chapa reforçada foi modelada usando o método dos elementos de contorno de reciprocidade dual (DRBEM). As tensões de cisalhamento na camada adesiva foram modeladas como forças de corpo.

Lourenço, 2000 analisou chapas metálicas isotrópicas com reparos adesivos e carregamento no plano usando o DRBEM para modelar as forças de interação entre a placa e o reparo como forças de corpo distribuídas. Esta formulação foi estendida por Lourenço et al., 2003 para a análise de reparos anisotrópicos com reforço estrutural de placas metálicas submetidas a carregamento estático no plano da chapa.

O trabalho de Dirgantara and Aliabadi, 1999 apresenta uma nova formulação mista de elementos de contorno para resolver problemas de deflexão em cascas metálicas isotrópicas considerando deformação de cisalhamento (formulação de Reissner). Os termos de curvatura da formulação da casca foram rearranjados junto com os termos de forças externas na equação governante. Foi acoplada uma formulação por elementos de contorno para placas considerando a deformação por cisalhamento com uma formulação do MEC para tensão elástica plana, completando assim o modelo de casca metálica com deformação por cisal-

hamento e deformação elástica no plano.

Nos trabalhos de Wen, 2000; Wen, 2000 foram analisadas cascas metálicas isotrópicas com deformação por cisalhamento usando o MEC. Novas equações integrais foram desenvolvidas usando o princípio do reciprocidade de Betti, e foram acopladas às formulações de elementos de contorno para placas com deformação por cisalhamento e tensão elástica no plano. Estes autores utilizaram duas técnicas para transformar as integrais do domínio em integrais de contorno: o método direto dos elementos de contorno (MDEC) e o método de reciprocidade dual.

Dirgantara and Aliabadi, 2001 desenvolveram uma formulação inovadora do MEC para análise de cascas metálicas isotrópicas trincadas considerando as deformações devidas ao esforço cortante. Eles desenvolveram uma equação integral hipersingular de contorno usando uma formulação de reciprocidade dual, aplicando uma equação integral de força de superfície em uma das superfícies da trinca e equações integrais de deslocamento na outra.

Widagdo and Aliabadi, 2001 apresentam uma formulação do MEC para a análise de placas metálicas reparadas por materiais compósitos parafusados. A chapa trincada é modelada usando uma formulação de reciprocidade dual. Os parafusos são modelados como molas lineares cujas forças são tratadas como forças pontuais. O reparo é modelado usando uma formulação MEC bidimensional para chapas anisotrópicas.

Recentemente, Wen et al., 2003 desenvolveram uma formulação do MEC para a análise de painéis metálicos curvos com trincas e reparos adesivos isotrópicos. O efeito da camada adesiva foi modelada considerando forças distribuídas. Uma formulação integral para a placa com tensão de cisalhamento acoplada com uma formulação integral para tensão plana foi usada para determinar os momentos fletores e as forças de membrana no reparo adesivo.

1.3 Descripção do trabalho

O objetivo deste projeto é o desenvolvimento de uma ferramenta computacional para a análise e desenho de estruturas aeronáuticas trincadas e reparadas utilizando compósitos laminados colados. As placas metálicas isotrópicas da estrutura aeronáutica são modeladas pelo método dos elementos de contorno considerando a presença de cisalhamento em planos normais á superfcie das placas (formulação de Reissner-Mindlin). A fím de modelar o reparo, uma formulação por elementos de contorno de três parámetros, baseada na teoría de Kirchhoff para placas laminadas simetricas é desenvolvida. A Interacção entre as forçãs e momentos da placa trincada e reparada foi modelada como cargas distribuídas. Equações de acoplamento, baseadas em considerações de compatibilidade cinemática e de equilíbrio para a camada do adesivo, são estabelecidas. Um modelo de rigidez cortante transversal é proposto a fím de modelar a resposta mecânica do adesivo. Os Fatores de intensificação de tensoes são calculados utilizando o método de apertura da trinca e extrapolação de deslocamentos. A análise validada com resultados analíticos, numéricos e experimentais disponiveis na literatura.

As contribuições principais do presente trabalho podem-se classificadas no que diz respeito ao grupo de pesquisa em Modelagem de Materiais Compósitos e Biomédicos do Departamento de Mecânica Computacional da Unicamp, e no que diz respeito ao avanço do conhecimento na análise de placas trincadas e reparadas com materiais compósitos colados, utilizando o método dos elementos de contorno.

No que diz respeito ao grupo de pesquisa, a principal contribuição encontra-se na geração de conhecimento e no desenvolvimento de programas computacionais para a análise de placas de Reissner trincadas utilizando o método dual de elementos de contorno. Estes programas permitirão o desenvolvimento de novos trabalhos na área de mecânica da fratura em estruturas.

Por outro lado, a contribuição do trabalho ao conhecimento na área de análise pelo método de elementos de contorno de placas espessas trincadas e reparadas com compósitos colados encontra-se representado nos seguintes avanços:

- Desenvolvimento e implementação computacional de uma formulação do método dos elementos de contorno de placas anisotrópicas laminadas simétricas baseadas na teoría de Kirchhoff, utilizando três parâmetros cinemáticos.

- Desenvolvimento e implementação computacional de uma formulação dual do método dos elementos de contorno para análise de placas isotrópicas espessas trincadas e reparadas com compósitos colados utilizando laminados simétricos.

Chapter 2

Two-dimensional elastostatics

2.1 Introduction

This chapter shows the boundary element formulation for two-dimensional elastostatics problems used to describe the in-plane mechanical behavior of isotropic elastic plates. First part of this chapter presents a general definition of plane stress problems in linear elasticity developing governing differential equations for isotropic elastic materials. Kelvin's fundamental solution for an infinite elastic plane is presented.

2.2 Plane stress elasticity

Thin flat objects (like the ones showed in figure 2.1), loaded in their plane, generates a *plane stress* state in the body. This situation is often referred to as *membrane* or *in-plane* type of action, and plane stress analysis is therefore also sometimes called membrane or in-plane analysis. The basic assumptions for the plane stress are (see Brebbia and Dominguez, 1989):

- The body is thin, i.e., h is small in comparison to the representative dimensions along x_1 or x_2.

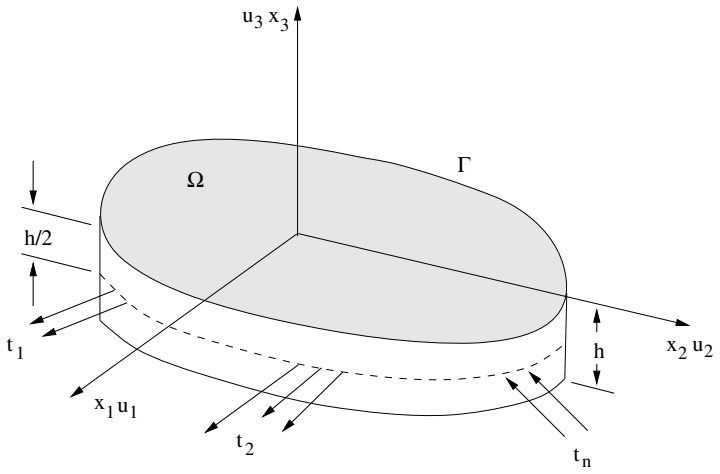

Figure 2.1: Plane stress definition

- There are no tractions acting at the end surfaces, i.e., at $x_3 = \pm h/2$, $t_k = 0$, where h is thickness and t_k are traction components acting on boundary Γ_t.

- Body forces acts on $x_1 - x_2$ planes and are independent of x_3, i.e. $f_3 = 0$ and f_1 and f_2 are functions of coordinates x_1 and x_2 only, where f_i are the components of body force vector acting on the domain Ω.

- Forces acting on the body are planar and independent of x_3 coordinate, i.e., $t_3 = 0$ and t_1 and t_2 are functions of the x_1 and x_2 coordinates.

Under these assumptions, it is assumed that the components σ_{3k} of the stress tensor are all small in comparison with the components $\sigma_{\alpha\beta}$ and that the variation of the latter with respect to coordinate x_3 are negligible (figure 10.4). Hence, one assumes: $\sigma_{3k} = 0$, and $\sigma_{\alpha\beta}$ are functions of the coordinates x_α only. This ability of thin objects to freely strain in the third dimension is exactly what puts them in a state where all components of the stress tensor in direction 3 are zero. It should be noted however that although these assumptions are reasonable in engineering practice, they are only approximation as they violate the compatibility equations.

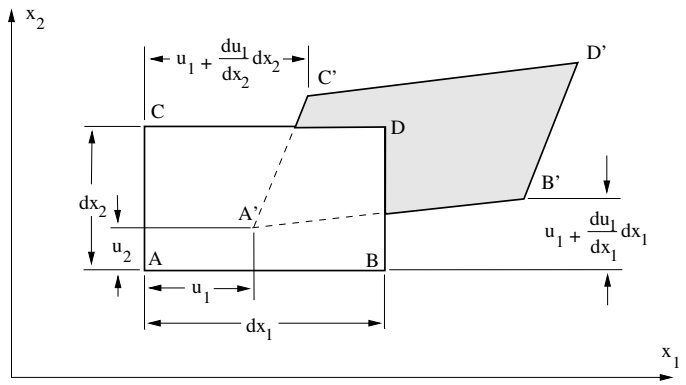

Figure 2.2: Strain definition

2.2.1 Strain-displacement relationships

In linear elasticity, the gradient of displacement vector is consider as infinitesimal order. Then, the strain tensor $\varepsilon_{\alpha\beta}$ is given by (figure 2.2):

$$\varepsilon_{11} = \frac{\partial u_1}{\partial x_1} \tag{2.1}$$

$$\varepsilon_{22} = \frac{\partial u_2}{\partial x_2} \tag{2.2}$$

$$\varepsilon_{12} = \frac{\partial u_1}{\partial x_2} + \frac{\partial u_2}{\partial x_1} \tag{2.3}$$

where u_α are the displacements components along of x_1 and x_2 coordinate axis. Indicial notation is used throughout this work. Greek index will vary from 1 to 2 and Roman index from 1 to 3. The partial derivative of any function with respect to the coordinate x_α will be denoted by comma subscript.

To ensure the uniticity of the displacement field, when the components of strain tensor has been arbitrary assigned, compatibility conditions between displacement components should

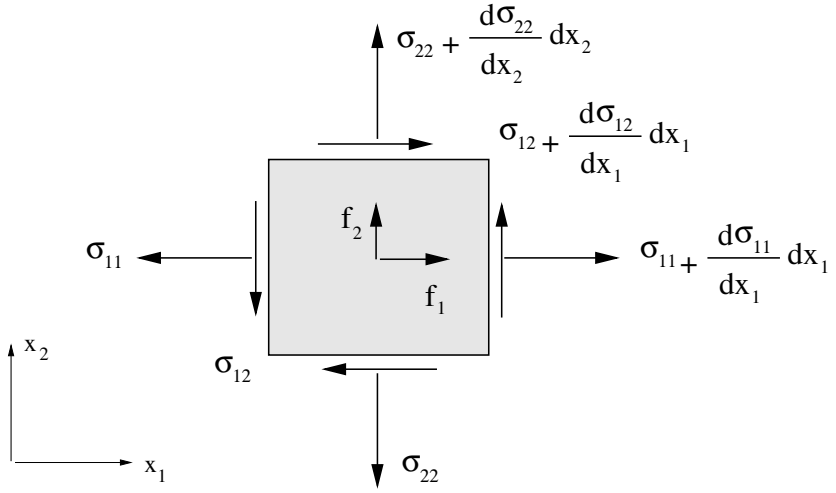

Figure 2.3: Stress components in plane-stress problems

be established. In two-dimensional problems the condition is given by the equation:

$$\frac{\partial}{\partial x_2}\left(\frac{\partial \varepsilon_{11}}{\partial x_2}\right) + \frac{\partial}{\partial x_1}\left(\frac{\partial \varepsilon_{22}}{\partial x_1}\right) = \frac{\partial}{\partial x_1}\left(\frac{\partial \varepsilon_{12}}{\partial x_2}\right) \tag{2.4}$$

2.2.2 Equilibrium equations

Considering figure 10.4, the static equilibrium equation for a differential element at a continuum body under plane stress condition can be written as (see Kane, 1994):

$$\frac{\partial \sigma_{11}}{\partial x_1} + \frac{\partial \sigma_{12}}{\partial x_2} + f_1 = 0 \tag{2.5}$$

$$\frac{\partial \sigma_{21}}{\partial x_1} + \frac{\partial \sigma_{22}}{\partial x_2} + f_2 = 0 \tag{2.6}$$

evaluated in Ω, which usually have to satisfy the following conditions:

$$u_\alpha = \bar{u}_\alpha \quad \text{in} \quad \Gamma_u \tag{2.7}$$

$$t_\alpha = \bar{t}_\alpha \quad \text{in} \quad \Gamma_\text{t} \tag{2.8}$$

where $\sigma_{\alpha\beta}$ represents the Cauchy stress tensor. Γ_u is a portion of the boundary Γ where known displacements are imposed. Finally, the traction vector, t_α at any point of the boundary Γ_t with normal n_β is given by:

$$t_\alpha = \sigma_{\alpha\beta} n_\beta \tag{2.9}$$

2.3 Isotropic elasticity

As discussed above, the object in a state of plane stress is free to contract or expand in the third direction. All components of the traction vector in direction 3 are equal to zero. Then, the stress-strain relationship based on Hooke's law for plane-stress can be written as:

$$\sigma_{11} = \frac{2\lambda G}{\lambda + 2G}\varepsilon_{11} + 2G\varepsilon_{11} \tag{2.10}$$

$$\sigma_{22} = \frac{2\lambda G}{\lambda + 2G}\varepsilon_{22} + 2G\varepsilon_{22} \tag{2.11}$$

$$\sigma_{12} = 2G\varepsilon_{12} \tag{2.12}$$

where $\lambda = 2\nu G/(1-2\nu)$, G is the elastic shear modulus, ν is the Poisson's modulus and $\delta_{\alpha\beta}$ is the Kronneker's delta. In plane stress the strain ε_{33} component can be obtained as:

$$\varepsilon_{33} = -\frac{\lambda}{(\lambda + 2G)}\varepsilon_{\alpha\alpha} \tag{2.13}$$

2.4 Isotropic fundamental solution

The formulation of the boundary integral equations for elastostatics require the knowledge of the solution of the elastic problem with the same material properties as the body under consideration, but corresponding to an infinite domain loaded with a concentrated unit point load. If the equilibrium equations are expressed in terms of the displacements components, we obtains the Navier's equations for two-dimensional elastostatics:

$$\mu \left(\frac{3\lambda + 2G}{\lambda + 2G} \right) u_{\alpha,\alpha\beta} + G u_{\beta,\gamma\gamma} + f_\beta = 0 \tag{2.14}$$

Kelvin solution is obtained from this equation when a unit concentrated load is applied at a point i, in the direction of the unit vector e_β:

$$f_\beta = \Delta^i e_\beta \tag{2.15}$$

Expressing the displacements terms through the Galerkin's vector, G_α, we obtain:

$$u_\alpha = G_{\alpha,\beta\beta} - \frac{1}{2\,(1-\nu)} G_{\beta,\alpha\beta} \tag{2.16}$$

Substituting equations (2.16) and (2.15) into equation (2.14) and solving for G_α, gives:

$$G_{\alpha\beta} = \frac{1}{8\pi G} r^2 \ln\left(\frac{1}{r}\right) e_\alpha \delta_{\alpha\beta} \tag{2.17}$$

$G_{\alpha\beta}$ is the α component of the Galerkin's vector at any point when a unit load is applied at point α in the β direction. The displacement at any point in the domain, considering each direction as independent is written as:

$$u^*_\alpha = u^*_{\beta\alpha} e_\beta \tag{2.18}$$

where $u^*_{\alpha\beta}$ represents the displacement at any point in the β direction when a unit load is applied at point "i" in the α direction. In accordance to the definition of equation (2.16), one can now write:

$$u^*_{\alpha\beta} = G_{\alpha\beta,\gamma\gamma} - \frac{1}{2\,(1-\nu)} G_{\alpha\gamma,\beta\gamma} \tag{2.19}$$

Substituting equations (2.17) into equation (2.19), we obtain the fundamental solution for the two dimensional plane stress problem:

$$U_{\alpha\beta} = \frac{1}{8\pi\mu\,(1-\bar{\nu})} \left[(3-4\bar{\nu}) \ln\left(\frac{1}{r}\right) \delta_{\alpha\beta} + r_{,\alpha} r_{,\beta} \right] \tag{2.20}$$

where $\bar{\nu} = \nu/(1+\nu)$.

Finally, the fundamental traction vector on any surface with normal n_α due to a concentrated load can be derived from equation (2.4):

$$T_{\alpha\beta} = -\frac{1}{4\pi\,(1-\bar{v})\,r} \left[r_{,n} \left[(1-2\bar{v})\,\delta_{\alpha\beta} + 2 r_{,\alpha} r_{,\beta} \right] + (1-2\bar{v}) \left(n_\beta r_{,\alpha} - n_\alpha r_{,\beta} \right) \right] \tag{2.21}$$

Chapter 3

Anisotropic plane elasticity

3.1 Introduction

This chapter presents constitutive equations for anisotropic materials in two-dimensional elastostatics and the fundamental solutions for infinite anisotropic planes. Chapter begins defining basic stress-strain relationships for anisotropic elastic materials represented by the general elastic constant tensor. The stress tensor and expression for displacements components are establish, based on the Airy's stress function defined for bi-dimensional anisotropic problems. As a special case of orthotropic laminae, stress-strain relationships are presented in order to obtain the basis for obtains the general stress-strain relations for composite laminates. Finally, fundamental solutions for displacements and tractions for infinite anisotropic plane is presented.

3.1.1 Anisotropic elasticity

In the anisotropic elasticity, the stress-strain relationship can be written in a general form as (see Lekhnitskii, 1968):

$$\sigma_{\alpha\beta} = C_{\alpha\beta\gamma\rho}\varepsilon_{\gamma\rho} \tag{3.1}$$

where $C_{\alpha\beta\gamma\rho}$ is a fourth-order tensor known as *elastic constants tensor* with 81 components. Because of symmetry restrictions and the existence of a strain energy function, the following conditions are required:

$$C_{ijkl} = C_{jikl}, \quad C_{ijkl} = C_{ijlk}$$
$$C_{ijkl} = C_{klji} \tag{3.2}$$

The symmetry of stresses and strains and the existence of a strain energy density function, reduces the number of elastic constant from 81 to 21. In general, principal direction of stress tensor do not have same direction of principal direction of the strain tensor. So only 18 out of 21 elastic constants are independents. Considering only 21 elastic constants, equation (3.1) can be written in a matrix form as:

$$\begin{Bmatrix} \sigma_{11} \\ \sigma_{22} \\ \sigma_{33} \\ \sigma_{23} \\ \sigma_{13} \\ \sigma_{12} \end{Bmatrix} = \begin{bmatrix} C_{1111} & C_{1122} & C_{1133} & C_{1123} & C_{1113} & C_{1112} \\ C_{1122} & C_{2222} & C_{2233} & C_{2223} & C_{2213} & C_{2212} \\ C_{1133} & C_{2233} & C_{3333} & C_{3323} & C_{3313} & C_{3312} \\ C_{1123} & C_{2223} & C_{3323} & C_{2323} & C_{2313} & C_{2312} \\ C_{1113} & C_{2213} & C_{3313} & C_{2313} & C_{1313} & C_{1312} \\ C_{1112} & C_{2212} & C_{3312} & C_{2312} & C_{1312} & C_{1212} \end{bmatrix} \begin{Bmatrix} \varepsilon_{11} \\ \varepsilon_{22} \\ \varepsilon_{33} \\ 2\varepsilon_{23} \\ 2\varepsilon_{13} \\ 2\varepsilon_{12} \end{Bmatrix} \tag{3.3}$$

Alternatively, equation (3.2) can be written as:

$$\varepsilon_{ij} = S_{ijkl}\sigma_{kl} \tag{3.4}$$

where, S_{ijkl} is a four order tensor named as flexibility tensor, and similar to tensor C_{ijkl} has only 18 independent constants. Equation (3.4) can be written as:

$$\begin{Bmatrix} \varepsilon_{11} \\ \varepsilon_{22} \\ \varepsilon_{33} \\ 2\varepsilon_{23} \\ 2\varepsilon_{13} \\ 2\varepsilon_{12} \end{Bmatrix} = \begin{bmatrix} S_{1111} & S_{1122} & S_{1133} & 2S_{1123} & 2S_{1113} & 2S_{1112} \\ S_{1122} & S_{2222} & S_{2233} & 2S_{2223} & 2S_{2213} & 2S_{2212} \\ S_{1133} & S_{2233} & S_{3333} & 2S_{3323} & 2S_{3313} & 2S_{3312} \\ 2S_{1123} & 2S_{2223} & 2S_{3323} & 4S_{2323} & 4S_{2313} & 4S_{2312} \\ 2S_{1113} & 2S_{2213} & 2S_{3313} & 4S_{2313} & 4S_{1313} & 4S_{1312} \\ 2S_{1112} & 2S_{2212} & 2S_{3312} & 4S_{2312} & 4S_{1312} & 4S_{1212} \end{bmatrix} \begin{Bmatrix} \sigma_{11} \\ \sigma_{22} \\ \sigma_{33} \\ \sigma_{23} \\ \sigma_{13} \\ \sigma_{12} \end{Bmatrix} \tag{3.5}$$

Using the reduced tensorial notation proposed by Lekhnitskii, this equation can be written as:

$$\begin{Bmatrix} \varepsilon_1 \\ \varepsilon_2 \\ \varepsilon_3 \\ \varepsilon_4 \\ \varepsilon_5 \\ \varepsilon_6 \end{Bmatrix} = \begin{bmatrix} a_{11} & a_{12} & a_{13} & a_{14} & a_{15} & a_{16} \\ a_{12} & a_{22} & a_{23} & a_{24} & a_{25} & a_{26} \\ a_{13} & a_{23} & a_{33} & a_{34} & a_{35} & a_{36} \\ a_{14} & a_{24} & a_{34} & a_{44} & a_{45} & a_{46} \\ a_{15} & a_{25} & a_{35} & a_{45} & a_{55} & a_{56} \\ a_{16} & a_{26} & a_{36} & a_{46} & a_{56} & a_{66} \end{bmatrix} \begin{Bmatrix} \sigma_1 \\ \sigma_2 \\ \sigma_3 \\ \sigma_4 \\ \sigma_5 \\ \sigma_6 \end{Bmatrix} \tag{3.6}$$

where:

$$\begin{Bmatrix} \varepsilon_1 \\ \varepsilon_2 \\ \varepsilon_3 \\ 2\varepsilon_4 \\ 2\varepsilon_5 \\ 2\varepsilon_6 \end{Bmatrix} = \begin{Bmatrix} \varepsilon_{11} \\ \varepsilon_{22} \\ \varepsilon_{33} \\ 2\varepsilon_{23} \\ 2\varepsilon_{13} \\ 2\varepsilon_{12} \end{Bmatrix} \tag{3.7}$$

and,

$$\begin{Bmatrix} \sigma_1 \\ \sigma_2 \\ \sigma_3 \\ \sigma_4 \\ \sigma_5 \\ \sigma_6 \end{Bmatrix} = \begin{Bmatrix} \sigma_{11} \\ \sigma_{22} \\ \sigma_{33} \\ \sigma_{23} \\ \sigma_{13} \\ \sigma_{12} \end{Bmatrix} \tag{3.8}$$

The elastic coefficients can be expressed in terms of engineering constants as:

$$\begin{aligned}
&a_{11} = 1/E_1 && a_{12} = v_{12}/E_1 = -v_{12}/E_2 \\
&a_{13} = -v_{13}/E_1 = -v_{13}/E_3 && a_{14} = \eta_{23,1}/E_1 = \eta_{1,23}/G_{23} \\
&a_{15} = \eta_{32,1}/E_1 = \eta_{1,32}/G_{23} && a_{16} = \eta_{12,1}/E_1 \\
&a_{22} = 1/E_2 && a_{23} = v_{32}/E_2 = -v_{23}/E_3 \\
&a_{24} = \eta_{23,1}/E_2 = \eta_{23,3}/G_{23} && a_{25} = \eta_{31,2}/E_2 = \eta_{2,31}/G_{13} \\
&a_{26} = \eta_{12,2}/E_2 = \eta_{2,12}/G_{12} && a_{33} = 1/E_3 \\
&a_{34} = \eta_{23,3}/E_3 = \eta_{3,23}/G_{23} && a_{35} = \eta_{31,1}/E_3 = \eta_{3,31}/G_{13} \\
&a_{36} = \eta_{12,3}/E_3 = \eta_{3,12}/G_{12} && a_{44} = 1/G_{23} \\
&a_{45} = \varsigma_{32,23}/G_{23} = \varsigma_{23,31}/G_{13} && a_{46} = \varsigma_{12,23}/G_{23} = \varsigma_{23,12}/G_{12} \\
&a_{55} = 1/G_{13} && a_{56} = \varsigma_{12,31}/G_{13} = \varsigma_{31,12}/G_{12} \\
&a_{66} = 1/G_{12}
\end{aligned} \tag{3.9}$$

were E_k are the Young modulus referenced to axis x_k, G_{ij} are the shear modulus or Coulomb's modulus for planes defined by axis $x_i xj$. Constants v_{ij} are the Poisson's coefficients. $\eta_{jk,l}$ are the first-kind mutual influence coefficients, that characterize the principal strains generated by shear stresses acting at principal planes. The constants $\eta_{l,jk}$ are the second-kind mutual influence coefficients that characterize shear strains at principal planes generated by normal stresses acting on this plane. Finally, $\varsigma_{ij,kl}$ are the Chentsov's coefficients, that characterize

the shear strain acting at principal planes, generated by shear stresses acting in this planes.

In a plane-stress state ($\sigma_3 = \sigma_4 = \sigma_5 = 0$), any material can be expressed using only six independent elastic constants. In this way, equation (3.6) can be written as:

$$\begin{Bmatrix} \varepsilon_1 \\ \varepsilon_2 \\ \varepsilon_3 \end{Bmatrix} = \begin{bmatrix} a_{11} & a_{12} & a_{16} \\ a_{12} & a_{22} & a_{26} \\ a_{16} & a_{26} & a_{66} \end{bmatrix} \begin{Bmatrix} \sigma_1 \\ \sigma_2 \\ \sigma_6 \end{Bmatrix} \tag{3.10}$$

Finally, substituting equations (2.3) and (3.1) into equation (2.6) the equilibrium equation for a general anisotropic elastostatic problems in term of displacements is obtained as:

$$C_{ijkl} u_{k,jl} + f_i = 0 \tag{3.11}$$

3.2 The Airy's stress function

In anisotropic elasticity, the stress-tensor can be written in function of the Airy's stress function $F(x_1, x_2)$ given by (Lekhnitskii, 1968):

$$\begin{aligned} \sigma_{11} &= F_{,22} + \Upsilon \\ \sigma_{22} &= F_{,11} + \Upsilon \\ \sigma_{12} &= -F_{,12} \end{aligned} \tag{3.12}$$

where Υ is a potential function with the property: $\Upsilon_{,i} = f_i$. Substituting equations (3.12) into constitutive equation (3.10) and then into compatibility equation (2.4), we obtains the

differential equation for the stress function $F(x_1, x_2)$:

$$\begin{aligned} &a_{11}F_{,2222} - 2a_{16}F_{,1222} + (2a_{12} + a_{66})\,F_{,1122} - 2a_{26}F_{,1112} + a_{22}F_{,1111} = \\ &-(a_{12} + a_{22})\,\vartheta_{,11} + (a_{16} + a_{26})\,\vartheta_{,12} - (a_{11} + a_{12})\,\vartheta_{,22} \end{aligned} \tag{3.13}$$

The special case of $f_i = 0$, the above equation can be written as:

$$a_{11}F_{,2222} - 2a_{16}F_{,1222} + (2a_{12} + a_{66})\,F_{,1122} - 2a_{26}F_{,1112} + a_{22}F_{,1111} = 0 \tag{3.14}$$

Defining the differential operator:

$$\Delta_k = \frac{\partial}{\partial x_2} - \mu_k \frac{\partial}{\partial x_1} \tag{3.15}$$

Applying this operator on stress function $F(x_1, x_2)$, we can write:

$$\Delta_1\Delta_2\Delta_3\Delta_4 F = 0 \tag{3.16}$$

Expanding this equation we have:

$$\begin{aligned} &F_{,2222} - (\mu_1\mu_2\mu_3\mu_4)\,F_{,1222} + (\mu_1\mu_2 + \mu_1\mu_3\mu_1\mu_4 + \mu_2\mu_3 + \mu_2\mu_4 + \mu_3\mu_4)\,F_{,1122} \\ &-(\mu_1\mu_2\mu_3 + \mu_1\mu_2\mu_4 + \mu_1\mu_3\mu_4 + \mu_2\mu_3\mu_4)\,F_{,1112} + (\mu_1\mu_2\mu_3\mu_4)\,F_{,1111} = 0 \end{aligned} \tag{3.17}$$

Equations (3.14) and (3.17) will be equal if μ_1 ,μ_2 ,μ_3 ,μ_4 are roots of the equation:

$$a_{11}\mu^4 - 2a_{16}\mu^3 + (2a_{12} + a_{66})\,\mu^2 - 2a_{26}\mu + a_{22} = 0 \tag{3.18}$$

Roots of equation (3.18) are complex or pure imaginary roots, occurring in pairs (μ_k and $\overline{\mu}_k$) as showed by Lekhnitskii, 1968.

Defining the variable z_k as:

$$z_\alpha = x_1 + \mu_\alpha x_2 \tag{3.19}$$

we have:

$$\Delta_k = \frac{\partial}{\partial x_2} - \mu_k \frac{\partial}{\partial x_1} = \frac{d}{dz_k} \tag{3.20}$$

Defining $F(x_1, x_2)$ as a real function, we have:

$$F\left(x_1, x_2\right) = 2\mathrm{Re}\left[F_1\left(z_1\right) + F_2\left(z_2\right)\right] \tag{3.21}$$

and introducing the notation:

$$\frac{dF_k\left(z_k\right)}{dz_k} = \Psi_k\left(z_k\right) \tag{3.22}$$

where the summation convention is applied for k, and replacing equation (3.21) into equation (3.12), we obtain the components of the stress tensor:

$$\sigma_{11} = 2\mathrm{Re}\left[\mu_1^2 \Psi_1^{(1)}\left(z_1\right) + \mu_2^2 \Psi_2^{(1)}\left(z_2\right)\right] \tag{3.23}$$

$$\sigma_{22} = 2\mathrm{Re}\left[\Psi_1^{(1)}\left(z_1\right) + \Psi_2^{(1)}\left(z_2\right)\right] \tag{3.24}$$

$$\sigma_{12} = -2\mathrm{Re}\left[\mu_1 \Psi_1^{(1)}\left(z_1\right) + \mu_2 \Psi_2^{(1)}\left(z_2\right)\right] \tag{3.25}$$

where $\psi_k^{(1)}$ represents the first derivative of ψ_k.

Replacing the above equation into equation (3.25) and then into equation (3.11) and integrating, we obtain:

$$u_1 = 2\mathrm{R_e}\left[q_{11}\Psi_1\left(z_1\right) + q_{12}\Psi_2\left(z_2\right)\right] \tag{3.26}$$

$$u_2 = 2\mathrm{R_e}\left[q_{21}\Psi_1\left(z_1\right) + q_{22}\Psi_2\left(z_2\right)\right] \tag{3.27}$$

where:

$$q_{\alpha\beta} = \begin{bmatrix} a_{11}\mu_\beta^2 + a_{12} - a_{16}\mu_\beta \\ a_{12}\mu_\beta + a_{22}/\mu_\beta - a_{26} \end{bmatrix} \tag{3.28}$$

are known as the complex parameter matrix.

If the boundary condition are established, the stress function given by equations (3.12) (with the condition : $\Upsilon_{,i} = f_i$) can be defined to satisfy this conditions. In this way the displacements and stress fields, given by equations (3.27) and (3.25) can be founded.

3.3 Constitutive equations for a laminae

An orthotropic laminae has the next stress-strain relationship given by:

$$\begin{Bmatrix} \sigma_{11} \\ \sigma_{22} \\ \sigma_{12} \end{Bmatrix} = \begin{Bmatrix} Q_{11} & Q_{12} & 0 \\ Q_{12} & Q_{22} & 0 \\ 0 & 0 & 2Q_{66} \end{Bmatrix} \begin{Bmatrix} \varepsilon_{11} \\ \varepsilon_{22} \\ \varepsilon_{12} \end{Bmatrix} \tag{3.29}$$

where Q_{ij} are the components of the stiffness tensor, i.e:

$$\begin{aligned} &Q_{11} = E_1/\left(1 - v_{12}v_{21}\right) && Q_{22} = E_2/\left(1 - v_{12}v_{21}\right) \\ &Q_{66} = G_{12} && Q_{16} = Q_{26} = 0 \\ &Q_{12} = v_{21}E_1/\left(1 - v_{12}v_{21}\right) = v_{12}E_2/\left(1 - v_{12}v_{21}\right) \end{aligned} \tag{3.30}$$

Since laminae is orthotropic (figure 3.1), it is totally characterized by four elastic constants: the Young modulus E_1 and E_2 in the directions 1 and 2, respectively, the transversal shear modulus G_{12} and the Poisson ratio, v_{12}. The fifth elastic constant v_{12} is determinated

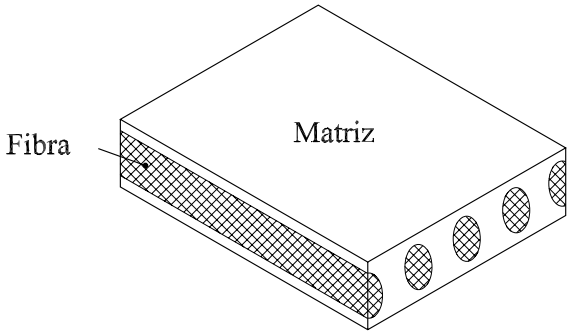

Figure 3.1: Orthotropic laminae

by the constitutive relationship:

$$v_{21}E_1 = v_{12}E_2 \tag{3.31}$$

In many situations the principal axis of the laminae (x_1x_2) are not coincident with the laminate axis ($\overline{x}_1\overline{x}_2$). In this case, the constitutive relationship for each laminae should be transformed to the laminated reference axis (figure 3.2) and then the constitutive relationship can be defined. This transformation is performed multiplying the stress and strain tensors by a matrix transformation:

$$\begin{aligned} \sigma^{'}_{\alpha\beta} &= \mathbf{T}\sigma_{\alpha\beta} \\ \varepsilon^{'}_{\alpha\beta} &= \mathbf{T}\varepsilon_{\alpha\beta} \end{aligned} \tag{3.32}$$

where $\sigma^{'}_{\alpha\beta}$ and $\varepsilon^{'}_{\alpha\beta}$ are the stress and strain tensor, respectively, referenced to laminated axis. Transformation matrix $\mathbf{T}$ is given by:

$$\mathbf{T} = \begin{bmatrix} m^2 & n^2 & 2mn \\ n^2 & m^2 & -2mn \\ -mn & mn & m^2 - n^2 \end{bmatrix} \tag{3.33}$$

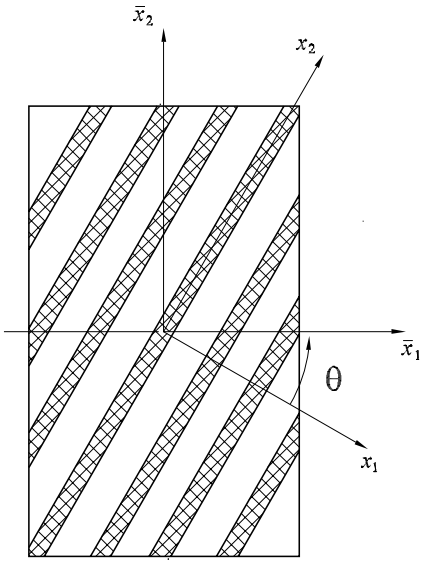

Figure 3.2: Laminae coordinate system

with: $m = \cos(\theta)$ and $n = \sin(\theta)$. Then, the constitutive equation is written as:

$$\left\{ \begin{array}{c} \sigma_{11}^{'} \\ \sigma_{22}^{'} \\ \sigma_{12}^{'} \end{array} \right\} = \mathbf{T}^{-1}\mathbf{Q}\left(\mathbf{T}^{-1}\right)^{'} \left\{ \begin{array}{c} \varepsilon_{11}^{'} \\ \varepsilon_{22}^{'} \\ \varepsilon_{12}^{'} \end{array} \right\} \tag{3.34}$$

that can be written as:

$$\left\{ \begin{array}{c} \sigma_{11}^{'} \\ \sigma_{22}^{'} \\ \sigma_{12}^{'} \end{array} \right\} = \left[\begin{array}{ccc} \overline{Q}_{11} & \overline{Q}_{12} & \overline{Q}_{16} \\ \overline{Q}_{12} & \overline{Q}_{22} & \overline{Q}_{26} \\ \overline{Q}_{16} & \overline{Q}_{26} & \overline{Q}_{66} \end{array} \right] \left\{ \begin{array}{c} \varepsilon_{11}^{'} \\ \varepsilon_{22}^{'} \\ \varepsilon_{12}^{'} \end{array} \right\} \tag{3.35}$$

where:

$$\begin{aligned} \overline{Q}_{11} &= Q_{11}\cos^4\theta + 2\left(Q_{12} + 2Q_{66}\right)\sin^2\theta\cos^2\theta + Q_{22}\sin^4\theta \\ \overline{Q}_{22} &= Q_{11}\sin^4\theta + 2\left(Q_{12} + 2Q_{66}\right)\sin^2\theta\cos^2\theta + Q_{22}\cos^4\theta \end{aligned}$$

$$\overline{Q}_{12} = (Q_{11} + Q_{22} - 4Q_{66})\sin^2\theta\cos^2\theta + Q_{12}\left(\sin^4\theta + \cos^4\theta\right)$$

$$\overline{Q}_{66} = (Q_{11} + Q_{22} - 2Q_{12} - 2Q_{66})\sin^2\theta\cos^2\theta + Q_{66}\left(\sin^4\theta + \cos^4\theta\right) \quad (3.36)$$

$$\overline{Q}_{16} = (Q_{11} - Q_{12} - 2Q_{66})\sin\theta\cos^3\theta + (Q_{12} - Q_{22} + 2Q_{66})\sin^3\theta\cos\theta \quad (3.37)$$

3.4 Symmetric laminates

A symmetric laminate has both, geometric and material property symmetric about the middle surface (see Gibson, 1992). That is, the lamina material, lamina orientation, and lamina thickness at a positive distance z from the middle surface are identical to the the corresponding values at an equal negative distance z from the middle surface.

This imply that bending-stretching coupling will not be present in such laminates. Consequently, in-plane loads will not generate bending and twisting curvatures that causes out-of-plane warping, and bending or twisting moments will not produce an extension of the middle surface.

Components of the tensor stress tensor acting at any laminate are obtained integrating these components that act in any lamina through the thickness of the laminate:

$$\sigma_{ij} = \frac{1}{h}\int_{-h_{l/2}}^{+h_{l/2}} \sigma_{ij}^{'} dx_3 \quad (3.38)$$

where $\sigma_{ij}^{'}$ is the stress tensor acting in any individual laminae and σ_{ij} is the mean tensor stress acting in the laminate.

Consider now the laminate as composed by N orthotropic laminae, as show in figure 3.3. Forces acting in the middle plane of this laminate can be obtained replacing the continuous

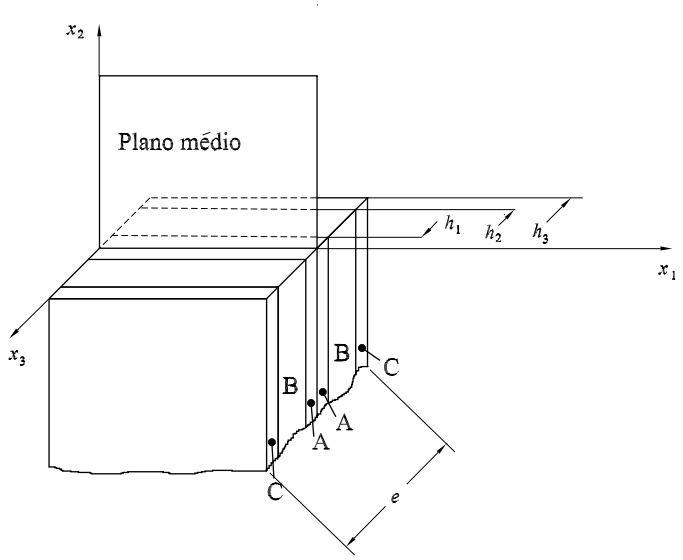

Figure 3.3: Symmetric laminate

integral by the summatory of integrals each laminae:

$$\left\{ \begin{array}{c} \sigma_{11} \\ \sigma_{22} \\ \sigma_{12} \end{array} \right\} = \frac{1}{h} \sum_{l=1}^{N} \int_{h_l - 1}^{h_l} \left\{ \begin{array}{c} \sigma_{11}^{'} \\ \sigma_{22}^{'} \\ \sigma_{12}^{'} \end{array} \right\}_l dx_3 \tag{3.39}$$

Replacing equation (3.34) into (3.39), we obtain:

$$\left\{ \begin{array}{c} \sigma_{11} \\ \sigma_{22} \\ \sigma_{12} \end{array} \right\} = \frac{1}{h} \sum_{l=1}^{N} \left\{ \int_{h_l - 1}^{h_l} \left[\begin{array}{ccc} \overline{Q}_{11} & \overline{Q}_{12} & \overline{Q}_{16} \\ \overline{Q}_{12} & \overline{Q}_{22} & \overline{Q}_{26} \\ \overline{Q}_{16} & \overline{Q}_{26} & \overline{Q}_{66} \end{array} \right]_l \left\{ \begin{array}{c} \varepsilon_{11} \\ \varepsilon_{22} \\ \varepsilon_{12} \end{array} \right\} dx_3 \right\} \tag{3.40}$$

Since $\overline{\mathbf{Q}}_l$ and ε_{ij} are constants through the thickness h (as principal hypothesis in this work),

equation (3.43) can be re-written as:

$$\left\{ \begin{array}{c} \sigma_{11} \\ \sigma_{22} \\ \sigma_{12} \end{array} \right\} = \frac{1}{h} \left[\sum_{l=1}^{N} \left[\begin{array}{ccc} \overline{Q}_{11} & \overline{Q}_{12} & \overline{Q}_{16} \\ \overline{Q}_{12} & \overline{Q}_{22} & \overline{Q}_{26} \\ \overline{Q}_{16} & \overline{Q}_{26} & \overline{Q}_{66} \end{array} \right]_l (h_l - h_{l-1}) \right] \left\{ \begin{array}{c} \varepsilon_{11} \\ \varepsilon_{22} \\ \varepsilon_{12} \end{array} \right\} \tag{3.41}$$

where:

$$\overline{\mathbf{Q}}_L = \frac{1}{h} \left[\sum_{l=1}^{N} \mathbf{Q}_l \left(h_l - h_{l-1} \right) \right] \tag{3.42}$$

In many cases is necessary to transform the tensor $\mathbf{Q}$ to another coordinate system. In this case, a similar transformation procedure applied to equations (3.35) is used:

$$\begin{aligned} a_{11}^{'} &= a_{11} \cos^4\theta + (2a_{12} + a_{66}) \sin^2\theta \cos^2\theta + a_{22} \sin^4\theta \\ &+ \left(a_{16} \cos^2\theta + a_{26} \sin^2\theta \right) \sin 2\theta \end{aligned} \tag{3.43}$$

$$\begin{aligned} a_{22}^{'} &= a_{11} \sin^4\theta + (2a_{12} + a_{66}) \sin^2\theta \cos^2\theta + a_{22} \cos^4\theta \\ &- \left(a_{16} \cos^2\theta + a_{26} \sin^2\theta \right) \sin 2\theta \end{aligned} \tag{3.44}$$

$$\begin{aligned} a_{12}^{'} &= a_{12} + (a_{11} + a_{22} - 2a_{12} - a_{66}) \sin^2\theta \cos^2\theta \\ &+ \frac{1}{2} (a_{26} - a_{16}) \sin 2\theta \cos 2\theta \end{aligned} \tag{3.45}$$

$$\begin{aligned} a_{66}^{'} &= \left[a_{22} \sin^2\theta - a_{11} \cos^2\theta + \frac{1}{2} (a_{12} - a_{66}) \cos 2\theta \right] \sin 2\theta \\ &+ a_{16} \cos^2\theta \left(\cos^2\theta - 3 \sin^2\theta \right) + a_{26} \sin^2\theta \left(3 \cos^2\theta - \sin^2\theta \right) \end{aligned} \tag{3.46}$$

$$\begin{aligned} a_{26}^{'} &= \left[a_{22} \cos^2\theta - a_{11} \sin^2\theta + \frac{1}{2} (2a_{12} + a_{66}) \cos 2\theta \right] \sin 2\theta \\ &+ a_{16} \sin^2\theta \left(3 \cos^2\theta - \sin^2\theta \right) + a_{26} \cos^2\theta \left(\cos^2\theta - 3 \sin^2\theta \right) \end{aligned} \tag{3.47}$$

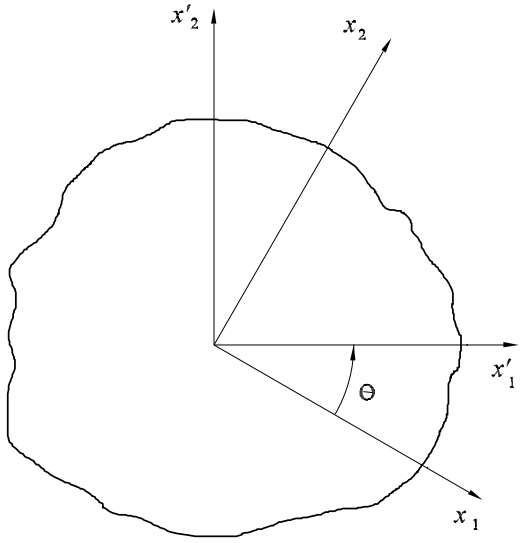

Figure 3.4: Transformation of the coordinate system

where a'_{ij} represents the elastic constants matrix represented in the $x'_1x'_2$ coordinate system and a_{ij} is the same matrix but related to coordinate system x_1x_2 (see figure 3.4).

Roots of characteristic equation can be written with reference to the new coordinate system by:

$$\mu'_k = \frac{\mu_k \cos\theta - \sin\theta}{\cos\theta + \mu_k \sin\theta} \tag{3.48}$$

where μ'_k are roots expressed in the new coordinate system.

3.5 Anisotropic fundamental solutions

Defining complex variables:

$$\mathbf{z}' = \left\{ \begin{array}{c} z'_1 \\ z'_2 \end{array} \right\} = \left\{ \begin{array}{c} x'_1 + \mu_1 x'_2 \\ x'_1 + \mu_2 x'_2 \end{array} \right\} \tag{3.49}$$

and

$$\mathbf{z}' = \left\{ \begin{array}{c} z_1 \\ z_2 \end{array} \right\} = \left\{ \begin{array}{c} x_1 + \mu_1 x_2 \\ x_2 + \mu_2 x_2 \end{array} \right\} \tag{3.50}$$

where $x_1^{'}$ and $x_2^{'}$ are the source point coordinates (point of application of the concentrated unit load) and x_1 and x_2 are the field point coordinates.

Considering a closed boundary around the source point and using the traction surface forces defined by equation (2.8) and stresses defined by equation (3.25), we have:

$$\int_{\Gamma_t} t_1 d\Gamma = 2\mathrm{Re}\left[\mu_1\Psi_1 + \mu_2\Psi_2\right] = -\delta_{\alpha 1} \tag{3.51}$$

$$\int_{\Gamma_t} t_2 d\Gamma = 2\mathrm{Re}\left[\Psi_1 + \Psi_2\right] = \delta_{\alpha 2} \tag{3.52}$$

For a loaded point in the direction x_1, the Airy stress function can be represented by $\Psi_{\alpha\beta}$. These equations can be satisfied for any closed boundary path $\mathbf{z}$' if we take:

$$\Psi_{\alpha\beta} = A_{\alpha\beta} \ln\left(\mathbf{z} - \mathbf{z}'\right) \tag{3.53}$$

Replacing (3.52) into (3.53) and considering $\ln\left(\mathbf{z} - \mathbf{z}'\right) = 2\pi i$ two equations for the unknows constants $A_{\alpha\beta}$ are obtained as:

$$\begin{aligned} A_{\alpha 1} - \overline{A}_{\alpha 1} + A_{\alpha 2} - \overline{A}_{\alpha 2} &= \delta_{\alpha 2}/(2\pi i) \\ \mu_1 A_{\alpha 1} - \overline{\mu}_1\overline{A}_{\alpha 1} + \mu_2 A_{\alpha 2} - \overline{\mu}_2\overline{A}_{\alpha 2} &= -\delta_{\alpha 1}/(2\pi i) \end{aligned} \tag{3.54}$$

Another two equations are necessary to compute $A_{\alpha\beta}$. These equations are obtained from the condition of uniques for displacements. Solving for $A_{\alpha\beta}$, using equation (3.53) and replacing into displacements equations (3.27), we obtain the displacement fundamental solution for

anisotropic plane-stress problems (see Albuquerque, 2001):

$$U_{\alpha\beta} = 2\mathrm{Re}\left[q_{\beta 1} A_{\alpha 1} \ln\left(z_1 - z_1^{'}\right) + q_{\alpha 2} A_{\beta 2} \ln\left(z_2 - z_2^{'}\right)\right] \tag{3.55}$$

Finally, the fundamental traction vector on any surface with normal n_α can be derived as:

$$T_{\alpha\beta} = 2\mathrm{Re}\left[\frac{1}{\left(z_1 - z_1^{'}\right)} g_{\alpha 1}\left(\mu_1 n_1 - n_2\right) A_{\beta 1} + \frac{1}{\left(z_2 - z_2^{'}\right)} g_{\alpha 2}\left(\mu_2 n_1 - n_2\right) A_{\beta 2}\right] \tag{3.56}$$

Chapter 4

Boundary element method for plane elastostatics

4.1 Introduction

In this chapter, the boundary element method (BEM) is applied to solve two-dimensional elasticity problems. For that, boundary integral equations are obtained using the weighted residual method applied to equilibrium equation in elastostatics, which is equivalent to the *Betti's reciprocity theorem* in solid mechanics. Initially, the boundary integral formulation (based on *Somigliana's* identity) is obtained. This formulation is discretizated using boundary elements and using fundamental solutions as weighted functions and then matrix equations of the BEM are established. In this work, two types of boundary element are used: continuous and discontinuous quadratic elements to discretizate the boundary. The continuous elements are used to approximate elements geometry and discontinuous to approximate the displacement and traction field in the elements. Finally, numerical examples considering isotropic and anisotropic material response are showed. Preliminary conclusions are presented.

4.2 Boundary integral formulation

The governing integral equations for elastostatics will be deduced using the weighted residual method. The weighted formulation of equations (2.6) can be written as (see for example Brebbia and Dominguez, 1989):

$$\int_{\Omega} \left(\sigma_{\alpha\beta,\beta} + f_{\alpha}\right) u_{\alpha}^{*} d\Omega = 0 \tag{4.1}$$

where u_{α}^{*} is the displacement weight function according to boundary conditions given by equations (2.2) and (2.3). Integrating by parts the first term of equation (4.1) and grouping the corresponding terms, we find the following expression:

$$\int_{\Omega} \sigma_{\alpha\beta}\varepsilon_{\alpha\beta}^{*} d\Omega + \int_{\Omega} f_{\alpha} u_{\alpha}^{*} d\Omega = -\int_{\Gamma} t_{\alpha} u_{\alpha}^{*} d\Gamma \tag{4.2}$$

Integrating by parts again we finds the adjoint of the equation (4.2):

$$\int_{\Omega} \sigma_{\alpha\beta}^{*} u_{\alpha} d\Omega + \int_{\Omega} f_{\alpha} u_{\alpha}^{*} d\Omega = -\int_{\Gamma} t_{\alpha} u_{\alpha}^{*} d\Gamma + \int_{\Gamma} t_{\alpha}^{*} u_{\alpha} d\Gamma \tag{4.3}$$

This expression corresponds to Betti's reciprocal theorem which will be used as the starting point for the boundary integral formulation in this work. Using as weighting function fundamental solutions for displacement and traction and considering the Dirac's property,

$$\int_{\Omega} \delta_{\alpha\beta} u_{\alpha} d\Omega = u_{\alpha} \tag{4.4}$$

we have:

$$u_{\alpha} + \int_{\Gamma} T_{\alpha\beta}\left(\mathbf{x}', \mathbf{x}\right) u_{\beta} d\Gamma = \int_{\Gamma} U_{\alpha\beta}\left(\mathbf{x}', \mathbf{x}\right) t_{\beta} d\Gamma - \frac{1}{h}\int_{A} U_{\alpha\beta}\left(\mathbf{x}', \mathbf{x}\right) f_{\beta} dA \tag{4.5}$$

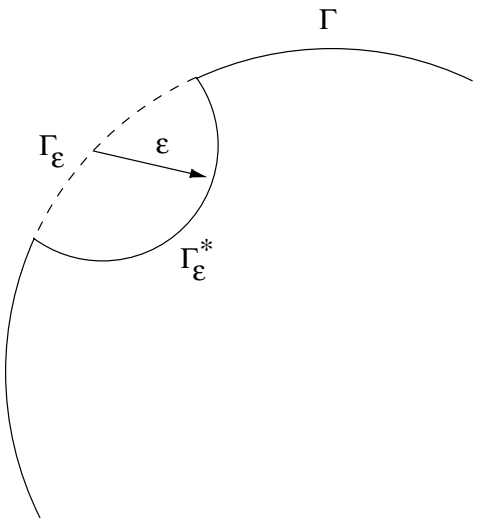

Figure 4.1: Source point placed at boundary and enclosed by a semi-circular region

where $d\Omega = hdA$, $h =$ the plate thickness. In this way, f_β represents a distributed body force per unit area[1]. This equation represents the *Somigliana's* identity for generalizated plane stress problems. This equation is the basis of the boundary element method.

4.3 Singular boundary integrals

When the source point is taken to the boundary, integrals have a singularity. If we consider that the boundary is smooth at source point, one can suppress it by a circle with center at this point and small radius ϵ which will afterward be taken to the limit (see figure 4.1).

There are two types of boundary integrals in equation (4.5). Consider first the one on R.H.S. and write it in function of Γ_ϵ:

$$\int_\Gamma U_{\alpha\beta} t_\beta \left(\mathbf{x}'\right) d\Gamma = \lim_{\epsilon \to 0} \left\{ \int_{\Gamma - \Gamma_\epsilon} U_{\alpha\beta} t_\beta \left(\mathbf{x}'\right) d\Gamma \right\} + \lim_{\epsilon \to 0} \left\{ \int_{\Gamma_\epsilon} U_{\alpha\beta} t_\beta \left(\mathbf{x}'\right) d\Gamma \right\} \tag{4.6}$$

[1] if b_β represents a distributed body force per unit of volume, this force can be written as: $b_\beta = 1/(hdA) b_\beta = 1/h f_\beta$

The first integral on the R.H.S. of (4.6) will simply become as integral on the whole boundary Γ when $\epsilon \to 0$. The second integral can be written as:

$$t_\beta(\mathbf{x}') \lim_{\epsilon \to 0} \left\{ \int_{\Gamma_\epsilon} U_{\alpha\beta} d\Gamma \right\} \tag{4.7}$$

Since the fundamental solution is of order $1/\epsilon$ and the boundary integral in (4.7) will tend to zero as $\epsilon \to 0$, we obtain:

$$\lim_{\varepsilon \to 0} \left\{ \int_{\Gamma_\varepsilon} U_{\alpha\beta} d\Gamma \right\} \equiv 0 \tag{4.8}$$

The L.H.S. integral in equation (4.5) however behaves differently. It can be written as:

$$\int_\Gamma T_{\alpha\beta} u_\beta(\mathbf{x}')\, d\Gamma = \lim_{\varepsilon \to 0} \left\{ \int_{\Gamma - \Gamma_\varepsilon} T_{\alpha\beta} u_\beta(\mathbf{x}')\, d\Gamma \right\} + \lim_{\varepsilon \to 0} \left\{ \int_{\Gamma_\varepsilon} T_{\alpha\beta} u_\beta(\mathbf{x}')\, d\Gamma \right\} \tag{4.9}$$

The limit of the last integral can be written as:

$$\lim_{\varepsilon \to 0} \left\{ \int_{\Gamma_\varepsilon} T_{\alpha\beta} u_\beta(\mathbf{x}')\, d\Gamma \right\} = u_\beta(\mathbf{x}') \lim_{\varepsilon \to 0} \left\{ \int_{\Gamma_\varepsilon} T_{\alpha\beta} d\Gamma \right\} \tag{4.10}$$

The values $T_{\alpha\beta}$ are now of order $1/\epsilon^2$ while the terms from integration over the boundary are of order ϵ^2. Hence integral (4.10) does not vanish when $\epsilon \to 0$ but produces a free term. Integrating over Γ_ϵ one finds:

$$\lim_{\varepsilon \to 0} \left\{ \int_{\Gamma_\varepsilon} T_{\alpha\beta} d\Gamma \right\} = -\frac{1}{2} \delta_{\alpha\beta} \tag{4.11}$$

Hence the L.H.S. integral (4.9) can be written in the limit as:

$$\int_\Gamma T_{\alpha\beta} u_\beta(\mathbf{x}')\, d\Gamma - \frac{1}{2} \delta_{\alpha\beta} u_\beta(\mathbf{x}') = \int_\Gamma T_{\alpha\beta} u_\beta(\mathbf{x}')\, d\Gamma - u_\alpha(\mathbf{x}') \tag{4.12}$$

where the integral on Γ is defined in the sense of Cauchy Principal Value. Therefore, for

boundary points, equation (4.5) transform into:

$$c_{\alpha\beta}u_{\beta}\left(\mathbf{x}'\right)+\int_{\Gamma}T_{\alpha\beta}\left(\mathbf{x}',\mathbf{x}\right)u_{\beta}d\Gamma=\int_{\Gamma}U_{\alpha\beta}\left(\mathbf{x}',\mathbf{x}\right)t_{\beta}d\Gamma+\frac{1}{h}\int_{A}U_{\alpha\beta}\left(\mathbf{x}',\mathbf{x}\right)f_{\beta}dA \tag{4.13}$$

where the integrals are in the sense of Cauchy principal value and where Γ is smooth at source point, $c_{\alpha\beta}=\frac{1}{2}\delta_{\alpha\beta}$.

4.4 Internal stresses

For an isotropic medium, the internal stresses can be computed by differentiating the displacements at internal points and introducing the corresponding strains and the stress-strain relationships into equation (4.13). After carrying out the derivatives inside the integral equations and taking the corresponding derivatives of the fundamental solution, it can be written as:

$$\sigma_{\alpha\beta}=\int_{\Gamma}D_{\alpha\beta\gamma}t_{\alpha}d\Gamma-\int_{\Gamma}S_{\alpha\beta\gamma}u_{\alpha}d\Gamma+\frac{1}{h}\int_{A}D_{\alpha\beta\gamma}f_{\alpha}dA \tag{4.14}$$

where the second order tensor components $D_{\alpha\beta\gamma}$ and $S_{\alpha\beta\gamma}$ are:

$$D_{\alpha\beta\gamma} = \frac{1}{4\pi r\left(1-v\right)}\left\{\left(1-2v\right)\left\{\delta_{\alpha\beta}r_{,\gamma}+\delta_{\beta\gamma}r_{,\beta}-\delta_{\beta\gamma}r_{,\alpha}\right\}+2r_{,\alpha}r_{,\beta}r_{,\gamma}\right\} \tag{4.15}$$

$$\begin{aligned} S_{\alpha\beta\gamma} &= \frac{2G}{4\pi r^{2}\left(1-v\right)}\left\{2r_{,n}\left[\left(1-2v\right)\delta_{\beta\gamma}r_{,\alpha}+v\left(\delta_{\beta\alpha}r_{,\gamma}+\delta_{\gamma\alpha}r_{,\beta}\right)-\gamma r_{,\alpha}r_{,\beta}r_{,\gamma}\right]\right. \\ &+ 2v\left(n_{\beta}r_{,\gamma}r_{,\alpha}+n_{\gamma}r_{,\beta}r_{,\alpha}\right) \\ &+ \left.\left(1-2v\right)\left(2n_{\alpha}r_{,\beta}r_{,\gamma}+n_{\gamma}\delta_{\beta\alpha}+n_{\beta}\delta_{\gamma\alpha}\right)-\left(1-4v\right)n_{\alpha}\delta_{\beta\gamma}\right\} \end{aligned} \tag{4.16}$$

4.5 Boundary element discretization

In order to solve the integral equation (4.13), the boundary will be discretized into a series of elements over which displacements and tractions are written in terms of their values at a

series of nodal points. In this way, a system of algebraic equations is obtained and consequently an approximated solution to the boundary value problem is obtained (see Brebbia and Dominguez, 1989).

In matrix form, the displacement, u_α, and the traction vector, t_α at any point on the boundary Γ_e can be written as:

$$\mathbf{u} = \mathbf{\Phi}\mathbf{u}^j \tag{4.17}$$

$$\mathbf{t} = \mathbf{\Phi}\mathbf{t}^j \tag{4.18}$$

where the interpolation function matrix $\mathbf{\Phi}$ is an array $2 \times$ ND array of shape functions:

$$\mathbf{\Phi} = \begin{bmatrix} \phi_1 & 0 & \phi_2 & 0 & \phi_3 & 0 \\ 0 & \phi_1 & 0 & \phi_2 & 0 & \phi_3 \end{bmatrix} \tag{4.19}$$

The body forces at any point on the domain Ω can also be expressed in a vector form. The fundamental solution coefficients can be expressed as,

$$\mathbf{T} = \begin{bmatrix} T_{11} & T_{12} \\ T_{21} & T_{22} \end{bmatrix} \tag{4.20}$$

and,

$$\mathbf{U} = \begin{bmatrix} U_{11} & U_{12} \\ U_{21} & U_{22} \end{bmatrix} \tag{4.21}$$

With this notation, equation (4.13) can be written as follows:

$$c\left(\mathbf{x}'\right)\mathbf{u}\left(\mathbf{x}'\right) + \int_\Gamma \mathbf{T}\left(\mathbf{x}', \mathbf{x}\right)\mathbf{u}d\Gamma = \int_\Gamma \mathbf{U}\left(\mathbf{x}', \mathbf{x}\right)\mathbf{t}d\Gamma + \frac{1}{h}\int_\Omega \mathbf{U}\left(\mathbf{x}', \mathbf{x}\right)\mathbf{f}dA \tag{4.22}$$

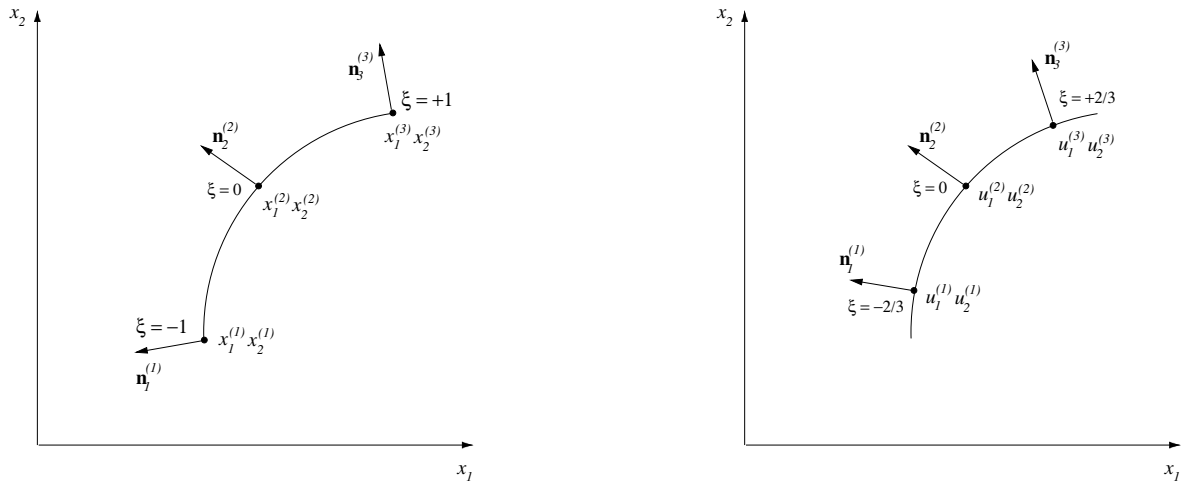

Figure 4.2: Continuous and dis-continuous quadratic elements

Discretizing the boundary, we obtaining the following equation for a nodal point:

$$c\left(\mathbf{x}'\right)\mathbf{u}\left(\mathbf{x}'\right)+\sum_{j=1}^{NE}\left\{\int_{\Gamma_j}\mathbf{T}\left(\mathbf{x}',\mathbf{x}\right)\mathbf{\Phi}d\Gamma\right\}\mathbf{u}^j = \sum_{j=1}^{NE}\left\{\int_{\Gamma_j}\mathbf{U}\left(\mathbf{x}',\mathbf{x}\right)\mathbf{\Phi}d\Gamma\right\}\mathbf{t}^j + \sum_{s=1}^{M}\left\{\frac{1}{h}\int_{A_s}\mathbf{U}\left(\mathbf{x}',\mathbf{x}\right)\mathbf{f}dA\right\} \tag{4.23}$$

where NE is the number of element on the boundary and Γ_j is the domain of j element, $\mathbf{u^j}$ and $\mathbf{t^j}$ are the nodal displacements and tractions, respectively, in the element j.

In equation (4.22) the body force integral has been treated using the cell method where the domain was divided into M internal cells over which these integral forces are computed.

4.6 Spatial integration

In this work, quadratic continuous and discontinuous interpolation functions (shape functions) are used (see figure 4.2). Continuous functions are used to modeling the geometry,

and discontinuous functions are used to approximate the displacement and traction fields at the boundary elements. Typically:

$$\mathbf{u} = \left\{ \begin{array}{c} u_1 \\ u_2 \end{array} \right\} = \left[\begin{array}{cccccc} \phi_1 & 0 & \phi_2 & 0 & \phi_3 & 0 \\ 0 & \phi_1 & 0 & \phi_2 & 0 & \phi_1 \end{array} \right] \left\{ \begin{array}{c} u_1^{(1)} \\ u_2^{(1)} \\ u_1^{(2)} \\ u_2^{(2)} \\ u_1^{(3)} \\ u_2^{(3)} \end{array} \right\} = \mathbf{\Phi u}^{(j)} \tag{4.24}$$

$$\mathbf{t} = \left\{ \begin{array}{c} t_1 \\ t_2 \end{array} \right\} = \left[\begin{array}{cccccc} \phi_1 & 0 & \phi_2 & 0 & \phi_3 & 0 \\ 0 & \phi_1 & 0 & \phi_2 & 0 & \phi_1 \end{array} \right] \left\{ \begin{array}{c} t_1^{(1)} \\ t_2^{(1)} \\ t_1^{(2)} \\ t_2^{(2)} \\ t_1^{(3)} \\ t_2^{(3)} \end{array} \right\} = \mathbf{\Phi t}^{(j)} \tag{4.25}$$

where discontinuous shape functions $\phi^{(i)}$ are given by:

$$\phi_1 = \frac{3}{4}\xi\left(\frac{3}{2}\xi - 1\right) \tag{4.26}$$

$$\phi_2 = \left(1 - \frac{3}{2}\xi\right)\left(1 + \frac{3}{2}\xi\right) \tag{4.27}$$

$$\phi_1 = \frac{3}{4}\xi\left(\frac{3}{2}\xi + 1\right) \tag{4.28}$$

Here ξ is a parametric coordinate. Geometry is represented by continuous quadratic elements as (figure 4.2):

$$\mathbf{x} = \left\{ \begin{array}{c} x_1 \\ x_2 \end{array} \right\} = \left[\begin{array}{cccccc} \psi_1 & 0 & \psi_2 & 0 & \psi_3 & 0 \\ 0 & \psi_1 & 0 & \psi_2 & 0 & \psi_3 \end{array} \right] \left\{ \begin{array}{c} x_1^{(1)} \\ x_2^{(1)} \\ x_1^{(2)} \\ x_2^{(2)} \\ x_1^{(3)} \\ x_2^{(3)} \end{array} \right\} = \mathbf{\Phi} \mathbf{x}^{(j)} \tag{4.29}$$

where:

$$\psi_1 = \frac{1}{2}\xi\left(\xi - 1\right) \tag{4.30}$$

$$\psi_2 = \left(1 - \xi\right)\left(1 + \xi\right) \tag{4.31}$$

$$\psi_3 = \frac{1}{2}\xi\left(\xi + 1\right) \tag{4.32}$$

In this way, boundary integrals in equation (4.22) can be written as:

$$\begin{aligned} \mathbf{c}\left(\mathbf{x}'\right)\mathbf{u}\left(\mathbf{x}'\right) + \sum_{j=1}^{NE}\left\{\int_{\Gamma_j}\mathbf{T}\left(\mathbf{x}', \mathbf{x}\right)\mathbf{\Phi}\left|\mathbf{J}\right|d\xi\right\}\mathbf{u}^j &= \sum_{j=1}^{NE}\left\{\int_{\Gamma_j}\mathbf{U}\left(\mathbf{x}', \mathbf{x}\right)\mathbf{\Phi}\left|\mathbf{J}\right|d\xi\right\}\mathbf{t}^j \\ &+ \frac{1}{h}\sum_{s=1}^{M}\left\{\int_{A_s}\mathbf{U}\left(\mathbf{x}', \mathbf{x}\right)\mathbf{b}\left|\mathbf{G}\right|d\xi d\eta\right\} \end{aligned} \tag{4.33}$$

where $|\mathbf{J}|$ is the modulus of Jacobian matrix for a uni-dimensional transformation:

$$\left|\mathbf{J}\right| = \frac{d\Gamma}{d\xi} = \left\{\left(\frac{dx_1}{d\xi}\right)^2 + \left(\frac{dx_2}{d\xi}\right)^2\right\}^{1/2} \tag{4.34}$$

And $|\mathbf{G}|$ is the modulus of Jacobian matrix for a bi-dimensional transformation:

$$|\mathbf{G}| = \frac{\partial x_1}{\partial \xi}\frac{\partial x_2}{\partial \eta} - \frac{\partial x_2}{\partial \xi}\frac{\partial x_1}{\partial \eta} \tag{4.35}$$

Applying numerical integration to the above formula we obtains:

$$\begin{aligned} \mathbf{c}\left(\mathbf{x}'\right)\mathbf{u}\left(\mathbf{x}'\right) &+ \sum_{j=1}^{NE}\left\{\sum_{k=1}^{NG} w_k \left(\mathbf{T}\left(\mathbf{x}',\mathbf{x}\right)\mathbf{\Psi}\right)_k |\mathbf{J}|\right\}\mathbf{u}^j \\ &= \sum_{j=1}^{NE}\left\{\sum_{k=1}^{NG} w_k \left(\mathbf{U}\left(\mathbf{x}',\mathbf{x}\right)\mathbf{\Psi}\right)_k |\mathbf{J}|\right\}\mathbf{t}^j \\ &+ \frac{1}{h}\sum_{s=1}^{M}\left\{\sum_{p=1}^{NG} w_p \left(\mathbf{U}\left(\mathbf{x}',\mathbf{x}\right)\mathbf{\Psi}\right)_p |\mathbf{G}|\right\} \end{aligned} \tag{4.36}$$

where NG is the number of integration points on the element and w_k are the weight at those points. This equation correspond to a particular node and once integrated can be written as:

$$\mathbf{c}\left(\mathbf{x}'\right)\mathbf{u}\left(\mathbf{x}'\right) + \sum_{j=1}^{N}\hat{\mathbf{H}}^{ij}\mathbf{u}^j = \sum_{j=1}^{N}\hat{\mathbf{G}}^{ij}\mathbf{t}^j + \sum_{s=1}^{M}\mathbf{B}^{is} \tag{4.37}$$

where N is the number of nodes, $\mathbf{u}^j$ and $\mathbf{t}^j$ are the displacements and tractions at node j. The influence matrices $\mathbf{H}$ and $\mathbf{G}$ are:

$$\hat{\mathbf{H}}^{ij} = \sum_t \int_{\Gamma_t} \mathbf{U}\left(\mathbf{x}',\mathbf{x}\right)\mathbf{\Psi}_q d\Gamma \tag{4.38}$$

$$\mathbf{G}^{ij} = \sum_t \int_{\Gamma_t} \mathbf{T}\left(\mathbf{x}',\mathbf{x}\right)\mathbf{\Psi}_q d\Gamma \tag{4.39}$$

where the summation extends to all the elements to which node j belongs and q is the number of order of the node j within element t. Additionally:

$$\mathbf{B}^{is} = \frac{1}{h}\int_{\Omega_s} \mathbf{U}\left(\mathbf{x}',\mathbf{x}\right)\mathbf{f} dA \tag{4.40}$$

Calling $\mathbf{H}^{ij} = \hat{\mathbf{H}}^{ij}$ if $i \neq j$ and $\mathbf{H}^{ij} = \hat{\mathbf{H}}^{ij} + \mathbf{c}\left(\mathbf{x}'\right)$ if $i = j$, equation (4.37) becomes,

$$\sum_{j=1}^{N} \mathbf{H}^{ij}\mathbf{u}^{j} = \sum_{j=1}^{N} \mathbf{G}^{ij}\mathbf{t}^{j} + \sum_{s=1}^{M} \mathbf{B}^{is} \tag{4.41}$$

The contribution for all i nodes can be written together in matrix form to give the global system equations:

$$\mathbf{Hu} = \mathbf{Gt} + \mathbf{B} \tag{4.42}$$

Vectors $\mathbf{u}$ and $\mathbf{t}$ represent all values of displacements and tractions before applying boundary conditions.

Singular integrals with order $O(ln\ r)$ are evaluated using Logarithmic quadrature developed by Stroud and Secrest, 1996. According to this method, terms that includes logarithmic singularities can be integrated by:

$$I = \int_{0}^{1} \ln\left(\frac{1}{\xi}\right) f\left(\xi\right) d\xi \cong \sum_{i=1}^{NG} w_i f\left(\xi\right) \tag{4.43}$$

Integration points ξ_i and the weights can be found in the literature. Strong singularity with order $O(1/r)$ are threated using rigid body considerations.

4.7 Numerical examples

4.7.1 Isotropic plate with central square hole

A 1.4 m x 1.4 m square plate with a central square hole of 0.1 m x 0.1 m is loaded at boundary with a uniform traction load of 0.1 MPa. Considering the symmetry of the plate, only one-quarter of its geometry will be discretized as shown in figure 4.3. The Young modulus and Poisson coefficient are $E = 210$ MPa and $v = 0.33$. The thickness of the plate is 0.01 m.

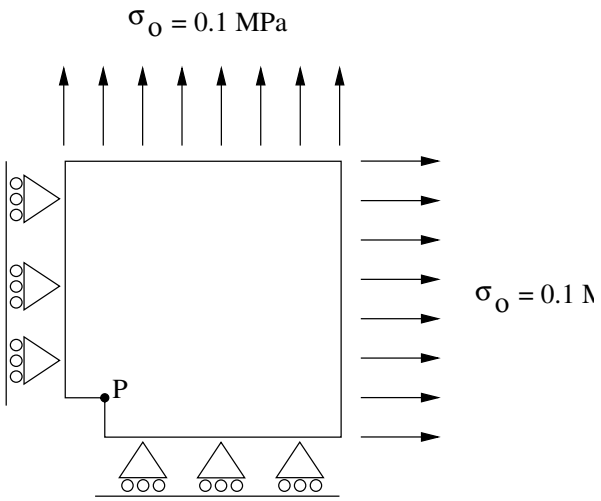

Figure 4.3: Isotropic plate with square hole under uniform traction load

Verification of the results consist to compare the displacements obtained with BEM model with those encountered using a finite element model of the plate. The norm of error proposed to compare the numerical solutions is given by:

$$\|u_{BEM} - u_{FEM}\| = \left(\int_{\Omega} |u_{BEM} - u_{FEM}|^2 \, d\Omega \right)^{1/2} \tag{4.44}$$

Figure 4.4 shows the BEM model proposed for the analysis. A convergence analysis was performed varing the number of boundary element between 5 and 43. In this way the number of nodes at boundary variated between 15 and 129.

The number of elements was uniform distributed along the edges of the plate. Figure 4.5 shows the variation in the norm of error given by equation (4.44) for total displacements as function of number of boundary nodes. Rapid convergence for displacements is obtained as figure shown. The difference in displacements using the BEM model and the FEM model was error less than 0.1% reached with 100 nodes.

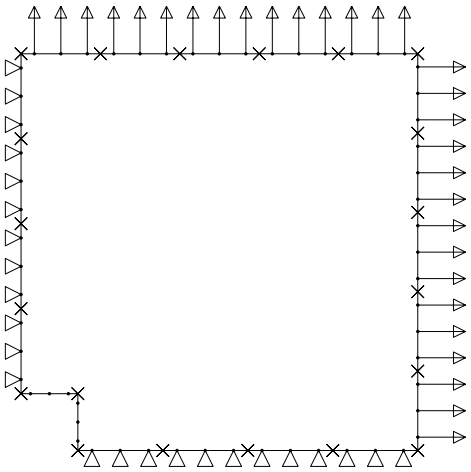

Figure 4.4: Boundary element model of square plate with central hole

Figure (4.6) shows the distribution of total displacement in the domain of the plate. For this, a uniform internal points was distributed in the domain. The components of displacements have been calculated using equation (4.36). A calculation of internal stresses can be performed using a discretizated version of equation (4.14), but is not presented here.

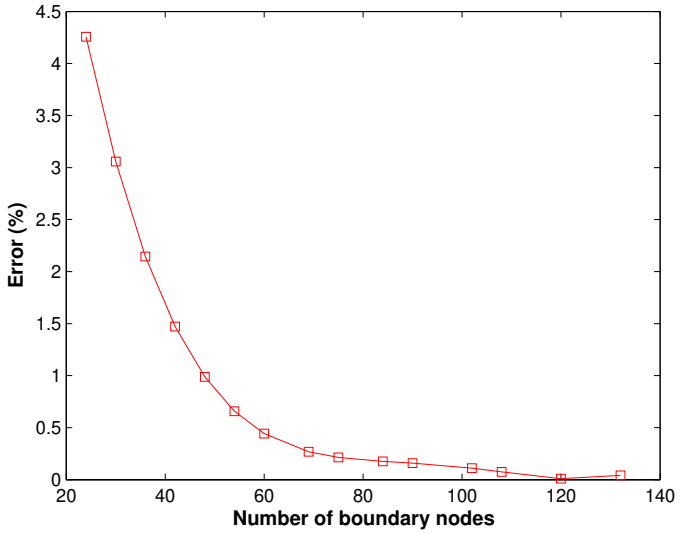

Figure 4.5: Convergence analysis for displacements

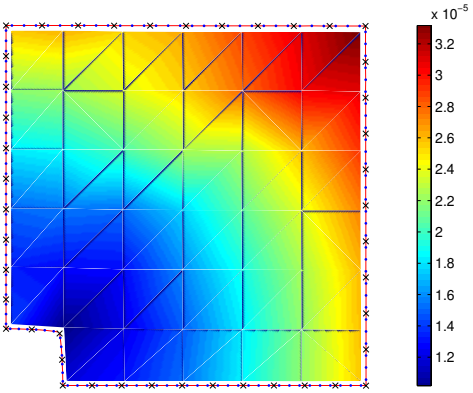

Figure 4.6: Total displacement distribution at plate domain

4.7.2 Orthotropic square plate with circular hole

A square orthotropic plate with edges of 0.4 m containing a circular hole with radius of 0.1 m, loaded with a traction of 100 MPa, is considered now. The mechanical properties are: E_1 = 220 GPa, E_2 = 118 Gpa, G_{12} = 77GPa and v_{12} = 0.4286. The thickness of the plate is 0.001 m. Again, symmetry considerations has been applied.

This problem is analyzed using the MATLAB program named '*composite*' developed by Albuquerque, 2001. This program performs static and dynamic two-dimensional analysis of composite plates and has been used to model the in-plane static response of composite patches in this work. Various papers reporting the performance of this program can be found in the literature (see: Albuquerque and Sollero, 1998; Albuquerque et al., 1999; Albuquerque et al., 1999). A total of 21 boundary elements were used and 160 internal points were used to calculate internal displacements and stresses were used. As representative numerical results, the stress distribution in direction y is showed in figure 4.7. Good agreement with the theoretical values for the stresses are obtained when comparing this results with that reported in literature (see Albuquerque, 2001).

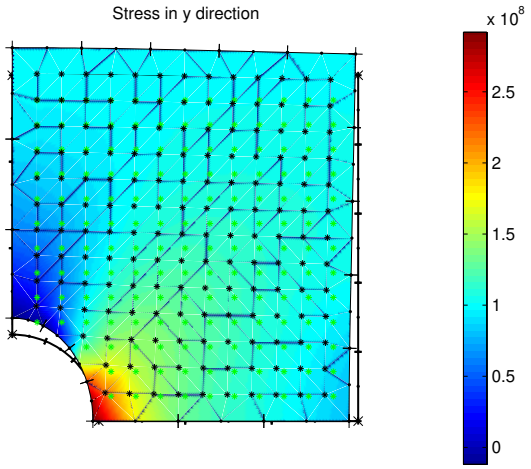

Figure 4.7: Normal stress distribution in y-axis direction

4.8 Conclusions

The displacement boundary integral formulation of two-dimensional equilibrium equations was presented. The discretizated version of this formulation is obtained from the boundary element method applied to plane-stress elastostatics problems. The integral equation for internal stresses has been obtained differentiating the displacement boundary integral formulation with respect to spacial variables. Continuous and discontinuous quadratic boundary elements were used to approximate the boundary geometry and to interpolate the displacements and traction fields in the boundary elements. Numerical results showing a representative plane-stress problems were presented and their numerical results were analyzed. Good agreement of results is obtained when compared with results from finite element models and those reported in literature.

Chapter 5

Boundary element formulation for Reissner plates

5.1 Introduction

This chapter presents the direct boundary element formulation of isotropic Reissner plates. The Reissner plate theory and governing equations for shear deformable plates are presented. Based in these equations, the boundary integral formulation is developed. Fundamental solutions, developed by Vander Weeën, 1982, for displacements and tractions for infinite elastic plane under transversal loads and in-plane bending moments are presented. Boundary element method is applied to discretizate the integral boundary equation. Procedures for treatment of the singular integrals are showed. Finally, numerical examples are showed and results are discussed. Preliminary conclusions are established.

5.2 Reissner plate theory

Both, the Kirchhoff's plate theory and the Reissner/Mindlin shear deformable plates theory are based on the following assumptions:

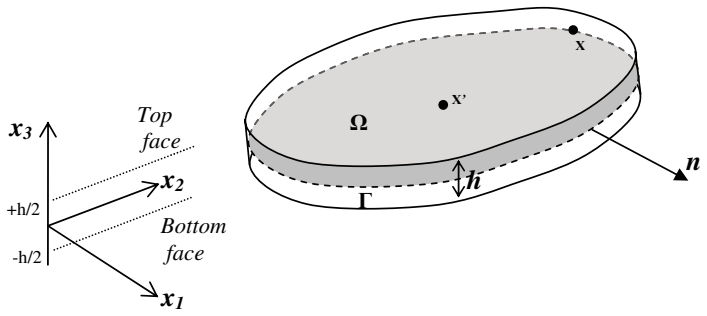

Figure 5.1: Thick plate geometry

- Plane section remains plane after the deformation, which implies the transverse normal strains are zeros.

- The displacements are small enough for changes in geometry to be negligible.

Therefore, the theory of plates can be regarded as an extension of small strain theory of elasticity, in particular, plane stress problems (see Dirgantara, 2000).

Plate theories are mainly simplified two-dimensional model of the original three-dimensional structure. The basic idea of the plate theories in general is to assume either stress distribution through the thickness as in the stress-based theories (such as the Reissner theory) or to assume displacement distribution through the thickness as in the displacement-based theories (such as Kirchhoff theory).

5.2.1 Internal stress resultants

Consider an arbitrary plate of thickness, h, as shown in figure 5.1 with a domain Ω and boundary Γ in the x_i space. The $x_1 - x_2$ plane is assumed to be located at the middle surface $x_3 = 0$. The generalized displacements are denoted as w_i, where w_α denotes rotations (ϕ_{x1} and ϕ_{x2}) and w_3 denotes the transverse deflection w (see Rashed, 1999).

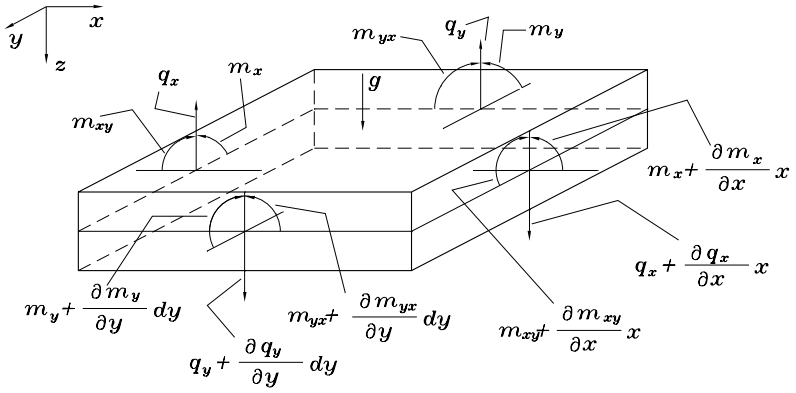

Figure 5.2: Equilibrium of differential plate element

The stress resultants at any internal point $\mathbf{x}' \in \Omega$ which are the bending moments $M_{\alpha\beta}$ and the shearing forces Q_α can be defined as follows:

$$M_{\alpha\beta} = \int_{-h/2}^{h/2} x_3 \sigma_{\alpha\beta} dx_3 \tag{5.1}$$

$$Q_\alpha = \int_{-h/2}^{h/2} x_3 \sigma_{\alpha 3} dx_3 \tag{5.2}$$

with $\alpha, \beta = 1, 2$. $\sigma_{\alpha\beta}$ are the three-dimensional components of the normal stresses through the plate thickness and $\sigma_{\alpha 3}$ are the components of the transverse shear stresses. The generalized tractions at a boundary point $\mathbf{x} \in \Gamma$ can be defined as:

$$\begin{aligned} q_\alpha &= M_{\alpha\beta} n_\beta \\ q_3 &= Q_\alpha n_\alpha \end{aligned} \tag{5.3}$$

where n_β are the components of the outward normal vector to the plate boundary Γ.

5.2.2 Equilibrium equations

The equilibrium equations can be formed by considering the equilibrium of a typical differential element shown in figure 5.2. This element has dimensions of $dx_1 \times dx_2 \times h$ and under uniform load q (per unit area), as regarded positive when applied in the x_3 direction. The equilibrium of moments about the x_1 and x_2 coordinate axis and the equilibrium of forces in the x_3 direction can be written as follows:

$$\frac{\partial M_{11}}{\partial x_1} + \frac{\partial M_{21}}{\partial x_2} - Q_1 = 0 \tag{5.4}$$

$$\frac{\partial M_{22}}{\partial x_2} + \frac{\partial M_{12}}{\partial x_1} - Q_2 = 0 \tag{5.5}$$

$$\frac{\partial Q_1}{\partial x_1} + \frac{\partial Q_2}{\partial x_2} + q = 0 \tag{5.6}$$

$$\frac{\partial Q_2}{\partial x_1} + \frac{\partial Q_1}{\partial x_2} + q = 0 \tag{5.7}$$

$$\tag{5.8}$$

These equations represent the governing equations in the differential form. It has to be noted that they contain five unknows, however they are three equations. The required additional equations to define the problem will be setup via the stress-displacement relationships and the application of suitable boundary conditions.

5.2.3 Stress resultant-strain relationships

For shear deformable plate bending, the normal stresses due to bending and twisting moments $\sigma_{\alpha\beta}$ vary linearly and the transverse shear stresses $\sigma_{\alpha 3}$ vary parabolically over the thickness.

Hence the stress components can be expressed via the following relationships:

$$\sigma_{\alpha\beta} = \frac{12x_3}{h^3} M_{\alpha\beta} \tag{5.9}$$

$$\sigma_{\alpha 3} = \frac{3}{2h}\left[1 - \left(\frac{2x_3}{h}\right)^2\right] Q_\alpha \tag{5.10}$$

The stress resultant-strain relationships are derived using the basic minimum principle for the stresses as presented in Reissner, 1947. The resultant tensor moment $M_{\alpha\beta}$ and the normal shear vector Q_α are given by:

$$M_{\alpha\beta} = D\frac{1-v}{2}\left(2\chi_{\alpha\beta} + \frac{2v}{1-v}\chi_{\gamma\gamma}\delta_{\alpha\beta}\right) \tag{5.11}$$

$$Q_\alpha = \frac{1-v}{2}\lambda^2\psi_\alpha \tag{5.12}$$

where:

$$\begin{aligned} 2\chi_{\alpha\beta} &= w_{\alpha,\beta} + w_{\beta,\alpha} \\ \psi_\alpha &= w_\alpha + w_{3,\alpha} \end{aligned} \tag{5.13}$$

where $\chi_{\alpha\beta}$ is the curvature tensor and ψ_α are the transversal shear strains. Equation (5.12) represents the generalized Hooke's law. This equation together with equation (5.13) presents the stress-resultant-displacement relationships. Constants C_s, C_n and D are given by:

$$D = \frac{Eh^3}{12\left(1-v^2\right)} \tag{5.14}$$

$$C_n = \frac{5}{6}\frac{Eh}{v} \tag{5.15}$$

$$C_s = \frac{5}{6}Gh \tag{5.16}$$

Replacing these constants into equation (5.12) we obtain:

$$\begin{aligned} M_{\alpha\beta} &= D\frac{1-v}{2}\left(w_{\alpha,\beta}+w_{\beta,\alpha}+\frac{2v}{1-v}w_{\gamma,\gamma}\delta_{\alpha\beta}\right)+\frac{vq}{(1-v)\,\lambda^2}\delta_{\alpha\beta} \\ Q_\alpha &= D\frac{1-v}{2}\lambda^2\left(w_\alpha+w_{3,\alpha}\right) \end{aligned} \tag{5.17}$$

where $D = Eh^3/12(1-v^2)$ is the *flexural rigity* of the plate and $\lambda = \sqrt{10}$ is called the *shear factor*.

5.3 Governing equations

The generalized governing equations for Reissner plates (*Naiver equations*)can be formed by substituting equation (5.17) into the equilibrium equations (5.8) to give:

$$D\nabla^2 w_1 + \frac{D}{2}(1+v)\frac{\partial}{\partial x_2}(-\frac{\partial w_1}{\partial x_2}+\frac{\partial w_2}{\partial x_1}) - Cw_1 - C\frac{\partial w_3}{\partial x_1} = 0 \tag{5.18}$$

$$\frac{D}{2}(1+v)\frac{\partial}{\partial x_1}(-\frac{\partial w_1}{\partial x_2}+\frac{\partial w_2}{\partial x_1}) + D\nabla^2 w_2 - Cw_2 - C\frac{\partial w_3}{\partial x_2} = 0 \tag{5.19}$$

$$C\nabla^2 w_3 + C\frac{\partial w_1}{\partial x_1} + C\frac{\partial w_2}{\partial x_2} + q_3 = 0 \tag{5.20}$$

$$B\nabla^2 u_1 + \frac{B}{2}(1+v)\frac{\partial}{\partial x_2}(-\frac{\partial u_1}{\partial x_2}+\frac{\partial u_2}{\partial x_1}) + q_1 = 0 \tag{5.21}$$

where $C = D(1-v)/2\lambda^2$.

5.4 Boundary integral formulation

The integral equation can be derived by considering the integral representation of the governing equations (5.8) via the following integral identity:

$$\int_{\Omega} \left[\left(M_{\alpha\beta,\beta} - Q_{\alpha} \right) W_{\alpha}^{*} + \left(Q_{\alpha,\alpha} + q \right) W_{3}^{*} \right] d\Omega = 0 \tag{5.22}$$

where W_i^* $(i = \alpha, 3)$ are weighting functions. Integrating by parts and making use of the relationships in equation (5.3), it gives:

$$\int_{\Gamma} p_j W_j^* d\Gamma + \int_{\Omega} q W_3^* d\Omega + \int_{\Omega} Q_{\alpha} \left(W_{\alpha}^{*} + W_{3,\alpha}^{*} \right) d\Omega + \int_{\Omega} M_{\alpha\beta} W_{\alpha,\beta}^{*} d\Omega = 0 \tag{5.23}$$

where $j = \alpha, 3$. Replace the stress resultants ($M_{\alpha\beta}$ and Q_{α}) with the generalized displacements and its derivatives using equation (5.17) and applying the Green's second identity for the $M_{\alpha}\beta$ integral gives:

$$\begin{aligned} \int_{\Gamma} p_j W_j^* d\Gamma \;+\; & \int_{\Omega} Q_{\alpha} \left(w_{\alpha} + w_{3,\alpha} \right) d\Omega \\ - \; & \int_{\Gamma} W_{\alpha,\beta}^{*} \left\{ \frac{D\left(1-v\right)}{2} \left(w_{\alpha} n_{\beta} + w_{\beta} n_{\alpha} + \frac{2v}{\left(1-v\right)} w_{\gamma} n_{\gamma} \delta_{\alpha\beta} \right) \right\} d\Gamma \\ - \; & \int_{\Gamma} \frac{D\left(1-v\right)}{2} \left(w_{\alpha} W_{\alpha,\beta\beta}^{*} + w_{\beta} W_{\alpha,\beta\alpha}^{*} + \frac{2v}{\left(1-v\right)} w_{\gamma} W_{\alpha,\beta\gamma}^{*} \delta_{\alpha\beta} \right) d\Gamma \\ + \; & \int_{\Omega} \left[q W_3^* + \frac{vq}{\left(1-v\right)\lambda^2} \delta_{\alpha\beta} W_{\alpha,\beta}^{*} \right] d\Omega \end{aligned} \tag{5.24}$$

The second integral on the left hand side of above equation can be decomposed using Green's second identity and making use of the relationships in equation (5.3) as follows:

$$\int_{\Omega} Q_{\alpha} \left(w_{\alpha} + w_{3,\alpha} \right) d\Omega = \int_{\Gamma} p_3 w_3 d\Gamma + \int_{\Omega} \left(Q_{\alpha}^{*} w_{\alpha} - Q_{\alpha,\alpha}^{*} w_3 \right) d\Omega \tag{5.25}$$

Substituting this equation into last equation and grouping it gives:

$$\begin{aligned}\int_{\Gamma}\left(W_j^* p_j - P_j^* w_j\right) d\Gamma \;&+\; \int_{\Omega}\left[W_3^* + \frac{v}{(1-v)\,\lambda^2} W_{\theta,\theta}^*\right] q d\Omega \\ &+\; \int_{\Omega}\left[\left(M_{\alpha\beta,\beta}^* - Q_{\alpha}^*\right) w_{\alpha} + Q_{\alpha,\alpha}^* w_3\right] d\Omega = 0 \end{aligned} \tag{5.26}$$

This equation represents a generalized Betti's reciprocal theorem for Reissner plates; It has to be noted that the weighting functions can be chosen to represents arbitrarily state. This state is defined for concentrated generalized loads: two bending moments ($i = \alpha = 1, 2$) and one concentrated shear force ($i = 3$) at an arbitrary point $\mathbf{x}' \in \Omega$. Then equation (5.26) can be rewritten after introducing the direction of the load i as follows:

$$\begin{aligned}\int_{\Gamma} W_{ij}^*(\mathbf{x}', \mathbf{x})\, p_j(\mathbf{x})\, d\Gamma \;&-\; \int_{\Gamma} P_{ij}^*(\mathbf{x}', \mathbf{x})\, w_j(\mathbf{x})\, d\Gamma \\ &+\; \int_{\Omega}\left[W_{i3}^*(\mathbf{x}', \mathbf{x}) + \frac{v}{(1-v)\,\lambda^2} W_{i\theta,\theta}^*(\mathbf{x}', \mathbf{x})\right] q d\Omega \\ &+\; \int_{\Omega}\left[\left(M_{i\alpha\beta,\beta}^*(\mathbf{x}', \mathbf{x}) - Q_{i\alpha}^*(\mathbf{x}', \mathbf{x})\right)\right] w_{\alpha}(\mathbf{x})\, d\Omega \\ &+\; \int_{\Omega} Q_{i\alpha,\alpha}^*(\mathbf{x}', \mathbf{x})\, w_3(\mathbf{x})\, d\Omega \end{aligned} \tag{5.27}$$

By choosing the weighting function as:

$$\begin{aligned} M_{i\alpha\beta,\beta}^*(\mathbf{x}', \mathbf{x}) - Q_{i\alpha}^*(\mathbf{x}', \mathbf{x}) &= -\delta(\mathbf{x}', \mathbf{x})\, \delta_{i\alpha} \\ Q_{i\alpha,\alpha}^*(\mathbf{x}', \mathbf{x}) &= -\delta(\mathbf{x}', \mathbf{x})\, \delta_{i3} \end{aligned} \tag{5.28}$$

and making use of the Dirac delta property:

$$\int_{\Omega} \delta(\mathbf{x}', \mathbf{x})\, w_i(\mathbf{x})\, d\Omega = w_i(\mathbf{x}') \tag{5.29}$$

then equation (5.27) can be written for an internal source point **x'** as:

$$\begin{aligned} w_j(\mathbf{x}') &+ \int_\Gamma P^*_{ij}(\mathbf{x}',\mathbf{x})\, w_j(\mathbf{x})\, d\Gamma = \int_\Gamma W^*_{ij}(\mathbf{x}',\mathbf{x})\, p_j(\mathbf{x})\, d\Gamma \\ &+ \int_\Omega \left(W^*_{i3}(\mathbf{x}',\mathbf{x}) - \frac{v}{(1-v)\,\lambda^2} W^*_{i\alpha,\alpha}(\mathbf{x}',\mathbf{x}) \right) q(\mathbf{x})\, d\Omega \end{aligned} \tag{5.30}$$

where $W^*_{ij}(\mathbf{x}',\mathbf{x})$ and $P^*_{ij}(\mathbf{x}',\mathbf{x})$ are the two-point fundamental solution kernels for the displacements and the tractions respectively. It represents the displacement or the tractions at the point $\mathbf{x}$ in the direction j due to unit load applied at $\mathbf{x}'$ at the direction i. The expressions for these kernels are given by Vander Weeën, 1982 as follows:

$$\begin{aligned} W^*_{\alpha\beta} &= \frac{1}{8\pi D(1-v)} \left\{ \left[8B(z) - (1-v)(2\ln(z)-1) \right] \delta_{\alpha\beta} \right. \\ &- \left. \left[8A(z) - 2(1-v) \right] r_{,\alpha} r_{,\beta} \right\} \\ W^*_{\alpha 3} &= -W^*_{3\alpha} = \frac{1}{8\pi D} (2\ln(z)-1)\, r r_{,\alpha} \\ W^*_{\alpha\beta} &= \frac{1}{8\pi D(1-v)\lambda^2} \left[(1-v) z^2 (\ln(z)-1) - 8\ln(z) \right] \end{aligned} \tag{5.31}$$

and

$$\begin{aligned} P^*_{\alpha\beta} &= -\frac{1}{4\pi r} \left[(4A(z) + 2zK_1(z) + 1 - v)(\delta_{\alpha\gamma} r_{,n} + r_{,\alpha} n_\gamma) \right. \\ &+ \left. (4A(z) + 1 + v) r_{,\gamma} n_\alpha - 2(8A(z) + 2zK_1(z) + 1 - v) r_{,\alpha} r_{,\gamma} r_{,n} \right] \\ P^*_{\gamma 3} &= \frac{\lambda^2}{2\pi} \left[B(z)\, n_\gamma - A(z)\, r_{,\gamma} r_{,n} \right] \\ P^*_{3\alpha} &= \frac{-(1-v)}{8\pi} \left[\left(2\frac{(1+v)}{(1-v)} \ln(z) - 1 \right) n_\alpha + 2 r_{,\alpha} r_{,n} \right] \\ P^*_{33} &= \frac{-1}{2\pi r} r_{,n} \end{aligned} \tag{5.32}$$

where

$$A(z) = K_0(z) + \frac{2}{z}\left[K_1(z) - \frac{1}{z} \right] \tag{5.33}$$

$$B(z) = K_0(z) + \frac{1}{z}\left[K_1(z) - \frac{1}{z}\right] \tag{5.34}$$

in which $K_0(z)$ and $K_1(z)$ are modified Bessel functions, $z = \lambda r$, r is the absolute distance between the source and the field points, $r_{,\alpha} = r_\alpha / r$ where $r_\alpha = x_\alpha(\mathbf{x}) - x_\alpha(\mathbf{x}')$ and $r_{,n} = r_{,\alpha} n_\alpha$. Equation (5.30) represents the generalized Somigliana's identity for Reissner plates. As can be demonstrate, $A(z)$ is a smooth function, whereas $B(z)$ is a weakly singular $O(ln(r))$. Therefore W^*_{ij} is a weakly singular and P^*_{ij} has a strong (Cauchy principal value) singularity $O(1/r)$.

In other hands, by taking the point $\mathbf{x}'$ to the boundary at the position $\mathbf{x}' \in \Gamma$, and assuming that the displacements w_i satisfy Hölder continuity, equation (5.30) can be written as follows:

$$\begin{aligned} c_{ij}(\mathbf{x}')\, w_j(\mathbf{x}') + \int_\Gamma P^*_{ij}(\mathbf{x}', \mathbf{x})\, w_j(\mathbf{x}')\, d\Gamma = \int_\Gamma W^*_{ij}(\mathbf{x}', \mathbf{x})\, p_j(\mathbf{x}')\, d\Gamma \\ + \int_\Omega \left(W^*_{i3}(\mathbf{x}', \mathbf{x}) - \frac{v}{(1-v)\,\lambda^2} W^*_{i\alpha,\alpha}(\mathbf{x}', \mathbf{x}) \right) q\, d\Omega \end{aligned} \tag{5.35}$$

Integral at left hand side is a Cauchy principal value integral; $\mathbf{x}', \mathbf{x} \in \mathbf{\Gamma}$ are source and field points respectively, and $c_{ij}(\mathbf{x}')$ are the jump terms arising from the terms of $O(1/r)$ in the kernel P^*_{ij}. Equation (5.35) represent three integral equations (two (i=1, 2) for rotations and one ($i = 3$) for deflection).

The domain integral in equation (5.35) can be transferred to the boundary (by applying the divergence theorem), in the case of a uniform load (q = constant) to give:

$$\int_\Omega \left(W^*_{i3}(\mathbf{x}', \mathbf{x}) - \frac{v}{(1-v)\,\lambda^2} W^*_{i\alpha,\alpha}(\mathbf{x}', \mathbf{x}) \right) q\, d\Omega =$$

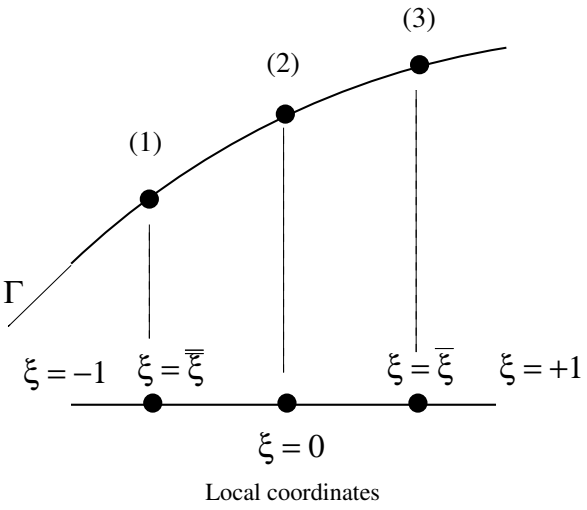

Figure 5.3: General quadratic element

$$q \int_{\Gamma} \left(V_{i,\alpha}\left(\mathbf{x}', \mathbf{x}\right) - \frac{v}{(1-v)\,\lambda^2} W^*_{i\alpha}\left(\mathbf{x}', \mathbf{x}\right) \right) n_\alpha d\Gamma \tag{5.36}$$

where V_i^* are the particular solutions of the equation $V^*_{i,\theta\theta} = W^*_{i3}$. According with Mindlin, the term: $v/((1-v)\lambda^2)$ has negligible contribution to the results. For the sake of simplicity, this term will be ignored in this work. The expressions for $V^*_{i,\beta}$ are given as follows:

$$V^*_{\alpha,\beta} = \frac{r^2}{128\pi D}\left[\left(4\ln\left(z\right)-5\right)\delta_{\alpha\beta} + 2\left(4\ln\left(z\right)-3\right) r_{,\alpha} r_{,\beta}\right] \tag{5.37}$$

$$V^*_{3,\beta} = \frac{-r r_{,\beta}}{128\pi D\,(1-v)\,\lambda^2}\left[32\left(2\ln\left(z\right)-1\right) - z^2\,(1-v)\left(4\ln\left(z\right)-5\right)\right] \tag{5.38}$$

5.5 Boundary element discretization

The analytical solution of the integral equations (5.35) is difficult even for a simple plate problem. Therefore, the numerical solution can be considered. In this work, the boundary has to be discretized into N_e elements, over which the unknows are approximated to vary quadratically using quadratic discontinuous elements.

After the discretization, equation (5.35) can be rewritten as:

$$\begin{aligned} c_{ij}\left(\mathbf{x}'\right) w_i\left(\mathbf{x}'\right) + \sum_{j=1}^{N_e}\sum_{m=1}^{3} w_j^m \int_{-1}^{+1} P_{ij}^*\left(\mathbf{x}', \mathbf{x}\left(\xi\right)\right) \Phi^m\left(\xi\right) J_j\left(\xi\right) d\xi \\ = \sum_{j=1}^{N_e}\sum_{m=1}^{3} p_j^m \int_{-1}^{+1} W_{ij}^*\left(\mathbf{x}', \mathbf{x}\left(\xi\right)\right) \Phi^m\left(\xi\right) J_j\left(\xi\right) d\xi \\ + q\sum_{j=1}^{N_e} \int_{-1}^{+1} V_{i,\alpha}^*\left(\mathbf{x}', \mathbf{x}\left(\xi\right)\right) n_\alpha\left(\xi\right) J_j\left(\xi\right) d\xi \end{aligned} \tag{5.39}$$

where J is the jacobian of the transformation and Φ is the element shape function, as presented in chapter 4. For a general quadratic element we as shown in figure 5.3 we have:

$$\Phi^1\left(\xi\right) = \frac{1}{\overline{\xi}\left(\overline{\xi} - \overline{\overline{\xi}}\right)} \xi\left(\xi - \overline{\overline{\xi}}\right) \tag{5.40}$$

$$\Phi^2\left(\xi\right) = \frac{1}{\overline{\xi}\,\overline{\overline{\xi}}} \left(\xi - \overline{\xi}\right)\left(\xi - \overline{\overline{\xi}}\right) \tag{5.41}$$

$$\Phi^3\left(\xi\right) = \frac{1}{\overline{\overline{\xi}}\left(\overline{\overline{\xi}} - \overline{\xi}\right)} \xi\left(\xi - \overline{\overline{\xi}}\right) \tag{5.42}$$

and

$$J\left(\xi\right) = \sqrt{\frac{\partial x_\theta\left(\xi\right)}{\partial \xi} \frac{\partial x_\theta\left(\xi\right)}{\partial \xi}} \tag{5.43}$$

$$n_\alpha\left(\xi\right) = \frac{1}{J\left(\xi\right)} \frac{\partial x_\beta\left(\xi\right)}{\partial \xi} \epsilon_{\alpha\beta 3} \tag{5.44}$$

where $\epsilon_{\alpha\beta 3}$ is the permutation symbol. After performing the collocation process, equation (5.44) can be written as follows:

$$\mathbf{Hw} = \mathbf{Gp} + \mathbf{Q} \tag{5.45}$$

5.6 Treatment of the singularities

The influence matrix $\mathbf{G}$ and the load vector $\mathbf{Q}$ contains weakly singular kernels, which can be canceled using a non-linear coordinate transformation (see Telles, 1987). In addition, for better numerical accuracy a suitable number of element sub-divisions (see Kane, 1994) along with the non-linear transformation will be used in this work.

The influence matrix $\underline{\mathbf{H}}$, on the other hand, contains a strongly singular kernel, which can be evaluated indirectly be expressing that the free stress problem admits non-trivial solutions which are arbitrary combinations of three basic rigid-body displacements (see Vander Weeën, 1982):

$$\begin{aligned} w_1 &= C, w_2 = 0, w_3 = -Cr_1 \\ w_1 &= 0, w_2 = C, w_3 = -Cr_1 \\ w_1 &= 0, w_2 = 0, w_3 = C \end{aligned} \tag{5.46}$$

where C is an arbitrary constant. In this way one obtains:

$$\begin{aligned} c_{i\beta}\left(\mathbf{x}'\right) &= -\int_{\Gamma}\left[P^*_{i\beta}\left(\mathbf{x}',\mathbf{x}\right) + r_\beta P_{i3}\left(\mathbf{x}',\mathbf{x}\right)\right] d\Gamma \\ c_{i3}\left(\mathbf{x}'\right) &= -\int_{\Gamma} P_{i3}\left(\mathbf{x}',\mathbf{x}\right) d\Gamma \end{aligned} \tag{5.47}$$

5.7 Internal stress resultants

The stress resultants at domain point $\mathbf{x}'$ can be evaluated from equations (5.35), by using relationships the resultant stress-displacement relationships:

$$M_{\alpha\beta}\left(\mathbf{x}'\right) = \int_{\Gamma} W^*_{\alpha\beta k}\left(\mathbf{x}',\mathbf{x}\right) p_k d\Gamma - \int_{\Gamma} P^*_{\alpha\beta k}\left(\mathbf{x}',\mathbf{x}\right) w_k d\Gamma$$

$$
\begin{aligned}
&+ \int_{\Omega} W^{*}_{\alpha\beta 3}\left(\mathbf{x}', \mathbf{x}\right) q_3 d\Omega \\
Q_{\alpha} &= \int_{\Gamma} W^{*}_{3\beta k}\left(\mathbf{x}', \mathbf{x}\right) p_k d\Gamma - \int_{\Gamma} P^{*}_{3\beta k}\left(\mathbf{x}', \mathbf{x}\right) w_k d\Gamma \\
&+ \int_{\Omega} W^{*}_{3\beta 3}\left(\mathbf{x}', \mathbf{x}\right) q_3 d\Omega
\end{aligned} \tag{5.48}
$$

In the case of a uniform load, the domain integral can be transferred to boundary integral, be applying the divergence theorem, to give:

$$
\int_{\Omega} W^{*}_{3\beta 3}\left(\mathbf{x}', \mathbf{x}\right) q_3 d\Omega = q_3 \int_{\Gamma} Q^{*}_{i\beta}\left(\mathbf{x}', \mathbf{x}\right) d\Gamma \tag{5.49}
$$

The kernels $W^{*}_{i\beta k}, P^{*}_{i\beta k}$ and $Q^{*}_{i\beta}$, are linear combination of the first derivatives of W^{*}_{ij}, P^{*}_{ij} and $V^{*}_{i,\beta}$, are given by:

$$
\begin{aligned}
W^{*}_{\alpha\beta\gamma} &= \frac{1}{4\pi r}\left[\left(4A\left(z\right) + 2zK_1\left(z\right) + 1 - v\right)\left(\delta_{\beta\gamma} r_{,\alpha} + \delta_{\alpha\gamma} r_{,\beta}\right)\right. \\
&- \left. 2\left(8A\left(z\right) + 2zK_1\left(z\right) + 1 - v\right) r_{,\alpha} r_{,\beta} r_{,\gamma} + \left(4A\left(z\right) + 2zK_1\left(z\right) + 1 - v\right)\delta_{\alpha\beta} r_{,\gamma}\right] \\
W^{*}_{\alpha\beta 3} &= \frac{-\left(1 - v\right)}{8\pi}\left[\left(2\frac{\left(1 + v\right)}{\left(1 - v\right)}\ln\left(z\right) - 1\right)\delta_{\alpha\beta} + 2 r_{,\alpha} r_{,\beta}\right] \\
W^{*}_{3\beta 3} &= \frac{1}{2\pi r} r_{,\beta}
\end{aligned}
$$

$$
\begin{aligned}
P^{*}_{\alpha\beta\gamma} &= \frac{D\left(1 - v\right)}{4\pi r^2}\left\{\left(4A\left(z\right) + 2zK_1\left(z\right) + 1 - v\right)\left(\delta_{\gamma\alpha} n_{\beta} + \delta_{\gamma\beta} n_{\alpha}\right)\right. \\
&+ \left. \left(4A\left(z\right) + 1 + 3v\right)\delta_{\alpha\beta} n_{\gamma} - \left(16A\left(z\right) + 6zK_1\left(z\right) + z^2 K_0\left(z\right) + 2 - 2v\right)\right. \\
P^{*}_{\alpha\beta 3} &= \frac{D\left(1 - v\right)\lambda^2}{4\pi r}\left[\left(2A\left(z\right) + zK_1\left(z\right)\right)\left(r_{,\beta} n_{\alpha} + r_{,\alpha} n_{\beta}\right)\right. \\
&- \left. 2\left(4A\left(z\right) + zK_1\left(z\right)\right) r_{,\alpha} r_{,\beta} r_{,n} + 2A\left(z\right)\delta_{\alpha\beta} r_{,n}\right. \\
P^{*}_{3\beta 3} &= \frac{D\left(1 - v\right)\lambda^2}{4\pi r^2}\left[\left(z^2 B\left(z\right) + 1\right) n_{\beta} - \left(z^2 A\left(z\right) + 2\right) r_{,\beta} r_{,n}\right]
\end{aligned}
$$

$$
\begin{aligned}
Q^{*}_{\alpha\beta} &= \frac{-r}{64\pi}\left\{\left(4\ln\left(z\right) - 3\right)\left[\left(1 - v\right)\left(r_{,\beta} n_{\alpha} + r_{,\alpha} n_{\beta}\right) + \left(1 + 3v\right)\delta_{\alpha\beta} r_{,n}\right]\right. \\
&+ \left. 4\left[\left(1 - v\right) r_{,\alpha} r_{,\beta} + v\delta_{\alpha\beta}\right] r_{,n}\right\}
\end{aligned}
$$

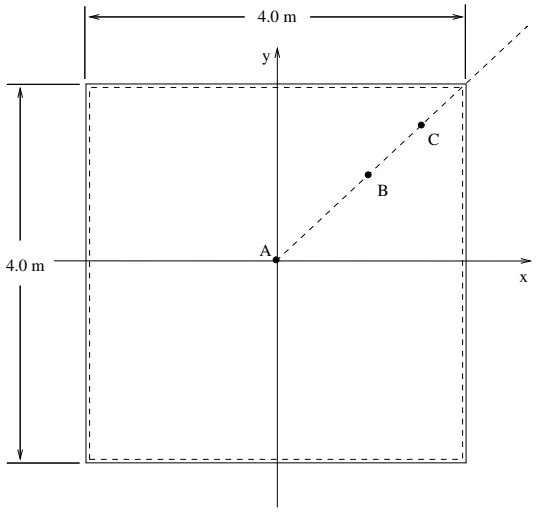

Figure 5.4: Simply supported thin plate

$$Q^*_{3\beta} = \frac{1}{8\pi}\left[\left(2\ln(z)-1\right)n_\beta + 2r_{,\beta}r_{,n}\right] \tag{5.50}$$

5.8 Numerical examples

5.8.1 Simply supported thin square plate

A clamped thick square plate of 4m side simply supported from all sides is considered (see figure 5.4). The BEM analysis is performed using the Reissner plate theory. The Young modulus was taken to be 0.1 MPa and the Poisson's ratio is 0.33. Thickness of the plate is take to be 1m. A uniform pressure of 102Pa is applied over the plate domain. Boundary plate was meshing using discontinuous quadratic boundary element. Figure 5.6 shows the BEM used for the analysis. Was found that 16 element boundary mesh generate an error of 0.02% in the internal forces when compared with analytic solution using the Kirchhoff plate theory. Figure 5.5 shows the transversal displacement component w_3 distribution. Table 5.1 presents the internal bending moments at points A, B and C. Good correlations when comparing with analytic solution are obtained.

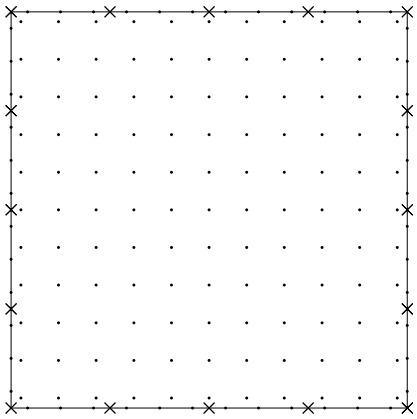

Figure 5.5: Boundary element mesh for simply supported thin plate

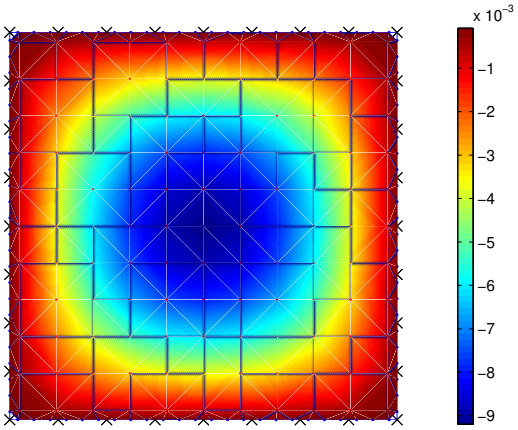

Figure 5.6: Transversal displacements for simply supported thin plate

5.8.2 Timoshenko beam

A Timoshenko beam of length 10m having a cross section of 3m depth × 1m width, showed in figure 5.7 is considered. The following material properties are considered: $\nu = 0.2$ and $E = 2 \times 10^6 t/m^2$. The beam is fixed from one end and left free as cantilever. A concentrated load of $P = 1$ ton is applied at the free end of the beam. A boundary element mesh of 20 elements

Table 5.1: Bending moments and shear forces at internal points for thin square plate

Point	$M_{11}(tf.m/m)$		$M_{12}(tf.m/m)$		$M_{22}(tf.m/m)$	
	BEM	Exact	BEM	Exact	BEM	Exact
Point A	-0.4904	-0.4905	0.0000	0.0000	-0.4905	-0.4904
Point B	-0.3766	0.3770	0.0814	0.0815	-0.3766	-0.3770
Point C	-0.1143	-0.1142	0.2521	0.2522	-0.1142	-0.1143

along the beam length and 4 elements along the beam width is used to model the beam. Figure 5.8 compares the numerical results for the beam deflection with those obtained using the using the Euler-Berboulli beam theory and the BEM solution obtained by Rashed et al., 1998.

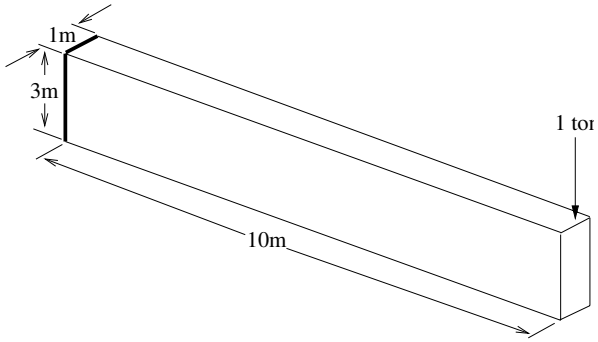

Figure 5.7: Timoshenko beam

5.9 Conclusions

The displacement boundary element method applied to analysis of isotropic shear deformable plates has been presented. Three boundary integral formulation involving three generalized displacements (two rotations and one deflection) and three generalized forces (two moments and one shear force), has been established. In addition, boundary integral equations for internal forces (bending moments and shear forces), were established. Fundamental solutions for displacements and tractions as given by Vander Weeën, 1982, are presented. Weak singular integrals integrals were threated using the Telles transformation and element subdi-

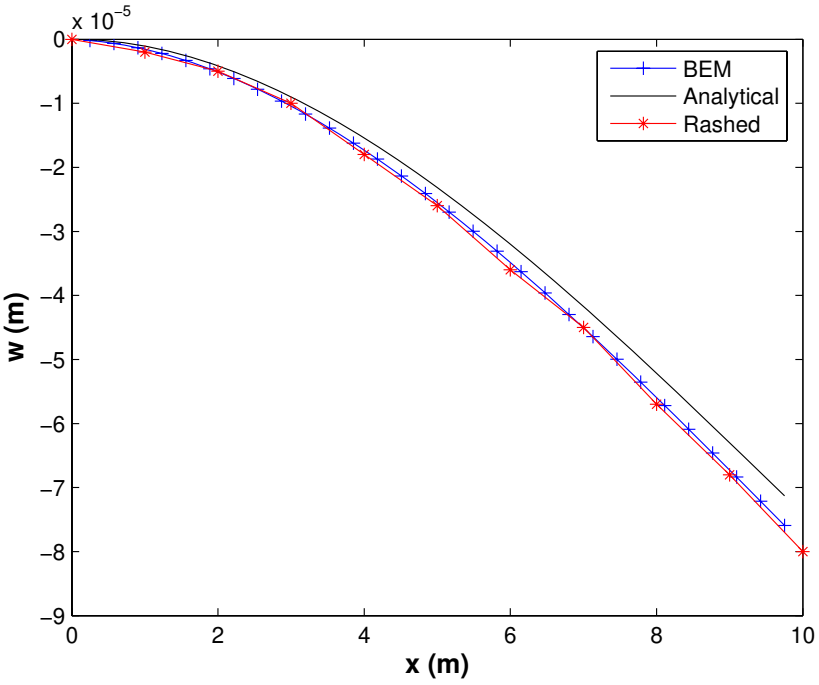

Figure 5.8: Transversal deflection along central axis of the Timoshenko beam

vision. Strong singular integrals were threated through rigid body considerations. Numerical examples were presented and good results correlations have been obtained.

Chapter 6

Boundary element formulation for anisotropic plates

6.1 Introduction

Chapter presents the boundary element method applied to the analysis of anisotropic Kirchhoff plates. The boundary element formulation developed in this chapter will be used for the modeling of the repair's bending response. Basic hypothesis of Kirchhoff theory are presented and the differential governing equation for anisotropic thin plates is developed. The boundary integral formulation for these equations are established and fundamental solutions for displacements, bending moments and shear forces are showed. Numerical examples and preliminary conclusions are presented.

6.2 Differential governing equation for anisotropic plates

A plate is a structural element defined by two flat parallel surfaces where loads are transversely applied, as explained in chapter 5. The distance between these two surfaces defines the thickness of the plate, which is small when compared to other plate dimensions.

Considering its material properties, a plate can be either anisotropic, with different properties in different directions, or isotropic, with equal properties in all directions. Depending on its thickness, a plate can be considered either a thin or a thick plate. In this work, formulations will be developed for anisotropic thin plates, based on the Kirchhoff's plate theory (see Kirchhoff, 1850).

The theory of anisotropic thin plates bending is based on the following assumptions (see Lekhnitskii, 1968):

1. Straight sections, which in the undeformed state are normal to its middle surface, remain straight and normal to the deformed middle surface after loading.

2. Normal stress σ_z in cross sections parallel to the middle plane is small if compared with stresses in the transverse cross section, i.e., σ_x, σ_y, τ_{xy}.

Consider a plate element following the assumptions previously defined. The equilibrium equation for this plate element is given by (see Timoshenko and Woinowski-Krieger, 1959):

$$\frac{\partial^2 m_x}{\partial x^2} + 2\frac{\partial^2 m_{xy}}{\partial x \partial y} + \frac{\partial^2 m_y}{\partial y^2} = -g. \tag{6.1}$$

The rotation of element an_1, initially placed in vertical position, is equal to $\frac{\partial w}{\partial x}$ (Figure 6.1). So, the displacement of a point in x direction, at a distance z from middle surface can be written as:

$$u = -z\frac{\partial w}{\partial x}. \tag{6.2}$$

Following similar procedure, the displacement of a point in y direction is given by:

$$v = -z\frac{\partial w}{\partial y}. \tag{6.3}$$

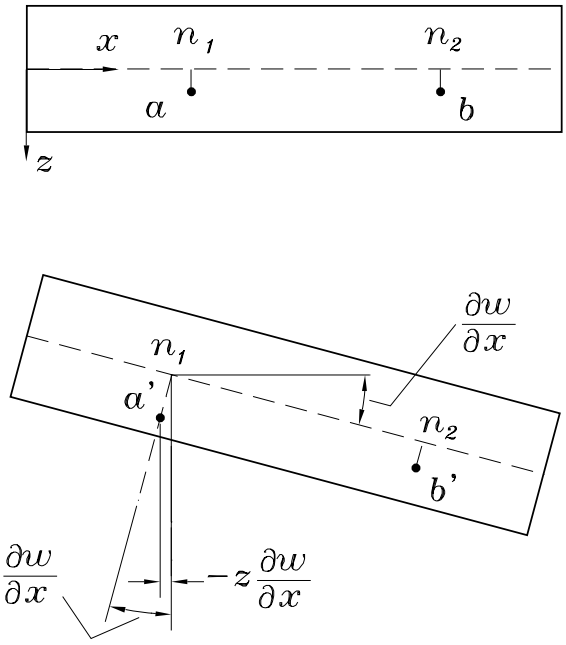

Figure 6.1: Rotation definition for Kirchhoff plates

Substituting equations (6.2) and (6.3) into strain-displacement equations (2.3), we can write:

$$\begin{aligned} \varepsilon_x &= -z\frac{\partial^2 w}{\partial x^2}, \\ \varepsilon_y &= -z\frac{\partial^2 w}{\partial x^2}, \\ \gamma_{xy} &= -2z\frac{\partial^2 w}{\partial x \partial y}. \end{aligned} \tag{6.4}$$

The constitutive equations for symmetric laminated plate can be obtained using equation (3.10) (see Lekhnitskii, 1968) [1]:

$$\begin{aligned} \varepsilon_x &= a_{11}\sigma_x + a_{12}\sigma_y + a_{16}\tau_{xy}, \\ \varepsilon_y &= a_{12}\sigma_x + a_{22}\sigma_y + a_{26}\tau_{xy}, \\ \gamma_{xy} &= a_{16}\sigma_x + a_{26}\sigma_y + a_{66}\tau_{xy}. \end{aligned} \tag{6.5}$$

[1] In this work only symmetric laminated composite repairs will be considered.

Substituting equations (6.4) into equations (6.5), we obtain:

$$\begin{aligned}
\sigma_x &= -z\left(B_{11}\frac{\partial^2 w}{\partial x^2} + B_{12}\frac{\partial^2 w}{\partial y^2} + 2B_{16}\frac{\partial^2 w}{\partial x \partial y}\right), \\
\sigma_y &= -z\left(B_{12}\frac{\partial^2 w}{\partial x^2} + B_{22}\frac{\partial^2 w}{\partial y^2} + 2B_{26}\frac{\partial^2 w}{\partial x \partial y}\right), \\
\tau_{xy} &= -z\left(B_{16}\frac{\partial^2 w}{\partial x^2} + B_{26}\frac{\partial^2 w}{\partial y^2} + 2B_{66}\frac{\partial^2 w}{\partial x \partial y}\right),
\end{aligned} \tag{6.6}$$

where B_{ij} are constants given by:

$$\begin{aligned}
B_{11} &= \frac{1}{\Delta}\left(a_{22}a_{66} - a_{26}^2\right), & B_{22} &= \frac{1}{\Delta}\left(a_{11}a_{66} - a_{16}^2\right), \\
B_{12} &= \frac{1}{\Delta}\left(a_{16}a_{26} - a_{12}a_{66}\right), & B_{66} &= \frac{1}{\Delta}\left(a_{11}a_{22} - a_{12}^2\right), \\
B_{16} &= \frac{1}{\Delta}\left(a_{12}a_{26} - a_{22}a_{16}\right), & B_{26} &= \frac{1}{\Delta}\left(a_{12}a_{16} - a_{11}a_{26}\right),
\end{aligned} \tag{6.7}$$

and

$$\Delta = \begin{vmatrix} a_{11} & a_{12} & a_{16} \\ a_{12} & a_{22} & a_{26} \\ a_{16} & a_{26} & a_{66} \end{vmatrix}. \tag{6.8}$$

Substituting equation (6.6) into bending moments equations (5.2) and integrating, we have:

$$\begin{aligned}
m_x &= -\left(D_{11}\frac{\partial^2 w}{\partial x^2} + D_{12}\frac{\partial^2 w}{\partial y^2} + 2D_{16}\frac{\partial^2 w}{\partial x \partial y}\right), \\
m_y &= -\left(D_{12}\frac{\partial^2 w}{\partial x^2} + D_{22}\frac{\partial^2 w}{\partial y^2} + 2D_{26}\frac{\partial^2 w}{\partial x \partial y}\right),
\end{aligned} \tag{6.9}$$

$$m_{xy} = -\left(D_{16}\frac{\partial^2 w}{\partial x^2} + D_{26}\frac{\partial^2 w}{\partial y^2} + 2D_{66}\frac{\partial^2 w}{\partial x \partial y}\right),$$

where

$$D_{ij} = B_{ij}\frac{t^3}{12}. \tag{6.10}$$

Substituting equation (6.10) into shear force equations given by (5.8), we can write:

$$\begin{aligned} q_x &= \left[D_{11}\frac{\partial^3 w}{\partial x^3} + 3D_{16}\frac{\partial^3 w}{\partial x^2 \partial y} + (D_{12} + 2D_{66})\frac{\partial^3 w}{\partial x \partial y^2} + D_{26}\frac{\partial^3 w}{\partial y^3}\right], \\ q_y &= \left[D_{16}\frac{\partial^3 w}{\partial x^3} + (D_{12} + 2D_{66})\frac{\partial^3 w}{\partial x^2 \partial y} + 3D_{26}\frac{\partial^3 w}{\partial x \partial y^2} + D_{22}\frac{\partial^3 w}{\partial y^3}\right]. \end{aligned} \tag{6.11}$$

Equation (6.1) can be rewritten using equations (6.10) as:

$$D_{11}\frac{\partial^4 w}{\partial x^4} + 4D_{16}\frac{\partial^4 w}{\partial x^3 \partial y} + 2(D_{12} + D_{66})\frac{\partial^4 w}{\partial x^2 \partial y^2} + 4D_{26}\frac{\partial^4 w}{\partial x \partial y^3} + D_{22}\frac{\partial^4 w}{\partial y^4} = g. \tag{6.12}$$

General solution to w in equation (6.12) depends on μ_1, μ_2, $\bar{\mu}_1$, and $\bar{\mu}_2$ roots of characteristic equation given by:

$$D_{22}\mu^4 + 4D_{26}\mu^3 + 2(D_{12} + 2D_{66})\mu^2 + 4D_{16}\mu + D_{11} = 0. \tag{6.13}$$

Roots of this equation, as shown by Lekhnitskii, 1968, are always complex for homogeneous material. The complex roots $\mu_1 = d_1 + e_1 i$ and $\mu_2 = d_2 + e_2 i$ are known as deflection complex parameters. In general, these roots are different complex numbers.

A general expression for the deflection has the form:

1. in case of different complex parameters ($\mu_1 \neq \mu_2$):

$$w = w_o + 2\mathrm{Re}[w_1(z_1) + w_2(z_2)]. \tag{6.14}$$

2. in case of equal complex parameters ($\mu_1 = \mu_2$):

$$w = w_o + 2\mathrm{Re}[w_1(z_1) + \bar{z_1} w_2(z_1)]. \tag{6.15}$$

where w_o is a particular solution of equation (6.12) that depends on the distributed load q in the plate surface, $w_1(z_1)$ and $w_2(z_2)$ are arbitrary analytic functions of complex variable $z_1 = x + \mu_1 y$ and $z_2 = x + \mu_2 y$.

Based on equations (6.10) and (6.11), general expressions for forces and moments can be obtained as (for the case $\mu_1 \neq \mu_2$):

$$\begin{aligned}
m_x &= m_x^o - 2\mathrm{Re}[p_1 w''(z_1) + p_2 w''(z_2)], \\
m_y &= m_y^o - 2\mathrm{Re}[q_1 w''(z_1) + q_2 w''(z_2)], \\
m_{xy} &= m_{xy}^o - 2\mathrm{Re}[r_1 w''(z_1) + r_2 w''(z_2)], \\
q_x &= q_x^o - 2\mathrm{Re}[\mu_1 s_1 w'''(z_1) + \mu_2 s_2 w'''(z_2)], \\
q_y &= q_y^o - 2\mathrm{Re}[s_1 w'''(z_1) + s_2 w'''(z_2)].
\end{aligned} \tag{6.16}$$

where m_x^o, m_y^o, m_{xy}^o, q_x^o, and q_y^o are moments and shear forces corresponding to function w_o

computed from equations (6.10) and (6.11). The other constants are given in Albuquerque, 2001.

6.2.1 Bending stiffness in an arbitrary direction

Considering that stiffness bending constants of a plate in a x, y, z coordinate system are given by D_{ij} $(i, j = 1, 2, 6)$ and in a x', y', z' coordinate system, rotated α with respect to the first coordinate system, are given by D'_{ij} $(i, j = 1, 2, 6)$, the equation relating these constants, as shown by Lekhnitskii, 1968, are given by:

$$D'_{11} = D_{11}\cos^4\phi + 2(D_{12} + 2D_{66})\sin^2\phi\cos^2\phi + D_{22}\sin^4\phi +$$

$$2(D_{16}\cos^2\phi + D_{26}\sin^2\phi)\sin 2\phi, \tag{6.17}$$

$$D'_{22} = D_{11}\sin^4\phi + 2(D_{12} + 2D_{66})\sin^2\phi\cos^2\phi + D_{22}\cos^4\phi +$$

$$2(D_{16}\sin^2\phi + D_{26}\cos^2\phi)\sin 2\phi, \tag{6.18}$$

$$D'_{12} = D_{12} + [D_{11} + D_{22} - 2(D_{12} + 2D_{66})]\sin^2\phi\cos^2\phi +$$

$$(D_{26} - D_{16})\cos 2\phi\sin 2\phi, \tag{6.19}$$

$$D'_{66} = D_{66} + [D_{11} + D_{22} - 2(D_{12} + 2D_{66})]\sin^2\phi\cos^2\phi +$$

$$(D_{26} - D_{16}) \cos 2\phi \sin 2\phi, \tag{6.20}$$

$$D'_{16} = \frac{1}{2}[D_{22} \sin^2 \phi - D_{11} \cos^2 \phi + (D_{12} + 2D_{66}) \cos 2\phi] \sin 2\phi +$$

$$D_{16} \cos^2 \phi(\cos^2 \phi - 3 \sin^2 \phi) + D_{26} \sin^2 \phi(3 \cos^2 \phi - \sin^2 \phi), \tag{6.21}$$

$$D'_{26} = \frac{1}{2}[D_{22} \cos^2 \phi - D_{11} \sin^2 \phi + (D_{12} + 2D_{66}) \cos 2\phi] \sin 2\phi +$$

$$D_{16} \sin^2 \phi(\cos^2 \phi - 3 \sin^2 \phi) + D_{26} \cos^2 \phi(3 \cos^2 \phi - \sin^2 \phi). \tag{6.22}$$

The stress components σ_n and τ_{ns}, normal and shear stress, respectively, are related with stress σ_x, σ_y, and τ_{xy} by:

$$\sigma_n = \sigma_x \cos^2 \alpha + \sigma_y \sin^2 \alpha + 2\tau_{xy} \sin \alpha \cos \alpha, \tag{6.23}$$

$$\tau_{ns} = (\sigma_y - \sigma_x) \sin \alpha \cos \alpha + \tau_{xy}(\cos^2 \alpha - \sin^2 \alpha). \tag{6.24}$$

The components of moment, initially written considering axis x and y, can now be rewritten in a generic coordinate system n, s (see Paiva, 1987). The bending moments referring to directions n and s are given by:

$$m_n = m_x \cos^2 \alpha + m_y \sin^2 \alpha + 2m_{xy} \sin \alpha \cos \alpha, \tag{6.25}$$

$$m_{ns} = (m_y - m_x) \sin \alpha \cos \alpha + m_{xy}(\cos^2 \alpha - \sin^2 \alpha). \tag{6.26}$$

Similarly, q_n, the shear force in the n axis, can be written as:

$$q_n ds = q_x ds \cos\alpha + q_y ds \sin\alpha, \tag{6.27}$$

or

$$q_n = q_x \cos\alpha + q_y \sin\alpha. \tag{6.28}$$

In order to solve the plate differential equation (6.12), it is necessary to impose boundary conditions to displacement w and its derivative $\partial w/\partial n$. Kirchhoff, 1850 has shown that the boundary conditions of shear force q_n and twisting moment m_{ns} can be written as one single boundary condition given by:

$$V_n = q_n + \frac{\partial m_{ns}}{\partial s}. \tag{6.29}$$

The other loading boundary condition is the moment m_n.

6.3 Boundary element method for anisotropic plates

Using Betti theorem, we can relate two states of stress-deformation of a linear material as:

$$\int_\Omega \sigma^*_{ij}\varepsilon_{ij} d\Omega = \int_\Omega \sigma_{ij}\varepsilon^*_{ij} d\Omega. \tag{6.30}$$

Writing the right hand side of equation (6.29) in von Karman's notation, we have:

$$\int_\Omega \sigma_{ij}\varepsilon^*_{ij} d\Omega = \int_\Omega \left(\sigma_x\varepsilon^*_x + \sigma_y\varepsilon^*_y + \sigma_z\varepsilon^*_z + \tau_{xy}\gamma^*_{xy} + \tau_{xz}\gamma^*_{xz} + \tau_{yz}\gamma^*_{yz}\right) d\Omega. \tag{6.31}$$

Neglecting stresses normal to the plate, equation (6.31) is given by:

$$\int_\Omega \sigma_{ij}\varepsilon^*_{ij} d\Omega = \int_\Omega \left(\sigma_x\varepsilon^*_x + \sigma_y\varepsilon^*_y + \tau_{xy}\gamma^*_{xy}\right) d\Omega. \tag{6.32}$$

Substituting equations (6.4) and (6.5) into equation (6.32), we can write the first term of the integral in the right hand side of equation (6.32) as:

$$\int_{\Omega} \sigma_x \varepsilon_x^* d\Omega = \int_{\Omega} \left[\int_z \left(B_{11} \frac{\partial^2 w}{\partial x^2} + B_{12} \frac{\partial^2 w}{\partial y^2} + 2B_{16} \frac{\partial^2 w}{\partial x \partial y} \right) \left(z \frac{\partial^2 w}{\partial x^2} \right) dz \right] d\Omega. \tag{6.33}$$

Integrating (6.33) throughout the thickness of the plate, we have:

$$\int_{\Omega} \sigma_x \varepsilon_x^* d\Omega = \int_{\Omega} \left(D_{11} \frac{\partial^2 w}{\partial x^2} + D_{12} \frac{\partial^2 w}{\partial y^2} + 2D_{16} \frac{\partial^2 w}{\partial x \partial y} \right) \frac{\partial^2 w}{\partial x^2} d\Omega = - \int_{\Omega} m_x \frac{\partial^2 w}{\partial x^2} d\Omega. \tag{6.34}$$

In order to obtain equations of the boundary element method, it is necessary to transform domain integrals into boundary integrals.

Consider two functions $f(x)$ and $g(x)$. The derivative of their product can be written as:

$$\frac{\partial}{\partial x}[f(x)g(x)] = \frac{\partial f(x)}{\partial x} g(x) + \frac{\partial g(x)}{\partial x} f(x). \tag{6.35}$$

Using the derivative property (6.35) in equation (6.34), we can write:

$$\int_{\Omega} \sigma_x \varepsilon_x^* d\Omega = - \int_{\Omega} \left[\frac{\partial}{\partial x} \left(m_x \frac{\partial w^*}{\partial x} \right) - \frac{\partial w^*}{\partial x} \frac{\partial m_x}{\partial x} \right] d\Omega. \tag{6.36}$$

Using Green theorem, equation (6.36) can be written as:

$$\int_{\Omega} \sigma_x \varepsilon_x^* d\Omega = - \int_{\Gamma} m_x \frac{\partial w^*}{\partial x} \cos \alpha d\Gamma + \int_{\Omega} \frac{\partial w^*}{\partial x} \frac{\partial m_x}{\partial x} d\Omega. \tag{6.37}$$

Applying the derivative property (6.35) in the second right hand side term of equation (6.37), we have:

$$\int_{\Omega} \sigma_x \varepsilon_x^* d\Omega = - \int_{\Gamma} m_x \frac{\partial w^*}{\partial x} \cos \alpha d\Gamma + \int_{\Omega} \left[\frac{\partial}{\partial x} \left(w^* \frac{\partial m_x}{\partial x} \right) - w^* \frac{\partial^2 m_x}{\partial x^2} \right] d\Omega. \tag{6.38}$$

After using Green theorem, we can write:

$$\int_\Omega \sigma_x \varepsilon_x^* d\Omega = \int_\Gamma \left(-m_x \frac{\partial w^*}{\partial x} \cos\alpha + w^* \frac{\partial m_x}{\partial x} \cos\alpha \right) d\Gamma - \int_\Omega w^* \frac{\partial^2 m_x}{\partial x^2} d\Omega. \tag{6.39}$$

Following similar procedure, we can show that:

$$\int_\Omega \sigma_y \varepsilon_y^* d\Omega = \int_\Gamma \left(-m_y \frac{\partial w^*}{\partial y} \sin\alpha + w^* \frac{\partial m_y}{\partial y} \sin\alpha \right) d\Gamma - \int_\Omega w^* \frac{\partial^2 m_y}{\partial y^2} d\Omega, \tag{6.40}$$

and

$$\int_\Omega \tau_{xy} \gamma_{xy}^* d\Omega = \int_\Gamma \left(-m_{xy} \frac{\partial w^*}{\partial y} \cos\alpha - m_{xy} \frac{\partial w^*}{\partial x} \sin\alpha + w^* \frac{\partial m_{xy}}{\partial x} \sin\alpha + \right.$$

$$\left. w^* \frac{\partial m_{xy}}{\partial y} \cos\alpha \right) d\Gamma - \int_\Omega 2 w^* \frac{\partial^2 m_{xy}}{\partial x \partial y} d\Omega. \tag{6.41}$$

Thus, equation (6.32) is written as:

$$\int_\Omega \sigma_{ij} \varepsilon_{ij}^* d\Omega = -\int_\Gamma \left(m_x \frac{\partial w^*}{\partial x} \cos\alpha + m_y \frac{\partial w^*}{\partial y} \sin\alpha + m_{xy} \frac{\partial w^*}{\partial y} \cos\alpha + \right.$$

$$\left. m_{xy} \frac{\partial w^*}{\partial x} \sin\alpha \right) d\Gamma + \int_\Gamma w^* \left[\left(\cos\alpha \frac{\partial m_x}{\partial x} + \frac{\partial m_{xy}}{\partial y} \right) \left(\sin\alpha \frac{\partial m_y}{\partial y} + \frac{\partial m_{xy}}{\partial x} \right) \right] d\Gamma -$$

$$\int_\Gamma w^* \left(\frac{\partial^2 m_x}{\partial x^2} + 2 \frac{\partial^2 m_{xy}}{\partial x \partial y} + \frac{\partial^2 m_y}{\partial y^2} \right) d\Gamma. \tag{6.42}$$

Substituting equations for shear forces given by (5.8) and using equation (6.28), equation (6.42) can be written as:

$$\int_\Omega \sigma_{ij} \varepsilon_{ij}^* d\Omega = -\int_\Gamma \left(m_x \frac{\partial w^*}{\partial x} \cos\alpha + m_y \frac{\partial w^*}{\partial y} \sin\alpha + m_{xy} \frac{\partial w^*}{\partial y} \cos\alpha + \right.$$

$$m_{xy}\frac{\partial w^*}{\partial x}\sin\alpha\Big)\,d\Gamma + \int_\Gamma w^* q_n d\Gamma + \int_\Omega g w^* d\Omega. \tag{6.43}$$

From the relation between two coordinate systems (x, y) and (n, s), we have:

$$\frac{\partial w^*}{\partial x} = \frac{\partial w^*}{\partial n}\cos\alpha - \frac{\partial w^*}{\partial s}\sin\alpha,$$

$$\frac{\partial w^*}{\partial y} = \frac{\partial w^*}{\partial n}\sin\alpha + \frac{\partial w^*}{\partial s}\cos\alpha. \tag{6.44}$$

Substituting equations (6.44) into equation (6.43), we have:

$$\int_\Omega \sigma_{ij}\varepsilon^*_{ij} d\Omega = -\int_\Gamma \Bigg[m_x \cos\alpha \left(\frac{\partial w^*}{\partial n}\cos\alpha - \frac{\partial w^*}{\partial s}\sin\alpha\right) +$$

$$m_y \sin\alpha \left(\frac{\partial w^*}{\partial n}\sin\alpha + \frac{\partial w^*}{\partial s}\cos\alpha\right) + m_{xy}\cos\alpha \left(\frac{\partial w^*}{\partial n}\sin\alpha + \frac{\partial w^*}{\partial s}\cos\alpha\right) +$$

$$m_{xy}\sin\alpha \left(\frac{\partial w^*}{\partial n}\cos\alpha - \frac{\partial w^*}{\partial s}\sin\alpha\right)\Bigg] d\Gamma + \int_\Gamma w^* q_n d\Gamma + \int_\Omega g w^* d\Omega. \tag{6.45}$$

After some algebraic manipulations, equation (6.45) can be rewritten as:

$$\int_\Omega \sigma_{ij}\varepsilon^*_{ij} d\Omega = -\int_\Gamma \Bigg\{ \frac{\partial w^*}{\partial n}\left(m_x \cos^2\alpha + m_y \sin^2\alpha + 2m_{xy}\sin\alpha\cos\alpha\right) +$$

$$\frac{\partial w^*}{\partial s}\left[m_{xy}\left(\cos^2\alpha - \sin^2\alpha\right) + (m_y - m_x)\sin\alpha\cos\alpha\right]\Bigg\} d\Gamma +$$

$$\int_\Gamma w^* q_n d\Gamma + \int_\Omega g w^* d\Omega. \tag{6.46}$$

Substituting equations (6.25) and (6.26) into equation (6.46), we have:

$$\int_{\Omega} \sigma_{ij}\varepsilon_{ij}^{*} d\Omega = -\int_{\Gamma} \left(m_n \frac{\partial w^*}{\partial n} + m_{ns} \frac{\partial w^*}{\partial s} - q_n w^* \right) d\Gamma + \int_{\Omega} g w^* d\Omega. \tag{6.47}$$

Computing the second term of the first integral in the right hand side of equation (6.47), we have:

$$\int_{\Gamma} m_{ns} \frac{\partial w^*}{\partial s} d\Gamma = m_{ns} w^* \Big|_{\Gamma_1}^{\Gamma_2} - \int_{\Gamma} \frac{\partial m_{ns}}{\partial s} w^* d\Gamma \tag{6.48}$$

where Γ_1 and Γ_2 are coordinates of ends of the boundary where the integration is being carried out. In the case of a closed boundary without corner, i.e., the function that describes the boundary curve and its derivative are continuous, the first term in the right hand side of equation (6.48) vanishes. In the case where there are corners, equation (6.48) can be written as:

$$\int_{\Gamma} m_{ns} \frac{\partial w^*}{\partial s} d\Gamma = -\sum_{i=1}^{N_c} R_{c_i} w_{c_i}^* - \int_{\Gamma} \frac{\partial m_{ns}}{\partial s} w^* d\Gamma \tag{6.49}$$

where

$$R_{c_i} = m_{ns_i}^{+} - m_{ns_i}^{-} \tag{6.50}$$

and the terms w_{c_i}, $m_{ns_i}^{+}$, $m_{ns_i}^{-}$ are values of displacements and twisting moments after and before the i corner of the plate, N_c are the total number of boundary corners (see Paiva, 1987).

From equation (6.47) and (6.49), we can write:

$$\int_{\Omega} \sigma_{ij}\varepsilon_{ij}^{*} d\Omega = \int_{\Gamma} \left(q_n w^* - m_n \frac{\partial w^*}{\partial n} + \frac{\partial m_{ns}}{\partial s} w^* \right) d\Gamma + \sum_{i=1}^{N_c} R_{c_i} w_{c_i}^* + \int_{\Omega} g w^* d\Omega. \tag{6.51}$$

From equations (6.51) and (6.29), we have:

$$\int_{\Omega} \sigma_{ij}\varepsilon_{ij}^{*} d\Omega = \int_{\Gamma} \left(V_n w^* - m_n \frac{\partial w^*}{\partial n} \right) d\Gamma + \sum_{i=1}^{N_c} R_{c_i} w_{c_i}^* + \int_{\Omega} g w^* d\Omega \tag{6.52}$$

Following a similar procedure to that used to obtain equation (6.52), the left hand side of equation (6.30) can be written as:

$$\int_{\Omega} \sigma_{ij}^{*} \varepsilon_{ij} d\Omega = \int_{\Gamma} \left(V_n^{*} w - m_n \frac{\partial w^{*}}{\partial n} \right) d\Gamma + \sum_{i=1}^{N_c} R_{c_i}^{*} w_{c_i} + \int_{\Omega} g^{*} w d\Omega. \tag{6.53}$$

Substituting equations (6.52) and (6.53) into equation (6.30), we can write:

$$\int_{\Gamma} \left(V_n w^{*} - m_n \frac{\partial w^{*}}{\partial n} \right) d\Gamma + \sum_{i=1}^{N_c} R_{c_i} w_{c_i}^{*} + \int_{\Omega} g w^{*} d\Omega =$$

$$\int_{\Gamma} \left(V_n^{*} w - m_n \frac{\partial w^{*}}{\partial n} \right) d\Gamma + \sum_{i=1}^{N_c} R_{c_i}^{*} w_{c_i} + \int_{\Omega} g^{*} w d\Omega. \tag{6.54}$$

Equation (6.54) relates two states of an elastic material. In order to apply this equation to solve bending problems, we need to consider one of states as known and other as the state which stands for the problem which we want to analyze. To obtain a boundary integral equation, the known state is chosen so that the domain integral given by:

$$\int_{\Omega} g^{*} w d\Omega \tag{6.55}$$

vanishes. Using the properties of Dirac delta function $\delta(\mathbf{x}', \mathbf{x})$, so that integral $g^{*} = \delta(\mathbf{x}', \mathbf{x})$, integral (6.55) is written as:

$$\int_{\Omega} \delta(\mathbf{x}', \mathbf{x}) w(\mathbf{x}) d\Omega(\mathbf{x}) = w(\mathbf{x}') \tag{6.56}$$

The state corresponding to a linear material under loading of a Dirac delta function is known as fundamental state and the variables of equation (6.54) related to this state (w^{*}, V_n^{*} and m_n^{*}) are known as fundamental solutions which are computed analytically from the differential equation (6.12).

Considering the state "*" as the fundamental state, equation (6.54) can be written as:

$$cw(\mathbf{x}) + \int_\Gamma \left[V_n^*(\mathbf{x}', \mathbf{x}) w(\mathbf{x}) - m_n^*(\mathbf{x}', \mathbf{x}) \frac{\partial w(\mathbf{x})}{\partial n} \right] d\Gamma + \sum_{i=1}^{N_c} R_{c_i}^*(\mathbf{x}', \mathbf{x}) w_{c_i}(\mathbf{x}) -$$

$$\int_\Gamma \left[V_n(\mathbf{x}) w^*(\mathbf{x}', \mathbf{x}) - m_n(\mathbf{x}) \frac{\partial w^*}{\partial n}(\mathbf{x}', \mathbf{x}) \right] d\Gamma + \sum_{i=1}^{N_c} R_{c_i}(\mathbf{x}) w_{c_i}^*(\mathbf{x}', \mathbf{x}) +$$

$$\int_\Omega q(\mathbf{x}) w^*(\mathbf{x}', \mathbf{x}) d\Omega. \tag{6.57}$$

The constant c is introduced in order to consider that the Dirac delta function can be applied in the domain, in the boundary, or outside the domain. If the Dirac delta function is applied in a point where the boundary is smooth, than $c = 1/2$.

Variables of equation (6.57) are displacements $w(\mathbf{x})$, rotations $\partial w(\mathbf{x})/\partial \mathbf{n}$, moments $m_n(\mathbf{x})$, and loads $V_n(\mathbf{x})$. For a given boundary condition, some of these variables are known. In order to have an equal number of equations and unknown variables, it is necessary to write an integral equation corresponding to the derivative of displacement $w(\mathbf{x}')$ in relation to a cartesian coordinate system fixed in the source point, i.e., the point where the Dirac delta of the fundamental state is applied. The axis directions of this coordinate system are coincident with normal and tangent to the boundary directions in the source point.

For a particular case where the of the source point is placed in a point where the boundary is smooth, the boundary equation is given by:

$$\frac{1}{2} \frac{\partial w(\mathbf{x}')}{\partial n_1} + \int_\Gamma \left[\frac{\partial V^*}{\partial n_1}(\mathbf{x}', \mathbf{x}) w(\mathbf{x}) - \frac{\partial m_n^*}{\partial n_1}(\mathbf{x}', \mathbf{x}) \frac{\partial w}{\partial n}(\mathbf{x}) \right] d\Gamma +$$

$$\sum_{i=1}^{N_c} \frac{\partial R_{c_i}^*}{\partial n_1}(\mathbf{x}', \mathbf{x}) w_{c_i}(\mathbf{x}) = \int_\Gamma \left\{ V_n(\mathbf{x}) \frac{\partial w^*}{\partial n_1}(\mathbf{x}', \mathbf{x}) - m_n(\mathbf{x}) \frac{\partial}{\partial n_1} \left[\frac{\partial w^*}{\partial n}(\mathbf{x}', \mathbf{x}) \right] \right\} d\Gamma +$$

$$\sum_{i=1}^{N_c} R_{c_i}(\mathbf{x}) \frac{\partial w^*_{c_i}}{\partial n_1}(\mathbf{x}', \mathbf{x}) + \int_\Omega g(\mathbf{x}) \frac{\partial w^*}{\partial n_1}(\mathbf{x}', \mathbf{x}) d\Omega \tag{6.58}$$

Its important to say that it is possible to use only equation (6.57) in a boundary element formulation by using as source points the boundary nodes and an equal number of points external to the domain of the problem.

6.3.1 Fundamental solutions for anisotropic plates

The transversal displacement plate bending fundamental solution is computed by placing the non-homogeneous term of the differential equation (6.12) equal to a concentrated force given by a Dirac delta function $\delta(\mathbf{x}', \mathbf{x}))$, i.e.,

$$\Delta\Delta w^*(\mathbf{x}', \mathbf{x}) = \delta(\mathbf{x}', \mathbf{x}) \tag{6.59}$$

where $\Delta\Delta(.)$ is the differential operator:

$$\Delta\Delta(.) = \frac{D_{11}}{D_{22}} \frac{\partial^4(.)}{\partial x^4} + 4\frac{D_{16}}{D_{22}} \frac{\partial^4(.)}{\partial^3 \partial y} + \frac{2(D_{12} + 2D_{66})}{D_{22}} \frac{\partial^4(.)}{\partial x^2 \partial y^2} + 4\frac{D_{26}}{D_{22}} \frac{\partial^4(.)}{\partial x \partial y^3} + \frac{\partial^4(.)}{\partial y^4}. \tag{6.60}$$

As shown by Shi and Bezine, 1988, the transversal displacement fundamental solution is given by:

$$w^*(\rho, \theta) = \frac{1}{8\pi} \left\{ C_1 R_1(\rho, \theta) + C_2 R_2(\rho, \theta) + C_3 \left[S_1(\rho, \theta) - S_2(\rho, \theta) \right] \right\} \tag{6.61}$$

where

$$\rho = \left[(x - x_o)^2 + (y - y_o)^2 \right]^{1/2} \tag{6.62}$$

x and y are the coordinates of the field point $\mathbf{x}$, x_o and y_o are the coordinates of source point $\mathbf{x}'$,

$$\theta = \arctan \frac{y - y_o}{x - x_o} \tag{6.63}$$

$$C_1 = \frac{(d_1 - d_2)^2 - (e_1^2 - e_2^2)}{GHe_1}, \tag{6.64}$$

$$C_2 = \frac{(d_1 - d_2)^2 + (e_1^2 - e_2^2)}{GHe_2}, \tag{6.65}$$

$$C_3 = \frac{4(d_1 - d_2)}{GH} \tag{6.66}$$

$$G = (d_1 - d_2)^2 + (e_1 + e_2)^2, \tag{6.67}$$

$$H = (d_1 - d_2)^2 + (e_1 - e_2)^2 \tag{6.68}$$

$$\begin{aligned} R_i = {} & \rho^2 \left[(\cos\theta + d_i \sin\theta)^2 - e_i^2 \sin^2\theta \right] \times \\ & \left\{ \log \left[\frac{\rho^2}{a^2} \left((\cos\theta + d_i \sin\theta)^2 + e_i^2 \sin^2\theta \right) \right] - 3 \right\} - \\ & 4\rho^2 e_i \sin\theta \left(\cos\theta + d_i \sin\theta \right) \arctan \frac{e_i \sin\theta}{\cos\theta + d_i \sin\theta} \end{aligned} \tag{6.69}$$

and

$$S_i = \rho^2 e_i \sin\theta \left(\cos\theta + d_i \sin\theta\right) \times$$

$$\left\{ \log\left[\frac{\rho^2}{a^2}\left(\left(\cos\theta + d_i \sin\theta\right)^2 + e_i^2 \sin^2\theta\right)\right] - 3 \right\} +$$

$$\rho^2 \left[\left(\cos\theta + d_i \sin\theta\right)^2 - e_i^2 \sin^2\theta\right] \arctan\frac{e_i \sin\theta}{\cos\theta + d_i \sin\theta} \tag{6.70}$$

The repeated index i in the terms of R_i and S_i does not imply summation. The coefficient a is an arbitrary constant taken as $a = 1$.

Other fundamental solutions are given by:

$$m_n^* = -\left(f_1 \frac{\partial^2 w^*}{\partial x^2} + f_2 \frac{\partial^2 w^*}{\partial x \partial y} + f_3 \frac{\partial^2 w^*}{\partial y^2}\right), \tag{6.71}$$

$$R_{c_i}^* = -\left(g_1 \frac{\partial^2 w^*}{\partial x^2} + g_2 \frac{\partial^2 w^*}{\partial x \partial y} + g_3 \frac{\partial^2 w^*}{\partial y^2}\right), \tag{6.72}$$

$$V_n^* = -\left(h_1 \frac{\partial^3 w^*}{\partial x^3} + h_2 \frac{\partial^3 w^*}{\partial x^2 \partial y} + h_3 \frac{\partial^3 w^*}{\partial x \partial y^2} + h_4 \frac{\partial^3 w^*}{\partial y^3}\right) -$$

$$\frac{1}{\bar{R}}\left(h_5 \frac{\partial^2 w^*}{\partial x^2} + h_6 \frac{\partial^2 w^*}{\partial x \partial y} + h_7 \frac{\partial^2 w^*}{\partial y^2}\right). \tag{6.73}$$

where $\bar{R}$ is the curvature radius at a smooth point of the boundary Γ. Other constants can be obtained from Albuquerque, 2001. As it can be seen, derivatives of R_i and S_i present weak $(\log r)$, strong $(1/r)$, and hyper $(1/r^2)$ singularities that will need special attention during their integration in boundary element kernels.

6.4 Numerical examples

In order to assess the accuracy of the proposed formulation some numerical problems are analyzed and their results compared with some results available in literature.

6.4.1 Orthotropic simply supported square plate

The first problem is a single lamina square plate of side length $a = 1$ m and thickness $h = 0.01$ m. The material is orthotropic and its material properties are: $E_x = 2.068 \times 10^{11}$ Pa, $E_y = E_x/15$, $\nu_{xy} = 0.3$, $G_{xy} = 6.055 \times 10^8$ Pa. The plate is under a uniformly distributed load $q = 1\ 10^4$ Pa applied along its domain (Figure 6.2) and simply supported along its four edges. This problem was analyzed by Shi and Bezine, 1988 using boundary element method and domain integration to treat the distributed load.

The problem is solved using different meshes and the results for transversal displacements at point A and at point B are compared with series solution for point A and for point B given by $w_{se.} = 8.1258 \times 10^{-3}$ m and $w_{se.} = 4.5211 \times 10^{-3}$ m, respectively. Table 6.1 shows transversal displacements computed by the present BEM technique using different meshes and their respective errors compared to Timoshenko and Woinowski-Krieger, 1959 series solution. It can be seen that a very poor agreement is obtained when 12 elements (3 elements per side) are used. However, the convergence to the series solutions is obtained as the number of elements is increased. When 48 boundary elements are used (Figure 6.3), transversal displacements in both points present errors below 1% when compared with series solutions.

6.4.2 Cross-laminate graphite-epoxy composite square plate

The second problem that has been analyzed in this work is a simply supported symmetric laminate $[0^o/90^o/0^o/90^o/0^o]_s$ of side length $a = 1$ m under a uniformly distributed load

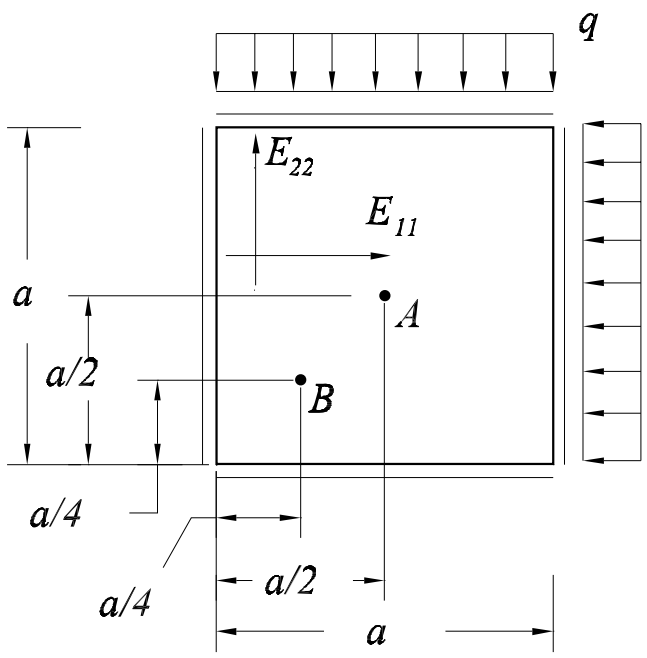

Figure 6.2: Square plate with simply-supported edges under uniformly distributed load

Table 6.1: Accuracy of transversal displacements obtained by BEM for the orthotropic square plate with simply supported edges under uniformly distributed loads.

Number of elements	Transversal displacements [10^{-6} m]		Errors [%]	
	Point A	Point B	Point A	Point B
12	-0.7985	-0.4415	1.7310	2.3545
24	-0.8014	-0.4430	1.3806	2.0100
48	-0.8081	-0.4481	0.5513	0.8875

$q = 6.9 \times 10^3$ Pa. The properties of each lamina of a high modulus graphite-epoxy composite material used in this analysis are: $E_x = 2.07 \times 10^9$ Pa, $E_y = 5.17 \times 10^9$ Pa, $G_{xy} = 3.10 \times 10^9$ Pa, and $\nu_{xy} = 0.25$. The total thickness of the laminate is taken as $h = 0.01$ m. All layers have equal thickness. This problem was analyzed by Lakshminarayana and Murthy, 1984 using finite element method. A series solution for the transversal displacement in the center of the plate was presented by Noor and Mathers, 1975 by treating the plate as an equivalent single lamina orthotropic plate. This solution is given by:

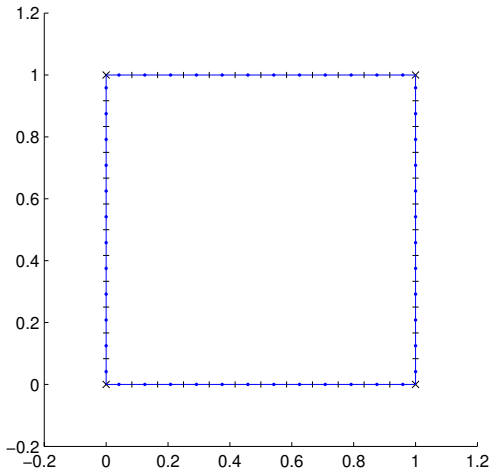

Figure 6.3: Boundary element mesh with 48 constant boundary elements

$$\frac{w_{an.}E_{22}h^3}{qa^4} \times 10^3 = 4.4718 \tag{6.74}$$

The center point transversal displacement obtained by the proposed formulation is compared in Table 6.2 with the finite element solution, presented by Lakshminarayana and Murthy, 1984, and with the analytical solution presented by Noor and Mathers, 1975. As it can be seen, it is obtained the same accuracy of the finite element results.

Table 6.2: Accuracy of transversal displacement obtained by BEM and FEM for the cross-laminate graphite-epoxy composite square plate with simply supported edges under uniformly distributed loads.

Numerical methods	Transversal displacements and errors	
	$wE_{22}h^3/(qa^4) \times 10^3$	Errors [%]
BEM	4.4507	0.47
FEM	4.4508	0.47

6.5 Conclusions

In this chapter, the boundary element method applied to analysis of anisotropic Kirchhoff

plates under static load conditions, was presented. Fundamental solutions for displacements and generalized forces (bending moments and shear forces) are established. Numerical examples was presented and results are compared with those reported in the literature. Good agreement was found.

Chapter 7

Dual boundary element method for plate fracture mechanics

7.1 Introduction

Some special techniques have been developed to treat problems in fracture mechanics using the boundary element method. Among these, the most important are: the crack Green's function method, the displacement discontinuity method, the subregions method and the dual boundary element method (see Portela and Aliabadi, 1992). The crack Green's function method is limited to problems with a single straight traction-free crack. The displacement discontinuity method introduces higher order singularities into the boundary integrals. The subregions method introduces artificial boundaries into the body. The dual boundary element method overcomes these drawbacks and, at present, is consider an effective technique for the treatment of problems in fracture mechanics, specifically in the boundary element analysis of cracked plates repaired with adhesively bonded isotropic patches (see Wen et al., 2003).

This chapter presents the Dual Boundary Element Method applied to plate fracture analysis considering membrane, bending moments and shear forces. In the first part, the hyper-

singular equations for plane elasticity and Reissner plate bending are developed obtaining the traction equations for these cases. Types of singularities that appears in these equations and their treatment using the Taylor series expansion methodology. The dual boundary element method is presented for the treatment of fracture mechanics problems and a general methodology is exposed. Finally, the stress intensity factors for plane elasticity and bending problems are defined. Numerical examples are presented and preliminary conclusions are established.

7.2 Hypersingular equations for plane elastostatics

The boundary integral representation of the displacement components u_i, at collocation point $\mathbf{x}'$, is given by equation (4.13) (Dirgantara, 2000):

$$c_{\alpha\beta}u_\alpha + \int_\Gamma T_{\alpha\beta}\left(\mathbf{x}', \mathbf{x}\right) u_\beta d\Gamma = \int_\Gamma U_{\alpha\beta}\left(\mathbf{x}', \mathbf{x}\right) t_\beta d\Gamma - \frac{1}{h}\int_A U_{\alpha\beta}\left(\mathbf{x}', \mathbf{x}\right) f_\beta dA \tag{7.1}$$

The stress components σ_{ij} are obtained by differentiation of equation (7.1), followed by the application of the Hooke's law, as given by equation (4.14):

$$\sigma_{\alpha\beta} + \int_\Gamma S_{ijk}\left(\mathbf{x}', \mathbf{x}\right) u_k d\Gamma = \int_\Gamma D_{ijk}\left(\mathbf{x}', \mathbf{x}\right) t_k d\Gamma - \frac{1}{h}\int_A D_{ijk}\left(\mathbf{x}', \mathbf{x}\right) f_k dA \tag{7.2}$$

In this equation, $S_{ijk}(\mathbf{x}', \mathbf{x})$ and $D_{ijk}(\mathbf{x}', \mathbf{x})$ are linear combinations of derivatives of $T_{\alpha\beta}(\mathbf{x}', \mathbf{x})$ and $U_{\alpha\beta}(\mathbf{x}', \mathbf{x})$ respectively, as explained in chapter 4. The integrals in equation (7.2) are regular, provided $r \neq 0$. As the internal point approaches the boundary, that is as $\mathbf{x}' \rightarrow \mathbf{x}$, the distance r tends to zero and $S_{ijk}\left(\mathbf{x}', \mathbf{x}\right)$ exhibits a hypersingularity of the order $1/r^2$, while $D_{ijk}\left(\mathbf{x}', \mathbf{x}\right)$ exhibits a strong singularity of the order $1/r$. Assuming continuity of both strains and tractions at $\mathbf{x}'$, the limiting process produces improper integrals and jumps terms in strains and tractions, in the first and second integrals of equation (7.2), respectively. For a

point on a smooth boundary, these jump terms are equivalent to boundary stresses. Hence, equation above equation can now be written as:

$$\frac{1}{2}\sigma_{\alpha\beta} + \int_{\Gamma} S_{ijk}\left(\mathbf{x}', \mathbf{x}\right) u_k d\Gamma = \int_{\Gamma} D_{ijk}\left(\mathbf{x}', \mathbf{x}\right) t_k d\Gamma - \frac{1}{h}\int_{A} D_{ijk}\left(\mathbf{x}', \mathbf{x}\right) f_k dA \tag{7.3}$$

where the first integral stands for the Hadamard principal value integral and the second integral stands for the Cauchy principal value integral. On a smooth boundary, the traction components t_j, are given by:

$$\frac{1}{2}t_j(\mathbf{x}') + n_i(\mathbf{x}')\int_{\Gamma} S_{ijk}\left(\mathbf{x}', \mathbf{x}\right) u_k d\Gamma = n_i(\mathbf{x}')\int_{\Gamma} D_{ijk}\left(\mathbf{x}', \mathbf{x}\right) t_k d\Gamma - n_i(\mathbf{x}')\frac{1}{h}\int_{A} D_{ijk}\left(\mathbf{x}', \mathbf{x}\right) f_k dA \tag{7.4}$$

Above equation is known as hypersingular integral equation for plane elasticity. Equations (7.1) and (7.4) constitutes the basis of the dual Boundary element method (DBEM).

On a traction-free crack, for example, these equations are simplified; the displacement and the traction equations are given by:

$$\begin{aligned} c_{ij}(\mathbf{x}')u_\alpha + \int_{\Gamma} T_{\alpha\beta}\left(\mathbf{x}', \mathbf{x}\right) u_\beta d\Gamma &= -\frac{1}{h}\int_{A} U_{\alpha\beta}\left(\mathbf{x}', \mathbf{x}\right) f_\beta dA \\ n_i(\mathbf{x}')\int_{\Gamma} S_{ijk}\left(\mathbf{x}', \mathbf{x}\right) u_k d\Gamma &= -n_i(\mathbf{x}')\frac{1}{h}\int_{A} D_{ijk}\left(\mathbf{x}', \mathbf{x}\right) f_k dA \end{aligned} \tag{7.5}$$

where the line integrals are evaluated at the crack boundary.

7.2.1 Treatment of finite-part integrals

The improper integrals, that arise in the dual integral equations, are easily handled by the classical singularity-subtraction method (see Aliabadi, 1997). In the vicinity of a collocation node the regular part of the integrand is expressed as a Taylor's expansion. If a sufficient

number of terms of the expansion are subtracted from the original improper integral and then added back, the singularity can be isolated. The original improper integral is thus transformed into the sum of a regular integral and an integral of the singular function. This latter integral is then evaluated analytically, while standard Gaussian quadrature is used for numerical integration of the regular integral.

Consider a discontinuous quadratic boundary element of general shape, Γ_e, that contains the collocation node. The local parametric co-ordinate ξ is defined in the range $-1 \leq \xi \leq 1$ and the collocation node ξ' is mapped onto $\mathbf{x}'$, via the continuous element shape functions, as presented in chapter 5. The displacement components u_j, are approximated in the local co-ordinate by means of the nodal values, u_j^n, and the discontinuous element shape functions. The first-order finite-part integral of equation (7.5) can be expressed in the local co-ordinate as:

$$\int_{\Gamma_e} T_{\alpha\beta}\left(\mathbf{x}', \mathbf{x}\right) u_j\left(\mathbf{x}\right) d\Gamma = u_j^n \int_{-1}^{+1} \frac{f_{\alpha\beta}^n\left(\xi\right)}{\xi - \xi'} d\xi \tag{7.6}$$

where $f_{ij}^n(\xi)$ is a regular function, given by the product of the fundamental solution, a shape function and the Jacobian of the co-ordinate transformation, multiplied by the term $\xi - \xi'$. The integral of the right hand side of equation (7.6) can be transformed with the aid of the first term of a Taylor's expansion of the function $f_{ij}^n(\xi)$ around the collocation node, to give:

$$\int_{-1}^{+1} \frac{f_{\alpha\beta}^n\left(\xi\right)}{\xi - \xi'} d\xi = \int_{-1}^{+1} \frac{f_{\alpha\beta}^n\left(\xi\right) - f_{\alpha\beta}^n\left(\xi'\right)}{\xi - \xi'} d\xi + f_{\alpha\beta}^n\left(\xi'\right) \int_{-1}^{+1} \frac{d\xi}{\xi - \xi'} \tag{7.7}$$

Now, the first integral of the right hand side is regular and the second one can be integrated analytically to give:

$$\int_{-1}^{+1} \frac{d\xi}{\xi - \xi'} = \ln \left| \frac{1 - \xi'}{1 + \xi'} \right| \tag{7.8}$$

In equation (7.6), the existence of the finite-part integral requires the Hölder continuity of

f_{ij}^n, at the collocation node. For the discontinuous element, this requirement is automatically satisfied, because the nodes are internal points of the element, where f_{ij}^n is continuously differentiable.

The second order finite-part integral of equation (7.7) can be expressed in the local parametric co-ordinate as:

$$\int_{\Gamma_e} S_{ijk}\left(\mathbf{x}', \mathbf{x}\right) u_k\left(\mathbf{x}\right) d\Gamma = u_k^n \int_{-1}^{+1} \frac{g_{ijk}^n\left(\xi\right)}{\left(\xi - \xi'\right)^2} d\xi \tag{7.9}$$

where $g_{ijk}^n(\xi)$ is a regular function, given by the product of the fundamental solution, a shape function and the Jacobian of the co-ordinate transformation, multiplied by the term $(\xi - \xi')^2$. The integral on the right hand side of equation (7.9) can be transformed with the aid of the first and second terms if a Taylor's expansion of the density function g_{ijk}^n, in the neighborhood of the collocation node, to:

$$\begin{aligned} \int_{-1}^{+1} \frac{g_{ijk}^n\left(\xi\right)}{\left(\xi - \xi'\right)^2} d\xi = & \int_{-1}^{+1} \frac{g_{ijk}^n\left(\xi\right) - g_{ijk}^n\left(\xi'\right) - g_{ijk}^{n(1)}\left(\xi'\right)\left(\xi - \xi'\right)}{\left(\xi - \xi'\right)^2} d\xi \\ & + g_{ijk}^n\left(\xi'\right) \int_{-1}^{+1} \frac{d\xi}{\left(\xi - \xi'\right)^2} + g_{ijk}^{n(1)}\left(\xi'\right) \int_{-1}^{+1} \frac{d\xi}{\xi - \xi'} \end{aligned} \tag{7.10}$$

where $g_{ijk}^{n(1)}$ denotes the first derivative of g_{ijk}^n. At the collocation node the function g_{ijk}^n is required to have continuity of its second derivative or, at least, a Hölder-continuous first derivative, for the finite-part integrals to exist. This requirement is automatically satisfaced by the discontinuous element, since the nodes are internal points of the element. Now, in equation (7.10), the first integral on the right hand side is regular and the third integral is identical with one given in equation (7.8). The second integral on the right hand side of

equation (7.10) can be integrated analytically to give:

$$\int_{-1}^{+1} \frac{d\xi}{(\xi - \xi')^2} = -\frac{1}{1+\xi'} - \frac{1}{1-\xi'} \tag{7.11}$$

For piece-wise flat cracks, all the integrals in equation (7.6) and (7.9) are most effectively carried out by direct analytic integration. Consider a flat discontinuous quadratic boundary element. The shape functions of this element are given by equations (5.42) and presented here again:

$$\begin{aligned} \psi_1 &= \xi\left(\frac{9}{8}\xi - \frac{3}{4}\right) \\ \psi_2 &= \xi\left(1 - \frac{3}{2}\xi\right)\left(1 + \frac{3}{2}\xi\right) \\ \psi_3 &= \xi\left(\frac{9}{8}\xi + \frac{3}{4}\right) \end{aligned} \tag{7.12}$$

For this element, the integral of equation (7.6) is represented by

$$\int_{\Gamma_e} T_{\alpha\beta}\left(\mathbf{x}', \mathbf{x}\right) u_j\left(\mathbf{x}\right) d\Gamma = u_j^n \int_{-1}^{+1} T_{\alpha\beta}\left(\xi', \xi\right) \psi_n\left(\xi\right) J\left(\xi\right) d\xi = \mathbf{h}_i^n \mathbf{u}^n \tag{7.13}$$

where $\mathbf{u^n}$ denotes the nodal displacement components and $J(\xi)$ is the Jacobian of the co-ordinate transformation. Because of the assumed flatness of the element, $J = l_e/2$, where l_e represents the element length and the matrix $\mathbf{h^n}$ is given by

$$\mathbf{h}^n = \frac{1-2v}{4\pi\left(1-v\right)} \begin{bmatrix} 0 & -1 \\ +1 & 0 \end{bmatrix} \int_{-1}^{+1} \frac{\psi_n}{\xi - \xi'} d\xi \tag{7.14}$$

The first-order finite-part integrals are integrated analytically to give:

$$\int_{-1}^{+1} \frac{\psi_1}{\xi - \xi'} d\xi = \frac{3}{4}\left(\frac{\xi'\left(3\xi' - 2\right)}{2} \ln\left|\frac{1-\xi'}{1+\xi'}\right| + 3\xi' - 2\right)$$

$$\begin{aligned}
\int_{-1}^{+1} \frac{\psi_2}{\xi - \xi'} d\xi &= \frac{1}{2}\left(\frac{(3\xi'-2)(3\xi'+2)}{2} \ln\left|\frac{1+\xi'}{1-\xi'}\right| - 9\xi'\right) \\
\int_{-1}^{+1} \frac{\psi_3}{\xi - \xi'} d\xi &= \frac{3}{4}\left(\frac{\xi'(3\xi'+2)}{2} \ln\left|\frac{1-\xi'}{1+\xi'}\right| + 3\xi' + 2\right)
\end{aligned} \tag{7.15}$$

The integral of equation (7.9) is represented by:

$$\int_{\Gamma_e} S_{ijk}(\mathbf{x}', \mathbf{x})\, u_k(\mathbf{x})\, d\Gamma = u_k^n \int_{\Gamma_e} S_{ijk}(\xi', \xi)\, N_n(\xi)\, J(\xi)\, d\Gamma = \bar{\mathbf{h}}_{ij}^n \mathbf{u}^n \tag{7.16}$$

where the matrix $\bar{\mathbf{h}}^{\mathbf{n}}$ is given by

$$\bar{\mathbf{h}}^n = \frac{E}{4\pi(1-v^2)} \frac{2}{l_e} \mathbf{S}' \int_{-1}^{+1} \frac{\psi_n}{(\xi - \xi')} d\xi \tag{7.17}$$

The matrix $\mathbf{S}'$ is given by:

$$\mathbf{S}' = \begin{bmatrix} +n_1(2n_2^2+1) & -n_2(-2n_2^2+1) \\ +n_1(2n_1^2-1) & -n_2(-2n_1^2-1) \\ -n_2(2n_1^2-1) & +n_1(-2n_2^2+1) \end{bmatrix} \tag{7.18}$$

where n_1 and n_2 are the components of the unit outward normal to the element. The second-order finite-part integrals of equation (7.11) are integrated analytically to give:

$$\begin{aligned}
\int_{-1}^{+1} \frac{\psi_1}{(\xi - \xi')^2} d\xi &= \frac{3}{4}\left((3\xi'-1) \ln\left|\frac{1-\xi'}{1+\xi'}\right| + \frac{6\xi'^2 - 2\xi - 3}{\xi'^2 - 1}\right) \\
\int_{-1}^{+1} \frac{\psi_2}{(\xi - \xi')^2} d\xi &= \frac{1}{2}\left(9\xi' \ln\left|\frac{1+\xi'}{1-\xi'}\right| - \frac{18\xi'^2 - 13}{\xi'^2 - 1}\right) \\
\int_{-1}^{+1} \frac{\psi_3}{(\xi - \xi')^2} d\xi &= \frac{3}{4}\left((3\xi'+1) \ln\left|\frac{1-\xi'}{1+\xi'}\right| + \frac{6\xi'^2 + 2\xi - 3}{\xi'^2 - 1}\right)
\end{aligned} \tag{7.19}$$

7.3 Hypersingular formulation for Reissner plates

The stress resultant boundary integral equations are formed by considering the behavior of equations (5.48) as $\mathbf{x}$' approaches to boundary Γ. A semi-circular domain with boundary Γ^*, similar to that showed in figure 4.1, is constructed around the point $\mathbf{x}'$. Taking the limit as $\mathbf{x}'$ tends to Γ equations (5.48) can be written as follows:

$$\begin{aligned} M_{\alpha\beta}(\mathbf{x}') &+ \lim_{\varepsilon\to 0}\int_{\Gamma^*} P^*_{\alpha\beta\gamma}(\mathbf{x}',\mathbf{x})\, w_\gamma(\mathbf{x})\, d\Gamma + \lim_{\varepsilon\to 0}\int_{\Gamma^*} P^*_{\alpha\beta 3}(\mathbf{x}',\mathbf{x})\, w_3(\mathbf{x})\, d\Gamma \\ &= \lim_{\varepsilon\to 0}\int_{\Gamma^*} W^*_{\alpha\beta\gamma}(\mathbf{x}',\mathbf{x})\, p_\gamma(\mathbf{x})\, d\Gamma + \lim_{\varepsilon\to 0}\int_{\Gamma^*} W^*_{\alpha\beta 3}(\mathbf{x}',\mathbf{x})\, p_3(\mathbf{x})\, d\Gamma \\ &+ \frac{1}{h}\int_A W^*_{\alpha\beta 3}(\mathbf{x}',\mathbf{x})\, q_3 dA \end{aligned} \tag{7.20}$$

and,

$$\begin{aligned} Q_\beta(\mathbf{x}') &+ \lim_{\varepsilon\to 0}\int_{\Gamma^*} P^*_{3\beta\gamma}(\mathbf{x}',\mathbf{x})\, w_\gamma(\mathbf{x})\, d\Gamma + \lim_{\varepsilon\to 0}\int_{\Gamma^*} P^*_{3\beta 3}(\mathbf{x}',\mathbf{x})\, w_3(\mathbf{x})\, d\Gamma \\ &= \lim_{\varepsilon\to 0}\int_{\Gamma^*} W^*_{3\beta\gamma}(\mathbf{x}',\mathbf{x})\, p_\gamma(\mathbf{x})\, d\Gamma + \lim_{\varepsilon\to 0}\int_{\Gamma^*} W^*_{3\beta 3}(\mathbf{x}',\mathbf{x})\, p_3(\mathbf{x})\, d\Gamma \\ &+ \frac{1}{h}\int_A W^*_{3\beta 3}(\mathbf{x}',\mathbf{x})\, q_3 dA \end{aligned} \tag{7.21}$$

where: $\Gamma^* = \Gamma - \Gamma_\varepsilon + \Gamma^*_\varepsilon$. In the limits, the kernels exhibits different order of singularity. The terms $P^*_{\alpha\beta\gamma}, P^*_{3\beta 3}$ are hypersingular of $O(1/r^2 + ln(r))$, while $P^*_{\alpha\beta 3}, P^*_{3\beta\gamma}, W^*_{\alpha\beta\gamma}, W^*_{3\beta 3}$ are strong singular of $O(1/r)$. Other remaining terms, namely $W^*_{\alpha\beta 3}, W^*_{3\beta\gamma}$ are weakly singular.

To satisfy continuity requirements, the point $\mathbf{x}'$ is assumed to be on a smooth boundary. In the limiting process, some integrals in above equations lead to a jump on the stress resultants. Taking into account all the limits and the jump terms, as $\epsilon \to 0$, for a source point on a smooth boundary, stress resultant integral equations are obtained as follows (see

Dirgantara, 2000):

$$\begin{aligned}\frac{1}{2}M_{\alpha\beta}(\mathbf{x}') &+ \int_{\Gamma} P^*_{\alpha\beta\gamma}(\mathbf{x}',\mathbf{x})\, w_\gamma(\mathbf{x})\, d\Gamma + \int_{\Gamma} P^*_{3\beta 3}(\mathbf{x}',\mathbf{x})\, w_3(\mathbf{x})\, d\Gamma \\ &= \int_{\Gamma} W^*_{\alpha\beta\gamma}(\mathbf{x}',\mathbf{x})\, p_\gamma(\mathbf{x})\, d\Gamma + \int_{\Gamma} W^*_{\alpha\beta 3}(\mathbf{x}',\mathbf{x})\, p_3(\mathbf{x})\, d\Gamma \\ &+ \frac{1}{h}\int_{A} W^*_{\alpha\beta 3}(\mathbf{x}',\mathbf{x})\, q_3 dA \end{aligned} \tag{7.22}$$

and,

$$\begin{aligned}\frac{1}{2}Q_{\beta}(\mathbf{x}') &+ \int_{\Gamma} P^*_{3\beta\gamma}(\mathbf{x}',\mathbf{x})\, w_\gamma(\mathbf{x})\, d\Gamma + \int_{\Gamma} P^*_{3\beta 3}(\mathbf{x}',\mathbf{x})\, w_3(\mathbf{x})\, d\Gamma \\ &= \int_{\Gamma} W^*_{3\beta\gamma}(\mathbf{x}',\mathbf{x})\, p_\gamma(\mathbf{x})\, d\Gamma + \int_{\Gamma} W^*_{3\beta 3}(\mathbf{x}',\mathbf{x})\, p_3(\mathbf{x})\, d\Gamma \\ &+ \frac{1}{h}\int_{A} W^*_{3\beta 3}(\mathbf{x}',\mathbf{x})\, q_3 dA \end{aligned} \tag{7.23}$$

Multiplying equations (7.22) and (7.23) by the outward normal n_β at the source point $\mathbf{x}'$, the traction integral equations for shear deformable plates are obtained:

$$\begin{aligned}\frac{1}{2}p_{\alpha}(\mathbf{x}') &+ n_\alpha(\mathbf{x}')\int_{\Gamma} P^*_{\alpha\beta\gamma}(\mathbf{x}',\mathbf{x})\, w_\gamma(\mathbf{x})\, d\Gamma + n_\alpha(\mathbf{x}')\int_{\Gamma} P^*_{3\beta 3}(\mathbf{x}',\mathbf{x})\, w_3(\mathbf{x})\, d\Gamma \\ &= n_\alpha(\mathbf{x}')\int_{\Gamma} W^*_{\alpha\beta\gamma}(\mathbf{x}',\mathbf{x})\, p_\gamma(\mathbf{x})\, d\Gamma + n_\alpha(\mathbf{x}')\int_{\Gamma} W^*_{\alpha\beta 3}(\mathbf{x}',\mathbf{x})\, p_3(\mathbf{x})\, d\Gamma \\ &+ \frac{1}{h}n_\alpha(\mathbf{x}')\int_{A} W^*_{\alpha\beta 3}(\mathbf{x}',\mathbf{x})\, q_3 dA \end{aligned} \tag{7.24}$$

and,

$$\begin{aligned}\frac{1}{2}p_{3}(\mathbf{x}') &+ n_\alpha(\mathbf{x}')\int_{\Gamma} P^*_{3\beta\gamma}(\mathbf{x}',\mathbf{x})\, w_\gamma(\mathbf{x})\, d\Gamma + n_\alpha(\mathbf{x}')\int_{\Gamma} P^*_{3\beta 3}(\mathbf{x}',\mathbf{x})\, w_3(\mathbf{x})\, d\Gamma \\ &= n_\alpha(\mathbf{x}')\int_{\Gamma} W^*_{3\beta\gamma}(\mathbf{x}',\mathbf{x})\, p_\gamma(\mathbf{x})\, d\Gamma + n_\alpha(\mathbf{x}')\int_{\Gamma} W^*_{3\beta 3}(\mathbf{x}',\mathbf{x})\, p_3(\mathbf{x})\, d\Gamma \end{aligned}$$

$$+ \quad \frac{1}{h} n_\alpha (\mathbf{x}') \int_A W^*_{3\beta 3} (\mathbf{x}', \mathbf{x}) \, q_3 dA \tag{7.25}$$

The first integrals at left hand side of these equations are evaluated in the sense of Haddamard principal value and seconds are evaluated in the Cauchy principal value.

7.3.1 Treatment of singularities

In the traction integral equations, the singularity order is higher than the displacement integral equations. In the $[H]$ matrix, the kernels $P^*_{\alpha\beta\gamma}$ and $P^*_{3\beta\gamma}$ are strongly singular, whereas, the kernels $P^*_{\alpha\beta\gamma}$ and $P^*_{3\beta 3}$ are hypersingular. In the off-diagonal sub-matrices, the shape functions will reduce the order of singularity by one. This means that, elements entries in $[H]$ matrix corresponding to the kernels $P^*_{\alpha\beta 3}$ and $P^*_{3\beta\gamma}$ become smooth, whereas, elements of the kernels $P^*_{\alpha\beta\gamma}$ and $P^*_{3\beta 3}$ still remain strongly singular (Dirgantara, 2000).

In $[G]$ matrix, the off-diagonal sub-matrices are smooth again due to the shape functions reducing the order of singularity. The diagonal matrices, on the other hand, contain the kernels $W^*_{\alpha\beta 3}$ and $W^*_{3\beta\gamma}$ which are weakly singular and the $W^*_{\alpha\beta\gamma}$ and $W^*_{3\beta 3}$ which are strongly singular.

The singular integrals mentioned above are treated individually based on their order of singularity. The weak singularity is treated using a nonlinear coordinate transformation as in Telles, 1987. The strong-singular and the hypersingular integrals are evaluated using Taylor series expansion around the singular point as presented in section 7.2.1.

A special type of singularity of $O(1/r^2 + ln(r))$ if observed in the $P_{\alpha\beta\gamma}$ kernel. This type

of hypersingular integrals can be solved as follows:

$$\begin{aligned}
&\int_{\Gamma_e} P^*_{\alpha\beta\gamma}(\xi',\xi)\,\Phi^n(\xi)\,J(\xi)\,d\xi \\
&= \int_{-1}^{+1}\left[P^*_{\alpha\beta\gamma}(\xi',\xi)\,\Phi^n(\xi)\,J(\xi) - \frac{g^n_{\alpha\beta\gamma}(\xi') + g^{n'}_{\alpha\beta\gamma}(\xi')(\xi-\xi')}{(\xi-\xi')^2} - h^n_{\alpha\beta\gamma}(\xi')\ln|\xi-\xi'|\right]d\xi \\
&+ g^n_{\alpha\beta\gamma}(\xi')\int_{-1}^{+1}\frac{d\xi}{(\xi-\xi')^2} + g^{n'}_{\alpha\beta\gamma}(\xi')\int_{-1}^{+1}\frac{d\xi}{\xi-\xi'} + h^n_{\alpha\beta\gamma}(\xi')\int_{-1}^{+1}\ln|\xi-\xi'|\,d\xi
\end{aligned} \tag{7.26}$$

where $g^n_{\alpha\beta\gamma}(\xi) = P^{*1}_{\alpha\beta\gamma}(\xi',\xi)\,\Phi^n(\xi)\,J(\xi)\,(\xi-\xi')^2$ on which $P^{*1}_{\alpha\beta\gamma}(\xi',\xi)$ are part of the kernels which contain $1/r^2$. The term $h^n_{\alpha\beta\gamma}(\xi) = P^{*2}_{\alpha\beta\gamma}(\xi',\xi)\,\Phi^n(\xi)\,J(\xi)\Big/\ln|\xi-\xi'|$, and $P^{*2}_{\alpha\beta\gamma}(\xi',\xi)$ are part of the kernels which contain $\ln|\xi-\xi'|$. The functions $g^n_{\alpha\beta\gamma}(\xi)$ and $h^n_{\alpha\beta\gamma}(\xi)$ are regular and can be expanded in terms of a Taylor series expansion about the singular point ξ' as before.

The first integral on the right hand side of equation (7.26) us now regular, the second integral on the right hand side which is hypersingular can be solve analytically using equation (7.11), the third integral is identical with the one given in equation (7.7). The last integral on the right hand side which is weakly singular can be integrated analytically to give:

$$\int_{-1}^{+1}\ln|\xi-\xi'|\,d\xi = \ln|(\xi-\xi')(\xi+\xi')| - \xi'\ln\left|\frac{1-\xi'}{1+\xi'}\right| - 2 \tag{7.27}$$

Detailed derivation of $f^n_{\alpha\beta\gamma}(\xi)$, $g^n_{\alpha\beta\gamma}(\xi)$ and $h^n_{\alpha\beta\gamma}(\xi)$ can be found in Dirgantara, 2000.

7.4 The dual boundary element method

The necessary conditions for the existence of principal-value integrals, assumed in the derivation of the dual boundary integral equations, impose special restrictions on the crack modeling.

Consider that collocation is always done at the boundary element nodes. Under this circumstance, the finite-part integral of first order, in the displacement equations, requires continuity of the displacement components at the nodes: any continuous or discontinuous boundary element satisfies this requirement. In the tractions, the finite-part integral of second order requires continuity of the displacement derivatives at the nodes, on a smooth boundary: discontinuous quadratic boundary elements implicitly have the necessary smoothness, since the nodes are internal points of element.

For the sake of simplicity of the standard boundary elements, the present work uses discontinuous quadratic flat elements for the crack modeling. The general modeling strategy implemented in this work is based closely to that used by Dirgantara, 2000, and can be summarized as follows:

- (i) The crack boundaries are modeled with discontinuous quadratic flat elements.
- (ii) The displacement equations is applied for collocation on one of the crack surfaces
- (iii) The traction equations is applied for collocation on the opposite surface.
- (iv) discontinuous quadratic flat elements are used along the remaining boundary of the body.

7.5 Stress intensity factor evaluation

In this thesis the opening crack displacement extrapolation method is used to calculate the stress intensity factors (SIF's). The presence of distributed body forces in the region of the repair, turns the J-integral method unsuitable for the SIF's calculation. For plate problems in combine bending and plane tension, the stress intensity factors can be represented by

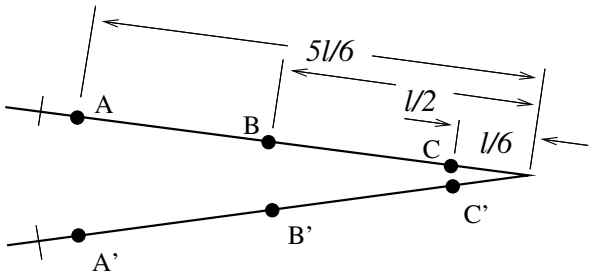

Figure 7.1: Crack tip element

superposition of five stress intensity factors, two due to membrane loads and three due to bending and shear loads. In this work, the stress resultant intensity factors for modes I, II and III are denoted by K_1, K_2 and K_3, respectively. Subscript m is added for stress intensity factors due to membrane loads, and subscript b is added for stress intensity factors due to bending and shear loads.

The displacements on the crack surfaces near the crack tip can be obtained as:

$$\begin{Bmatrix} \Delta\phi_2 \\ :\Delta\phi_1 \\ w_3 \\ u_2 \\ u_1 \end{Bmatrix} = \begin{Bmatrix} \phi_2 \\ \phi_1 \\ w_3 \\ u_2 \\ u_1 \end{Bmatrix}_{\theta=180^\circ} - \begin{Bmatrix} \phi_2 \\ \phi_1 \\ w_3 \\ u_2 \\ u_1 \end{Bmatrix}_{\theta=-180^\circ}$$

$$= \begin{bmatrix} \frac{48}{Eh^3}\sqrt{\frac{2r}{\pi}} & 0 & 0 & 0 & 0 \\ 0 & \frac{48}{Eh^3}\sqrt{\frac{2r}{\pi}} & 0 & 0 & 0 \\ 0 & 0 & \frac{24(1+v)}{5Eh}\sqrt{\frac{2r}{\pi}} & 0 & 0 \\ 0 & 0 & 0 & \frac{8}{Eh}\sqrt{\frac{2r}{\pi}} & 0 \\ 0 & 0 & 0 & 0 & \frac{8}{Eh}\sqrt{\frac{2r}{\pi}} \end{bmatrix} \begin{Bmatrix} K_{1b} \\ K_{2b} \\ K_{3b} \\ K_{1m} \\ K_{2m} \end{Bmatrix} \tag{7.28}$$

The stress resultant intensity factors can then be written in terms of displacements on

the crack surfaces as,

$$\{K\} = \frac{1}{\sqrt{r}}\mathbf{C}\{\Delta w\} \tag{7.29}$$

where,

$$K = \left\{ \begin{array}{c} K_{1b} \\ K_{2b} \\ K_{3b} \\ K_{1m} \\ K_{2m} \end{array} \right\} \quad \Delta\{w\} = \left\{ \begin{array}{c} \Delta\phi_2 \\ \Delta\phi_1 \\ w_3 \\ u_2 \\ u_1 \end{array} \right\} \tag{7.30}$$

and,

$$\mathbf{C} = \left[\begin{array}{ccccc} \frac{Eh^3}{48}\sqrt{\frac{\pi}{2}} & 0 & 0 & 0 & 0 \\ 0 & \frac{Eh^3}{48}\sqrt{\frac{\pi}{2}} & 0 & 0 & 0 \\ 0 & 0 & \frac{5Eh(1+v)}{24(1+v)}\sqrt{\frac{\pi}{2}} & 0 & 0 \\ 0 & 0 & 0 & \frac{Eh}{8}\sqrt{2\pi} & 0 \\ 0 & 0 & 0 & 0 & \frac{Eh}{8}\sqrt{2\pi} \end{array} \right] \tag{7.31}$$

When discontinuous elements are used for modeling crack surfaces, then at crack tip elements the distance of every node to the crack tip is given in (see figure 7.1). Hence,

$$\{K\}^{AA'} = \sqrt{\frac{6}{5l}}\mathbf{C}\left(\{w\}^{A} - \{w\}^{A'}\right)$$

$$\{K\}^{BB'} = \sqrt{\frac{2}{l}}\mathbf{C}\left(\{w\}^{B} - \{w\}^{B'}\right) \tag{7.32}$$

Then, SIF values are extrapolated to the crack tip using relationship (Dirgantara, 2000):

$$\{K\}^{tip} = \frac{r_{AA'}}{r_{AA'} - r_{BB'}}\left(\{K\}^{BB} - \frac{r_{BB'}}{r_{AA'}}\{K\}^{AA'}\right) \tag{7.33}$$

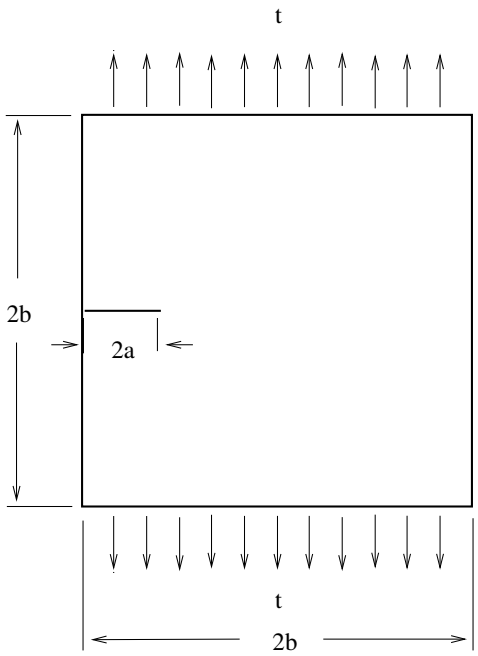

Figure 7.2: Sheet with border crack

7.6 Numerical examples

7.6.1 Square sheet with border crack

Consider a rectangular plate, with a single border crack as showed in figure (7.2). The crack length is noted by a, the width of the plate is b and the height is a. The plate is subjected to the action of a uniform traction t, symmetrically applied at ends. Five cases were considered, with $a/w = 0.2$, 0.3, 0.4, 0.5 and 0.6, respectively. Figure 7.3 shows a boundary element mode used. Table 10.1 shows the stress intensity factors in mode I obtained with a converged mesh containing 57 boundary elements, in which the crack was discretized with 7 quadratic discontinuous boundary elements on each surface. In this table, SIFs are compared with those reported by Portela and Aliabadi, 1992. Good agreement is obtained for a/w relations of 0.3, 0.4 and 0.5 when using the extrapolation technique for evaluate the K_I factor. Figure 7.3 shows the deformed geometry of the plate.

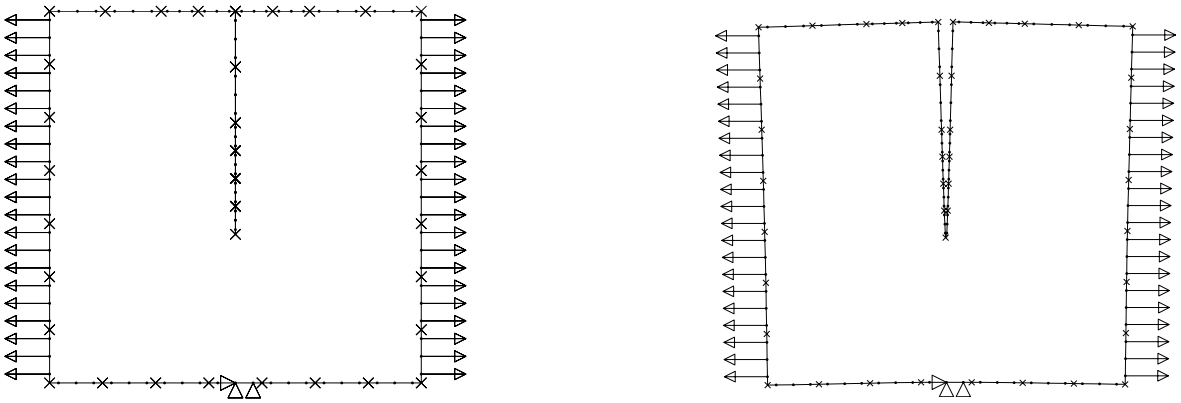

Figure 7.3: Boundary element mesh for border crack problem and deformed geometry

Table 7.1: KI stress intensity factor for square sheet with border crack

a/w	$K_I/(t.\sqrt{\pi a})$ **- Useche**	$K_I/(t.\sqrt{\pi a})$ **- Portela**	*% error*
0.2	1.607	1.618	0.68
0.3	2.016	2.014	0.10
0.4	2.511	2.537	1.02
0.5	3.275	3.292	0.52
0.6	4.528	4.558	0.66

7.6.2 Square sheet with central slant crack

A central slant crack in a rectangular plate is presented in figure 7.4. The plate is loaded with a uniform traction t, symmetrically applied at the ends. The ratio between the height and width of the plate is given by $h/w = 2$. The crack has the length $2a$ and makes an angle of $\Theta = 45°$ with the horizontal direction. A boundary element converged mesh of 50 quadratic elements was set up, in which 10 discontinuous elements were used on each side of the crack with ratios 0.2 to 0.6 (see in figure 7.5). The results obtained are presented in tables 7.2 and 7.3. As can be seen, high percentual errors for K_I and K_{II} were obtained when compared with theoretical values given by Portela and Aliabadi, 1992.

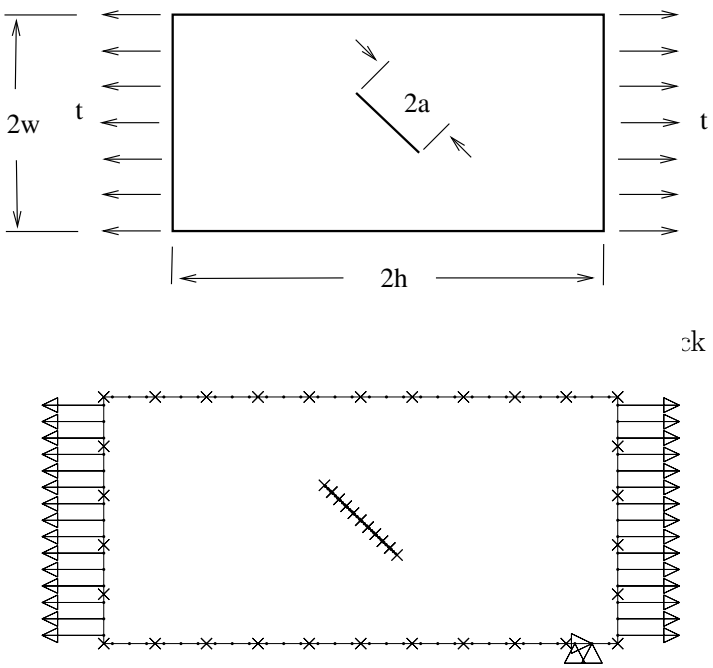

Figure 7.5: DBEM model for rectangular sheet with central slant crack

7.6.3 Plate with a center crack loaded by bending and tension

A rectangular plate with a central crack loaded by edge bending and tension is analyzed (see figure 7.6. The properties of the plate are: $b/h = 2$; $c/b = 2$; $M_o = 1.0$; $t = 1.0$,$E = 210000$ and $\nu = 0.3$. For DBEM analysis, 32 boundary elements for plate border and 16 discontinuous quadratic elements for each faces of the crack has been used (see figure 7.7). Table 7.4 shows SIF for K_{1b} factor for different a/b relations. The DBEM results show good agreement when compared with those obtained by Dirgantara, 2000. Bending deflection distribution is showed in figure 7.7.

Table 7.2: KI stress intensity factor for square sheet with central slant crack

a/w	$K_I/(t.\sqrt{\pi a})$ **- Useche**	$K_I/(t.\sqrt{\pi a})$ **- Portela**	*% error*
0.2	0.529	0.531	0.377
0.3	0.552	0.554	0.361
0.4	0.586	0.588	0.340
0.5	0.630	0.632	0.316
0.6	0.686	0.686	0.000

Table 7.3: KII stress intensity factor for square sheet with central slant crack

a/w	$K_{II}/(t.\sqrt{\pi a})$ **- Useche**	$K_{II}/(t.\sqrt{\pi a})$ **- Portela**	*% error*
0.2	0.517	0.519	0.385
0.3	0.526	0.528	0.380
0.4	0.539	0.541	0.370
0.5	0.556	0.558	0.360
0.6	0.577	0.579	0.345

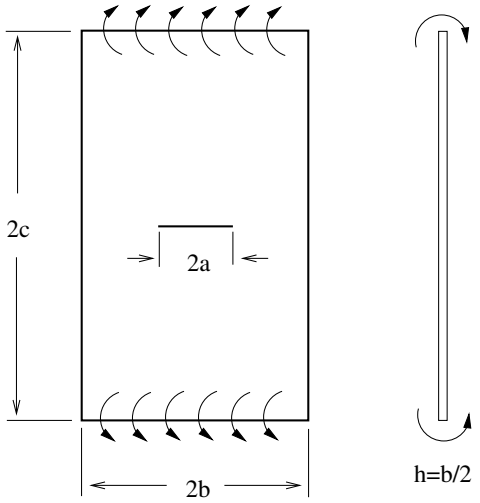

Figure 7.6: Rectangular plate with central crack

Table 7.4: K_{1b} stress intensity factor for rectangular plate with central crack

a/b	$K_{1b}/M_o\sqrt{\pi a}$ **- Useche**	$K_{1b}/M_o\sqrt{\pi a}$ **- Dirgantara**	**% error**
0.1	0.993	0.995	0.20
0.2	0.992	0.990	0.20
0.4	0.845	0.850	0.59
0.6	0.095	0.100	0.50
0.8	0.134	0.135	0.74

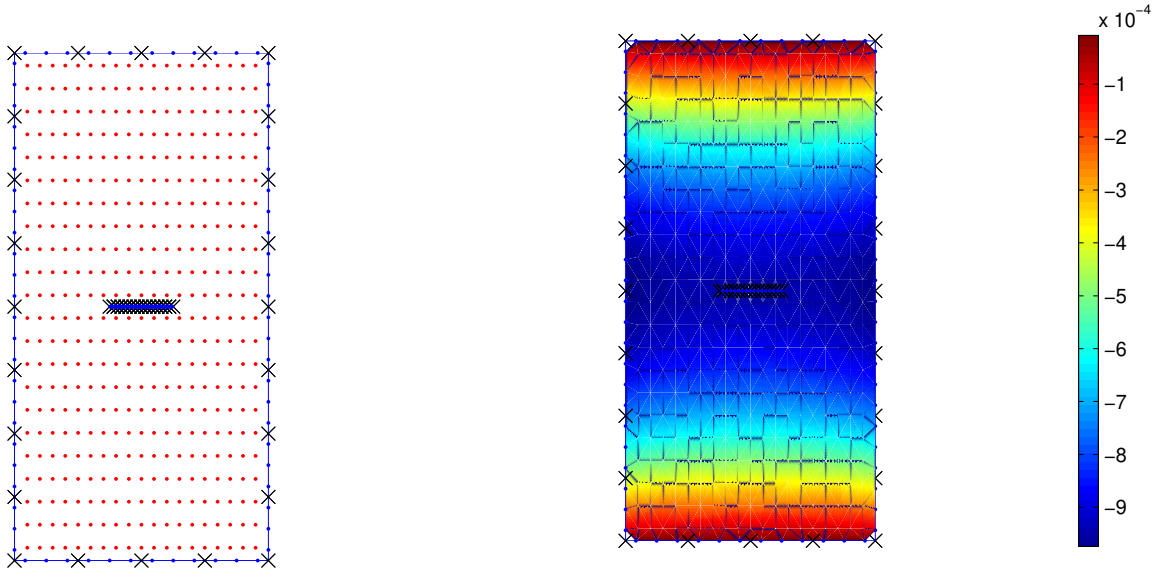

Figure 7.7: DBEM model for rectangular plate with central crack

7.6.4 Square plate with a center crack: uniform pressure

A simply supported square plate with a central crack loaded by uniform pressure $p_o = 1.0$ is analyzed. The properties of the plate are: $b = 1$; $b/h = 2$; $E = 1000$ and $\nu = 0.3$. DBEM contains 4 elements per side of the plate and 16 elements for each crack surface as shown in figure 7.8. Table 7.5 shows SIF for K_{1b} factor for different a/b relations. DBEM results show good agreement when compared with those obtained by Dirgantara, 2000. Bending deflection distribution is showed in figure 7.9 and figure 7.10 compares bending deflection along $y-$axis with deflection calculated using the Kirchhoff plate theory without crack.

Table 7.5: K_{1b} stress intensity factor for square plate with central crack

a/b	$K_{1b}/p_o b^2\sqrt{\pi a}$ **- Useche**	$K_{1b}/p_o b^2\sqrt{\pi a}$ **- Dirgantara**	**% error**
0.1	0.149	0.150	0.67
0.2	0.139	0.138	0.72
0.4	0.120	0.119	0.84
0.6	0.099	0.098	1.02
0.8	0.061	0.060	1.67

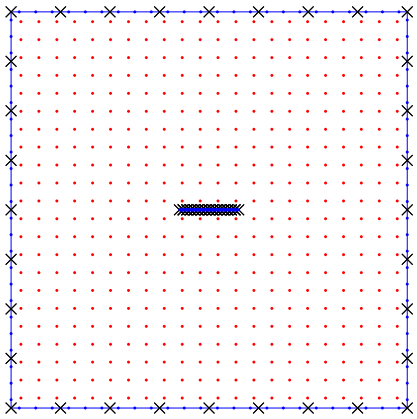

Figure 7.8: DBEM for Simply supported square plate with a central crack

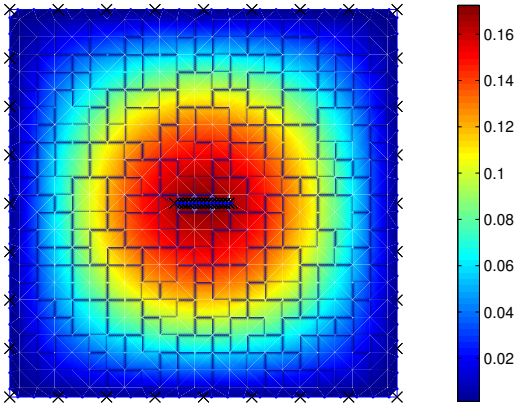

Figure 7.9: Displacement distribution for a square plate with a central crack

7.7 Conclusions

The Dual Boundary Element Method applied to plate fracture analysis considering membrane, bending moments and shear forces was presented. The hypersingular equations for plane elasticity and Reissner plate bending were establish for in-plane and plate bending problems. Types of singulars appearing in the traction equations has been identify and the

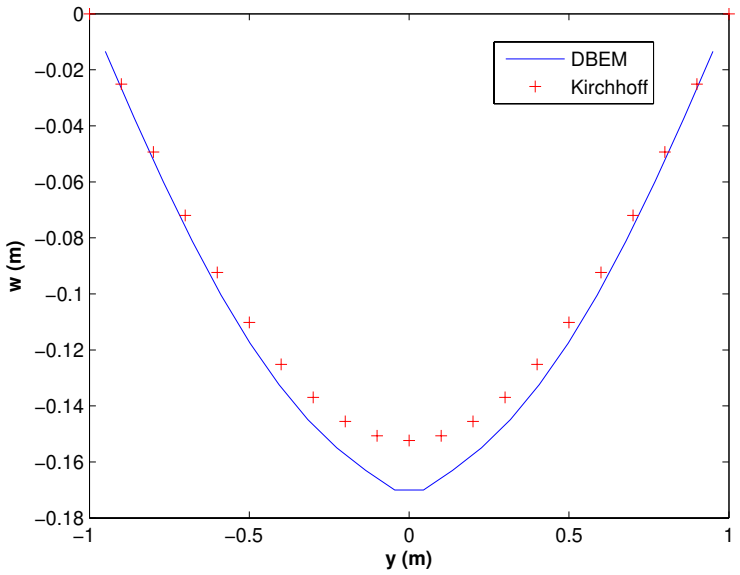

Figure 7.10: Displacement along y-axis ($x = 0$) for a square plate with a central crack

Taylor series expansion methodology has been presented to threated it. A general methodology for application of the dual boundary element method was presented. Numerical examples shows a good agreement for SIF's calculated with those reported in the literature.

Chapter 8

Mechanics of Bonded repairs

8.1 Introduction

This chapter presents the mechanics of bonded repairs, with emphasis in those analytical models used at present to design and evaluation of composite repairs. Due to the laminate structure of bonded repairs, which involve bonding orthotropic composite patches to cracked plates using polymeric adhesives, the stress states that exists in a bonded repair are very complex (see Rose and Wang, 2002). Their primary function is to sufficiently reduce the stress-intensity factor of the crack being repaired so that (1) the residual strength has been restored to an acceptable level, and (2) the growth rate of the crack under fatigue condition is sufficiently slow to ensure and an acceptable residual life. Therefore, the stress-intensity factor of a repaired is a predominant variable in design and evaluation of repairs. Since a bonded repair may fail in a number of modes, such as failure of the adhesive layer, failure of the plate near the termination of the patch, and failure of the patch, analytical formulas for stress-intensity factor calculation and the maximum shear stress in the adhesive are established in this chapter.

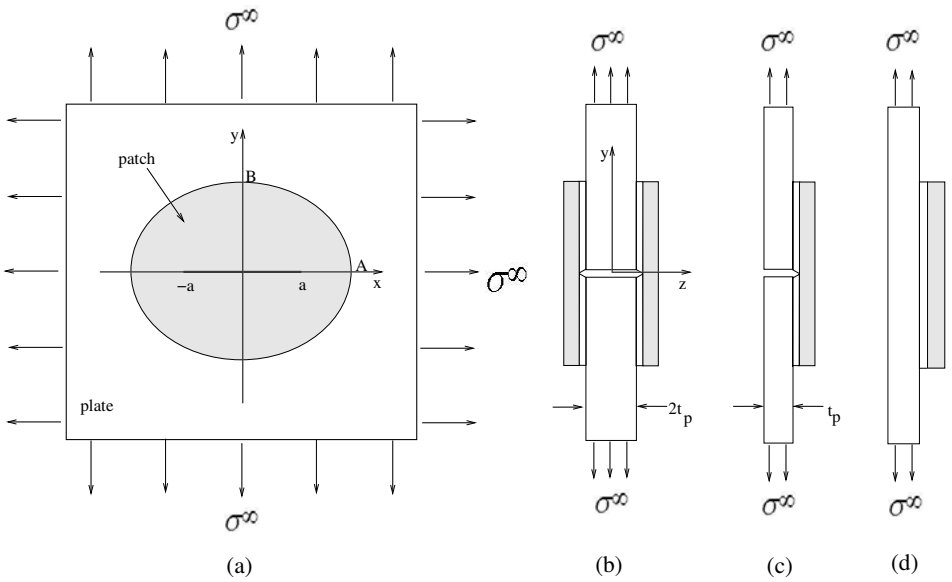

Figure 8.1: Repair configurations and coordinates. (a) Plan view, (b) Cross section along zy-plane, (c) one-side repair, (d) plate without crack with repair

8.2 Mechanics of the repair

The problem to be considered in this work, is a cracked plate with a patch adhesively bonded (see figure 8.1). The plate, which has a thickness of t_p contains a through-thickness crack of length $2a$. The thickness of the patch and the adhesive layer are respectively t_R and t_A. The cross sections in the yz and xz planes are depicted in figures 7.2(b) and (c). The Young modulus and the Poisson's ratio of each individual layer are denoted as E and v; Here and in the following subscripts P, R and A refers to distinguish properties pertaining respectively to the plate, the reinforcement and the adhesive layer. In addition, the shear modulus of the adhesive will be denoted as μ_A. The crack is along the line segment $|a| \leq a, y = 0$, and patch is over an elliptical region defined by,

$$\left(\frac{x}{A}\right)^2 + \left(\frac{y}{B}\right)^2 \leq 1 \tag{8.1}$$

which completely covers the crack ($A > a$). After this repair, the plate is subjected to a remote stress specified by,

$$\sigma_{yy}^{P} = \sigma^{\infty}, \quad \sigma_{xx}^{P} = \lambda\sigma^{\infty}, \quad \tau_{xy}^{P} = \tau^{\infty}, \quad (x^2 + y^2 \to \infty) \tag{8.2}$$

From a geometrical consideration, bonded repairs fall into two categories: two-sided (symmetric) and one-sided (asymmetric) (Rose and Wang, 2002). In the former case two identical reinforcements are bonded on the two surfaces of a cracked plate. This symmetric arrangement ensures that there is no out-of-plane deflection over the repaired region, provided that the cracked plate is subjected to extensional loads. In actual repairs, however, one-side repair is often adopted in which composite patches are applied to only one side of the plate.

The displacement of two coincident points at the plate and the patch have to be compatible with the shear deformation of the attachment (Salgado, 1998). Two different approaches have been used for the evaluation of the attachment shear flexibility. The first, which is the most widely used, is to neglect the shear deformation of the sheet and patch and assume the shear deformation of the adhesive layer to be uniform through its thickness, as showed in figure (8.2). The second approach is to assume that the sheet and patch deform linearly in shear and that this deformation contributes to the shear flexibility of the bonded structure. Considering that the shear deflection takes place predominantly in the adhesive layer and that the shear deflection of the sheet and patch is only significant near the interfaces, in this work, the shear deflection of the sheet and patch are neglected.

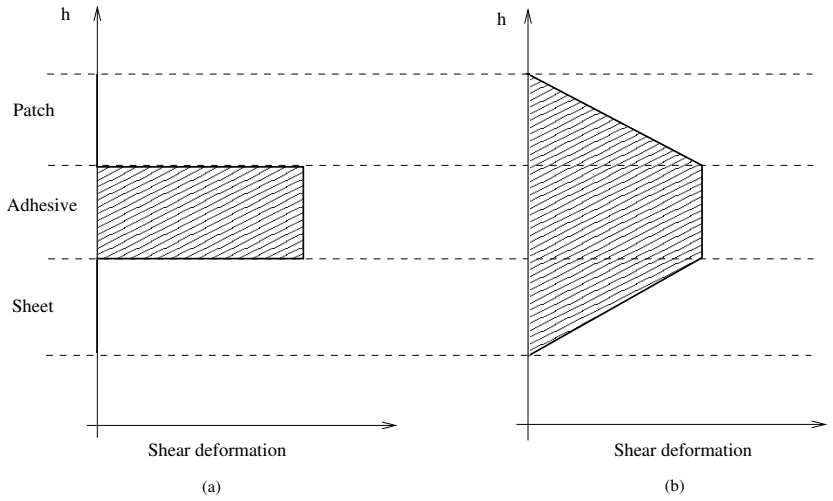

Figure 8.2: Left: Constant shear deformation approach. Right: Linear variation shear deformation approach

8.3 Load transfer of bonded reinforcement for plane stress problems

8.3.1 Uncracked sheet with isotropic patch

Consider the simple reinforcement configuration shown in figure (8.3), in which a reinforcing strip of length $2B$ and thickness t_R bonded to an infinite strip of thickness t_P; both strips are under plane strain conditions. The stresses and displacements in this reinforced can be calculated explicitly using the conventional 1D theory of bonded joints, which is based on the following assumptions:

1. Sheet and patch is treated as an elastic continuum whose deformation under plane strain conditions is specified by longitudinal displacement u and a longitudinal tensile stress σ^{∞} (see figure (8.3)). The stress-displacement relations for the plate and the reinforcement

respectively are:

$$\begin{aligned} \sigma_p &= \frac{E_p}{1-v_p^2}\frac{du_p}{dy} \\ \sigma_R &= \frac{E_R}{1-v_R^2}\frac{du_R}{dy} \end{aligned} \tag{8.3}$$

2. The adhesive layer acts as shear spring with the adhesive shear stress τ_A given by:

$$\tau_A = \mu_A \frac{u_R - u_p}{h_A} \tag{8.4}$$

3. The shear traction exerted by the adhesive on the plate and the reinforcement ca be replaced by an equivalent body force of Y_p and Y_R, respectively:

$$\begin{aligned} Y_P &= \frac{\tau_A}{h_p} \\ Y_R &= -\frac{\tau_A}{h_R} \end{aligned} \tag{8.5}$$

In the present case, using the above equations, the equilibrium equation for the shear stress can be written as:

$$\frac{d^2\tau_A}{dx^2} - \beta^2\tau_A = 0 \tag{8.6}$$

where:

$$\beta^2 = \frac{\mu_A}{h_A}\left[\frac{1-v_P^2}{E_P h_P} + \frac{1-v_R^2}{E_R h_R}\right] \tag{8.7}$$

The solution of this equation is given by (Rose and Wang, 2002):

$$\tau_A = -\sigma^\infty \frac{\left(1-v_p^2\right)\mu_A}{\beta h_A E_P \cosh(\beta B)} \sinh(\beta y) \tag{8.8}$$

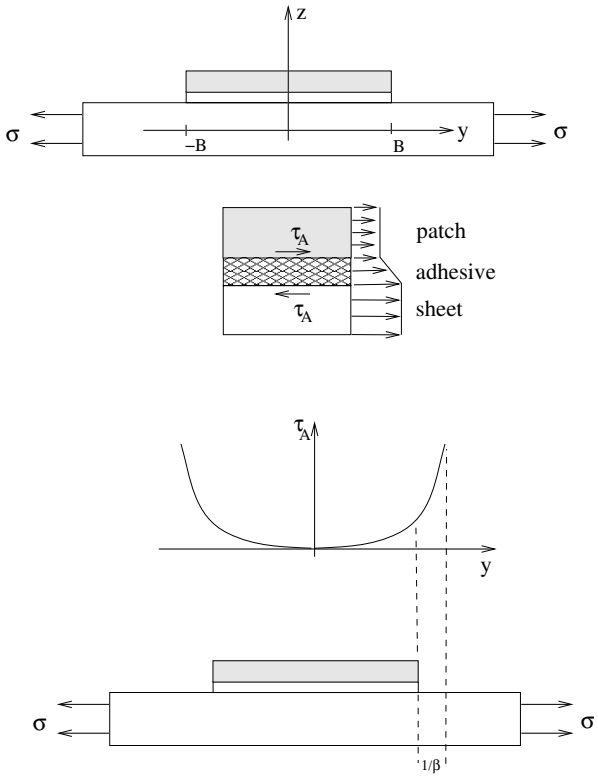

Figure 8.3: Load transfer of bonded reinforcement in uncracked sheet

This results reveals that for $\beta B << 1$, the adhesive shear stress decays exponentially from ends ($y = \pm B$) of the overlap, as showed in figure 8.3; i.e., the load transfer effectively occurs over a length of order β^{-1} at the ends of the overlap.

8.3.2 Load transfer in cracked sheet

Once the stress at the prospective crack location in known, one can proceed to *cut* the sheet along the line segment ($|x| \leq a, y = 0$) and a pressure equal to σ_0 is applied internally to the faces of this cut to make these faces stress-free. Provided that the load transfer to the reinforcement under this condition takes place in the intermediate neighborhood of the crack, the reinforcement may be assumed to be infinite extent. Using this condition, the solution

to the equation (7.4) is given by:

$$\tau_A = \beta h_P \sigma_0 e^{-\beta y} \tag{8.9}$$

For symmetric repairs or when the repaired structure is supported against out-of-plane bending, σ_0 is given by:

$$\sigma_0 = \frac{1}{Z}\left[4 + 2\frac{B}{A} + 2\frac{A}{B} + S\left(3 + v + 2\frac{B}{A}\right) + S\lambda\left(1 - v - 2v\frac{B}{A}\right)\right]\sigma^{\infty} \tag{8.10}$$

where:

$$Z = 3\left(1+S\right)^2 + 2\left(1+S\right)\left(B/A + A/B + vS\right) + 1 - v^2S^2 \tag{8.11}$$

It is important to recall that the idealization used to find σ_0 relies on β^{-1} and considering that the repair has elliptical form.

Finally, the stress intensity factor limit for cracked sheet with semi-infinite crack is obtained using the strain-energy release rate G_{inf} as Rose and Wang, 2002 shown:

$$K_{\infty} = \frac{\sigma_0}{k} = \frac{\sigma_0}{\sqrt{\frac{S\beta}{(1+S)\left(1-v_p^2\right)}}} \tag{8.12}$$

For the crack with finite size, K_r depends on the crack length and varies between the lower-bound $K_0 = \sigma_0\sqrt{\pi a}$ and the upper bound $K_{\infty} = \sigma_0/\sqrt{k}$. In general the stress-intensity factor K_r can be expressed as,

$$K_r = F\sigma_0\sqrt{\pi a} \tag{8.13}$$

The reduction factor F depends strongly on the parameter k and to a lesser extent on the stiffness ratio S. The following interpolation function is proposed by Rose and Wang, 2002:

$$F\left(ka\right) = \left[\frac{1}{\pi ka}\tanh\left(\frac{\pi ka}{1 + B\pi ka}\right)\right]^{1/2} \tag{8.14}$$

where constant B takes value of 3.0 for balanced repairs ($S = 1.0$) and 0.1 for infinitely-rigid patch ($S \to \infty$).

8.3.3 Cracked sheet with orthotropic patch

Similar to the previous case, the problem of estimating the reduction in the crack extension force when a cracked sheet is repaired by reinforcing orthotropic patches, starting with an uncracked plate and finding the prospective stress at the crack's location. In a second step, a crack is introduced into reduced stress field and a new stress field is founded. Similar equations to the previous ones are obtained for orthotropic repairs, to calculate shear stress distribution and K_∞, as presented in Rose and Wang, 2002. Since this formulation is very involved, an approximate solution for K_∞ is proposed:

$$K_\infty = \sigma_0 \sqrt{\pi\lambda} \tag{8.15}$$

where,

$$\sigma_0 = \frac{\sigma E_P t_P}{(E_P t_P + E_R t_R)} \tag{8.16}$$

$$\pi\lambda = \sqrt{\frac{E_P t_P}{\beta\left(1 + \frac{E_P t_P}{E_R t_R}\right)}} \tag{8.17}$$

$$\beta = \frac{\left(\frac{t_A}{G_A} + \frac{t_R}{3G_R} + \frac{t_P}{3G_P}\right)}{\left(\frac{t_A}{G_A} + \frac{3t_R}{8G_R} + \frac{3t_P}{8G_P}\right)^2} \tag{8.18}$$

8.4 Bonded reinforcement for plate bending problems

8.4.1 Uncracked plate analysis

The preceding analysis is valid only when the tendency of out-of-plane bending is neglected as in the case of symmetric repairs or one-side repairs to fully supported structures (Rose and Wang, 2002).

For the case of unsupported one-side repairs, stress distribution in the plate and the reinforcement can be determinated using the conventional theory of cylindrical bending of plates. The position of the neutral plane of the composite plate consisting of the plate and rigidly-bonded reinforcement is denoted by $\bar{z}$ (see figure 8.4):

$$\bar{z} = \frac{S\left(t_P + t_R + 2t_A\right)}{2\left(1+S\right)} \tag{8.19}$$

The moment of inertia of the reinforced region I_t is,

$$I_t = I_P + I_R \frac{E'_R}{E'_p} \tag{8.20}$$

where E' refers to the plane-strain Young's modulus ($E' = E/(1-\nu^2)$), and,

$$I_P = \frac{t_P^3}{12} + t_p \bar{z}^2 \tag{8.21}$$

$$I_R = \frac{t_R^3}{12} + \frac{t_R\left(t_P + t_R - 2\bar{z}\right)^2}{4} \tag{8.22}$$

The stress distribution in the patched plate is assumed to be linear in the thickness direction, so that it can be specified in terms of the membrane force N_0 and a bending

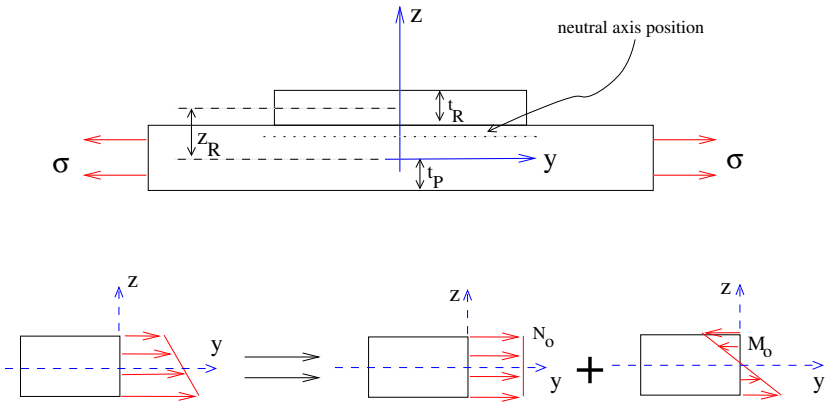

Figure 8.4: Stress distribution in an uncracked plate reinforced with a patch

moment M_0 per unit length in the direction x, as showed in figure 8.5:

$$N_0 = \frac{\sigma^{\infty} t_P}{1+S} + \frac{\sigma^{\infty} t_P^2 \bar{z}^2}{I_t} \tag{8.23}$$

$$M_0 = \frac{\sigma^{\infty} t_P^4 \bar{z}}{12 I_t} \tag{8.24}$$

First equation shows that the plate in a one-side repair is transferring more membrane stress than in an equivalent two-sided repairs. In addition, there is a bending moment acting on the prospective crack faces (see Rose and Wang, 2002). Consequently, due to the shift neutral plane, one-side repairs would experience not only an increase in the net force that the plate is transmitting, but also a secondary bending moment; both contributing to a considerable increase in stress-intensity factor (see figure 8.5).

8.4.2 Cracked plate analysis

The analysis of the stress-intensity factor for a cracked plate requires the use of the shear deformation theory, which yields that this factor varies linearly through the plate thickness:

$$K(z) = K_{mean} + K_b \frac{2z}{t_P} \tag{8.25}$$

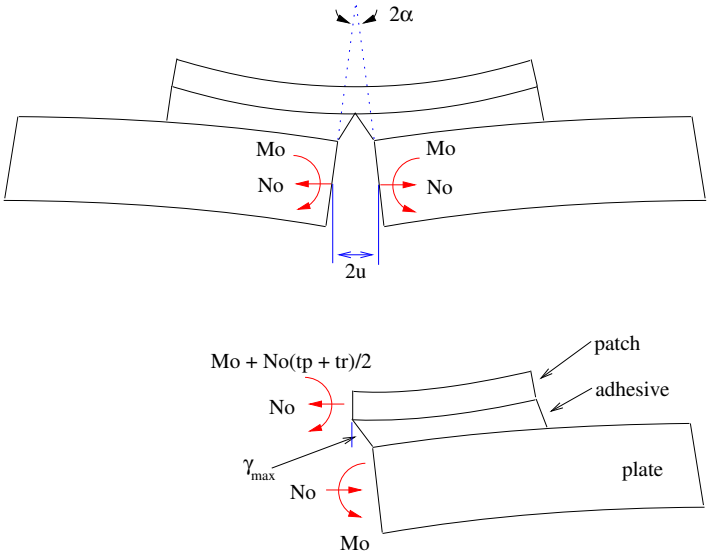

Figure 8.5: One-sided patch subjected to membrane tension and bending moment

where K_{mean} and K_b denotes the membrane and bending stress intensity factors, respectively. As in the case of plane stress problems, these factors can be founded using the strain-energy release rate approach, to obtain:

$$K_{rms}(a) = \frac{\sigma^{\infty}}{1+S}\sqrt{\pi a}F(k^{*}a) \tag{8.26}$$

where $k^{*} = k/w^{2}$, with:

$$w^{2} \approx 2 + \frac{3t_P}{2t_R} + \frac{3\beta t_P}{\kappa t_R}\left(1+\frac{t_P}{t_R}\right) + (1+S)\left(2+\frac{3t_P}{2t_R}\right)\frac{\bar{z}^{2}t_P}{I_t} \tag{8.27}$$

$$+ \quad (1+S)\frac{\beta}{\kappa}\left(1+\frac{t_P}{t_R}\right)\frac{\bar{z}^{3}t_P}{t_R I_t}\left(\frac{3\bar{z}}{t_P}-1\right) \tag{8.28}$$

and,

$$\kappa^{4} = \frac{3E_A^{'}}{t_A}\left[\frac{1}{E_P^{'}t_P^{3}} + \frac{1}{E_R^{'}t_R^{3}}\right] \tag{8.29}$$

K_{rms} is the root-mean-square stress-intensity factor, that is related to K_{mean} and K_b, as,

$$K_{rms}^2 = K_{mean}^2 + \frac{1}{3}K_b^2 \tag{8.30}$$

Finally, the root-mean-square stress-intensity factor $K_{RMS\infty}$ is given by:

$$K_{\infty,RMS} = \frac{\sigma^\infty}{1+S}\frac{w}{\sqrt{k}} \tag{8.31}$$

8.5 Conclusions

In this chapter, the mechanics of bonded repairs and the analytical models used to design and evaluation of composite repairs was presented. Kinematic models, for coupling actions between plate and repairs, through the mechanical analysis of adhesive layer were showed. Formulas for the calculation of shear stress distribution in the adhesive layer and the upper bound for stress intensity factor for cracked plates repaired with isotropic and orthotropic adhesive repairs, considering in-plane and out-of-plane problems, were presented.

Chapter 9

Boundary element analysis of cracked sheets repaired with bonded anisotropic patches

9.1 Introduction

A boundary element formulation for the analysis of isotropic cracked sheets, repaired with adhesively bonded anisotropic patches is presented. The sheet and the patch are modeled using the boundary element method. The crack in the isotropic sheet is modeled using the dual boundary element method. The interaction between the isotropic sheet and the patch is modeled considering shear body forces uniformly distributed on the interaction zone using a linear elastic relationship. Two different techniques are used in the present boundary element implementation to treat the domain integrals that arise in the formulation due to shear interaction forces. These techniques are the cell domain integration and the dual reciprocity boundary element method. The current work analyze a composite repair patch adhesively bonded in a metallic cracked sheet. The DBEM is used to model the isotropic cracked sheet and the BEM is used to model the anisotropic composite patch. The interaction loading

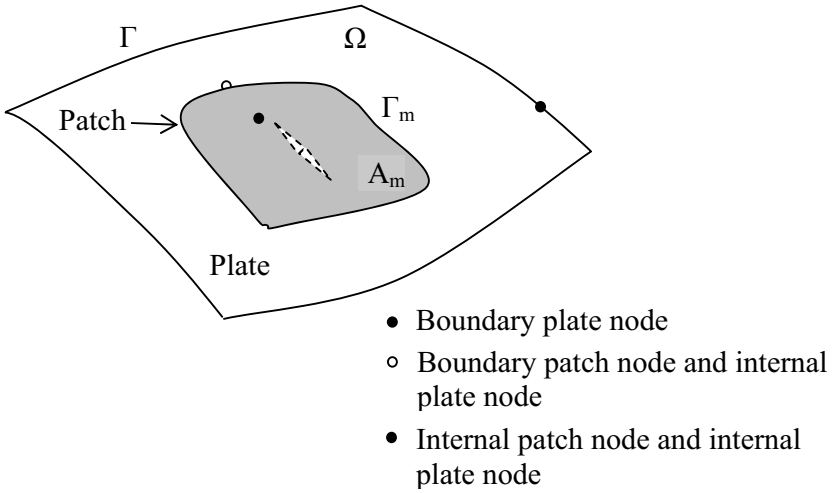

Figure 9.1: Cracked sheet repaired with adhesive patch

between the sheet and the patch is modeled considering the shear forces in the adhesive layer uniformly distributed using a linear elastic relationship. Two different techniques are used to treat domain the integrals that arise in the formulation due to the interaction shear forces: the cell domain integration and the DRBEM. Numerical examples of the adhesive stress analysis in cracked plate, repaired with a circular and rectangular composite patches, are presented.

9.2 Boundary element formulation

Figure 9.1 presents a finite isotropic sheet, containing an inner crack and an adhesive patch. In this case, the interaction forces can be treated as unknown body forces exchanged by the sheet and the patch in the attachment sub-region. Considering that the sheet and the patch remain flat after deformation, the two-dimensional elasticity theory can be used to model this problem. In this case, displacements at the sheet and at the patch have to be compatible with the shear deformation of the adhesive layer connecting them.

When the sheet is deformed due to applied loads on its boundaries, interaction forces

occur between the sheet, with contour Γ_S, and the repair patch, with contour Γ_R. In this two-dimensional case, interaction forces in the plate directly underneath the repair patch, and in the patch itself, can be treated as unknown body forces (action-reaction pair). As presented in chapters 3 and 4, for plane elasticity the boundary integral equation for the displacement of a source point **x'** on the sheet is given by:

$$c_{ij}^{S}\left(\mathbf{x}'\right)u_{j}^{S}\left(\mathbf{x}'\right)+\int_{\Gamma_S}T_{ij}^{*S}\left(\mathbf{x}',\mathbf{x}\right)u_{j}^{S}\left(\mathbf{x}\right)d\Gamma=\int_{\Gamma_S}U_{ij}^{*S}\left(\mathbf{x}',\mathbf{x}\right)t_{j}^{S}\left(\mathbf{x}\right)d\Gamma+\frac{1}{h_S}\int_{\Omega_R}U_{ij}^{*S}\left(\mathbf{x}',\mathbf{x}\right)f_{j}^{S}\left(\mathbf{x}\right)d\Omega_R \qquad i,j=1,2 \tag{9.1}$$

where c_{ij}^{S} is a coefficient which depends on the position of the source point in relation to the boundary of the sheet Γ_S; $U_{ij}^{*S}(\mathbf{x}',\mathbf{x})$ and $T_{ij}^{*S}(\mathbf{x}',\mathbf{x})$ are the Kelvin's isotropic fundamental solutions for displacements and tractions, respectively, for the two-dimensional sheet media; u_j^S and t_j^S are the displacements and tractions vectors at the boundary of the sheet; f_j^S are the interaction forces exchanged between the sheet and the patch in the domain Ω_R of the patch; and h_S is the thickness of the sheet.

Similarly, the displacement of a source point $\mathbf{x}'$ on the repair is given by (see chapters 3 and 4):

$$c_{ij}^{R}\left(\mathbf{x}'\right)u_{j}^{R}\left(\mathbf{x}'\right)+\int_{\Gamma}T_{ij}^{*R}\left(\mathbf{x}',\mathbf{x}\right)u_{j}^{R}\left(\mathbf{x}'\right)d\Gamma=\int_{\Gamma}U_{ij}^{*R}\left(\mathbf{x}',\mathbf{x}\right)t_{j}^{R}\left(\mathbf{x}'\right)d\Gamma+\frac{1}{h_R}\int_{\Omega_R}U_{ij}^{*R}\left(\mathbf{x}',\mathbf{x}\right)b_{j}^{R}\left(\mathbf{x}'\right)d\Omega_R \qquad i,j=1,2 \tag{9.2}$$

where c_{ij}^{R} is a coefficient which depends on the position of the source point in relation to the boundary of the sheet Γ_R; $U_{ij}^{*R}(\mathbf{x}',\mathbf{x})$ and $T_{ij}^{*R}(\mathbf{x}',\mathbf{x})$ are anisotropic fundamental solutions for the two-dimensional composite repair; u_j^R and t_j^R are the displacements and tractions vectors at the boundary of the repair; b_j^R are the interaction forces exchanged between the

sheet and the patch in the domain Ω_R of the patch; and h_R is the thickness of the sheet.

The crack in the isotropic sheet was modeled using the DBEM. The traction integral equation is applied in one of the crack faces and the displacement integral equation is applied in the other crack face. As showed in chapter 7, the traction integral equation is given by:

$$\frac{1}{2}t_j^S(\mathbf{x}') + n_i(\mathbf{x}') \int_{\Gamma_S} S_{ijk}^{*S}(\mathbf{x}', \mathbf{x}) u_j^S(\mathbf{x})\, d\Gamma = n_i(\mathbf{x}') \int_{\Gamma_S} D_{ijk}^{*S}(\mathbf{x}', \mathbf{x})\, t_j^S(\mathbf{x})\, d\Gamma + \frac{1}{h_S} \int_{\Omega_R} D_{ijk}^{*S}(\mathbf{x}', \mathbf{x})\, b_j^S(\mathbf{x})\, d\Omega_R \qquad i, j = 1, 2 \tag{9.3}$$

where $S_{ijk}^{*S}(\mathbf{x}', \mathbf{x})$ and $D_{ijk}^{*S}(\mathbf{x}', \mathbf{x})$ are linear combinations of derivatives of fundamentals solutions for traction and displacement $T_{ij}^{*R}(\mathbf{x}', \mathbf{x})$ and $U_{ij}^{*R}(\mathbf{x}', \mathbf{x})$, respectively, and n_i are the components of a unit vector outward to the boundary in the collocation point.

Now, considering a uniform shear deformation through the adhesive thickness, as proposed by Salgado and Aliabadi, 1998, and neglecting shear deformations in the sheet and in the patch, the body force $f_j(\mathbf{x}')$, that is equal to the shear stress in the adhesive $\tau_j(\mathbf{x}')$, can be written as a function of the difference Δu_j between the displacements u_j^S of a point $\mathbf{x}'$ ($\mathbf{x}' \in \Omega_R$) on the sheet and u_j^R of a corresponding point on the repair patch, as:

$$f_j(\mathbf{x}') = \tau_j(\mathbf{x}') = \frac{G_A}{h_A}\left\{u_j^S(\mathbf{x}') - u_j^R(\mathbf{x}')\right\} \qquad j = 1, 2 \tag{9.4}$$

where h_A is the thickness of the adhesive layer, G_A is the transversal stiffness modulus of the adhesive material.

9.3 Domain integral techniques

As can be seen, equations (9.1) and (9.2) require the calculation of domain integrals. Different techniques has been proposed to treat these integrals. Among them, the cell integration method and the dual reciprocity boundary element method (DRBEM) are the most used (see Patridge et al., 1992). Recently, Albuquerque, 2001 develop the Radial Integration Method (RIM) to treat domain integrals. In this method, the body force term is approximated with the use of radial basis functions, as in the dual reciprocity boundary element method. The transformation of domain integrals into boundary integrals is based on pure mathematical treatments. Although the proposed method is more time-consuming, it presents some advantages over the dual reciprocity boundary element method as accuracy and the absence of particular solutions in the formulation.

In this work, two different techniques were used and compared to treat the domain integrals that arise in the formulation due to the shear interaction forces. These techniques are the cell domain integration method and the dual reciprocity boundary element method (DRBEM).

9.3.1 Cell domain integration

In the cell domain technique, the attachment region Ω_R between the plate and the patch was subdivided in elementary cells. The distribution of the shear stress, $\tau_j(\mathbf{x}')$ in the adhesive in this area is described in terms of nodal values associates to each cell. In this work two types of cells were used. Since there exist two coincident nodes at any one crack elements, these nodes can't be used as collocation points because no coincident nodes can not exist in the patch. Then, constants cells with a central node has been used to approximate the shear stress distribution at neighborhood of the crack. Nine node quadrilateral isoparametric cells

were used to approximate the variation of the adhesive's shear stress in the remaining attach area.

Then, in the cell integration method the domain integral in the equation (9.1) can be expressed as (see Salgado and Aliabadi, 1997):

$$\frac{1}{h_S}\int\limits_{\Omega_R} U_{ij}^{*S}\left(\mathbf{x}',\mathbf{x}\right) f_j\left(\mathbf{x}\right) d\Omega_R \cong \frac{1}{h_S}\sum_{k=1}^{ncells}\int\limits_{\Omega_k} U_{ij}^{*S}\left(\mathbf{x}',\mathbf{x}\right) f_j\left(\mathbf{x}\right) d\Omega_k \tag{9.5}$$

and the integration is carried out on each cell. Using equation (9.4) and the bi-quadratic isoparametric approximation proposed in this work we can write:

$$\frac{1}{h_S}\sum_{k=1}^{ncells}\int\limits_{\Omega_k} U_{ij}^{*S} f_j\left(\mathbf{x}\right) d\Omega_k \cong \frac{1}{h_S}\sum_{k=1}^{ncells}\left[\int\limits_{\Omega_k} \underline{\mathbf{U}}^{*}\underline{\mathbf{N}} d\Omega_k\right]\mathbf{a}_k \tag{9.6}$$

where, $\underline{\mathbf{N}}$ is the matrix of bi-quadratic Lagrange shape functions and $\mathbf{a}_k = \left\{\mathbf{u}_d^S, \mathbf{u}^R\right\}^T$ is the vector of nodal displacements at cell k. In this vector, $\mathbf{u}_d^S$ refers to sheet displacement at Ω_R and $\mathbf{u}^R$ refers to repair displacements. Similar expression can be obtained for domain integrals at equations (9.2) and (9.3).

In this work the integral at right hand side of equation (9.6) is evaluate using ten-point Gaussian quadrature. However, when the source point $\mathbf{x}'$ is placed within the cell, this integral becomes weakly singular which will cause numerical error if Gaussian quadrature is used directly. In this case the integrand in (9.6) can be regularized at singular point by subtracting suitable singular term, which may be treated separately as follow (Young and Rooke, 1992):

$$\int\limits_{\Omega_k} U_{ij}^{*S} N_{jk} d\Omega_k = \int\limits_{-1}^{1}\int\limits_{-1}^{-1}\left\{U_{ij}^{*S} N_{jk} J - \lambda_{ij}\ln\left(R\right) J\right\} d\xi d\eta$$

$$+\lambda_{ij} J \int_{-1}^{1} \int_{-1}^{-1} \ln(R)\, d\xi d\eta \tag{9.7}$$

where, $R = \sqrt{(\xi - \xi_o)^2 + (\eta - \eta_o)^2}$. The second integral at right hand side may be evaluated analytically. The constant λ_{ij} is given by:

$$\lambda_{ij} = -\frac{1}{16\pi} \frac{(3-v)}{G_S} \delta_{ij} \tag{9.8}$$

where G_S is the shear modulus of the sheet.

9.3.2 DRBEM integration technique

In the dual reciprocity boundary element method (Patridge et al., 1992), interaction forces are approximated as a sum of unknown coefficients α_k^d multiplied by approximating functions $f_{jk}^d(\mathbf{x}', \mathbf{x})$, so that:

$$f_j(\mathbf{x}) = \sum_{d=1}^{D} \alpha_k^d f_{jk}^d \left(\mathbf{x}^d, \mathbf{x}\right) \tag{9.9}$$

The coefficients α_k^d have no physical meaning. But they are related to attachment shear forces through equation (9.4):

$$u_j^S(\mathbf{x}') - u_j^R(\mathbf{x}') = \frac{h_A}{G_A} \sum_{d=1}^{D} \alpha_j^d f_{jk}^d \left(\mathbf{x}^d, \mathbf{x}\right) \qquad j = 1, 2 \tag{9.10}$$

In this work a linear approximation function $f_{jk}^d(\mathbf{x}', \mathbf{x})$ was used for the isotropic sheet:

$$f_{jk}^d \left(\mathbf{x}^d, \mathbf{x}\right) = (1 - r)\, \delta_{jk} \tag{9.11}$$

For the anisotropic patch, an approximation function given by Albuquerque and Sollero, 1998 was used:

$$f_{jk}^d = C_{jilm} \left[cr \left(r_{,m} r_{,i} \delta_{lk} + \delta_{im} \delta_{lk}\right)\right] \tag{9.12}$$

Finally, domain integral at equation (9.5) can be expressed as:

$$\int_{\Omega_R} U_{ij}^{*S}\left(\mathbf{x}',\mathbf{x}\right) f_j\left(\mathbf{x}\right) d\Omega_R = -\frac{1}{h_S}\sum_{d=1}^{D}\alpha_k^d\left[c_{ij}\left(\mathbf{x}^d\right)\hat{u}_{kj}^d\left(\mathbf{x}^d\right) + \int_{\Gamma_R} T_{ij}^{*S}\left(\mathbf{x}',\mathbf{x}\right)\hat{u}_{kj}^d d\Gamma_R - \int_{\Gamma_R} U_{ij}^{*S}\left(\mathbf{x}',\mathbf{x}\right)\hat{t}_{kj}^d d\Gamma_R\right] \tag{9.13}$$

where $\hat{u}_{kj}^d$ and $\hat{t}_{kj}^d$ are particular solutions for displacements and tractions corresponding to a pre-defined function f_{kj}^d for the sheet. A similar approach was used to model body forces in the patch.

9.4 Matrix formulation

9.4.1 Cell integration technique

In matrix form, equation (9.6) can be write as:

$$\frac{1}{h_S}\sum_{k=1}^{ncells}\left(\int_{\Omega_k}\underline{\mathbf{U}}^*\cdot\underline{\mathbf{N}}d\Omega_k\right)_k\mathbf{a}_k = \underline{\mathbf{F}}_c^S\mathbf{u}_d^S - \underline{\mathbf{F}}_c^S\mathbf{u}^S \tag{9.14}$$

Discretizing the boundary, the equations for isotropic sheet (including traction equation) can be write in compact form as:

$$\begin{aligned}\underline{\mathbf{H}}_c^S\mathbf{u}_c^S &= \underline{\mathbf{G}}_c^S\mathbf{t}_c^S + \underline{\mathbf{F}}_c^S\mathbf{u}_d^S - \underline{\mathbf{F}}_c^S\mathbf{u}^R \\ \underline{\mathbf{I}}\mathbf{u}_d^S + \underline{\mathbf{H}}_d^S\mathbf{u}_c^S &= \underline{\mathbf{G}}_d^S\mathbf{t}_c^S + \underline{\mathbf{F}}_d^S\mathbf{u}_d^S - \underline{\mathbf{F}}_d^S\mathbf{u}^R\end{aligned} \tag{9.15}$$

where subindex c and d identify boundary and domain collocation points on the sheet. The

matrix of influence coefficients $\underline{\mathbf{H}}^S$ and $\underline{\mathbf{G}}^S$ are defined as:

$$\begin{aligned}\underline{\mathbf{H}}^S &= \sum_{e=1}^{nelem} \int_{\Gamma_e} T_{ij}^{*S} \phi_j d\Gamma_e \\ \underline{\mathbf{G}}^S &= \sum_{e=1}^{nelem} \int_{\Gamma_e} U_{ij}^{*S} \phi_j d\Gamma_e \end{aligned} \tag{9.16}$$

Here, ϕ_j are the shape functions for the elements. In this work, quadratic discontinuous elements are used to interpolate the displacement and traction variations in the boundaries of the plate and the repair.

In a similar way, matrix equations for repair can be write as (without consider traction forces applied at boundary repair):

$$\begin{aligned}\underline{\mathbf{H}}_c^R \mathbf{u}_c^R &= \underline{\mathbf{F}}_c^R \mathbf{u}^R - \underline{\mathbf{F}}_c^R \mathbf{u}_d^P \\ \underline{\mathbf{I}} \mathbf{u}_d^R + \underline{\mathbf{H}}_d^R \mathbf{u}_c^R &= \underline{\mathbf{F}}_d^R \mathbf{u}^R - \underline{\mathbf{F}}_d^R \mathbf{u}^P \end{aligned} \tag{9.17}$$

In this case, similar significance has the $\underline{\mathbf{H}}^R$ and $\underline{\mathbf{G}}^R$ matrices as those in the sheet case. In the general case, when the sheet and the patch are made of different materials, the $\mathbf{F}^S$ and $\mathbf{F}^R$ matrices in equations (9.15) and (9.17) are not equals.

After some mathematical manipulation the coupling equations for the sheet and the repair using the cell integration technique can be written as:

$$\begin{bmatrix} \underline{\mathbf{M}}^S & \underline{\mathbf{F}}^S \\ \underline{\mathbf{M}}^R & \underline{\mathbf{Q}}^R \end{bmatrix} \begin{Bmatrix} \mathbf{u}^S \\ \mathbf{u}^R \end{Bmatrix} = \begin{Bmatrix} \underline{\mathbf{G}}^S \mathbf{t}_c^S \\ \mathbf{0} \end{Bmatrix} \tag{9.18}$$

where $\underline{\mathbf{M}}^P$, $\underline{\mathbf{M}}^R$ and $\underline{\mathbf{Q}}^R$ matrices involving the $\underline{\mathbf{F}}$ matrices for sheet and repair.

9.4.2 DRBEM integration technique

In DRBEM integration technique, equation (9.13) can be write in matrix form as:

$$\int_{\Omega_R} U_{ij}^{*S}\left(\mathbf{x}', \mathbf{x}\right) f_j\left(\mathbf{x}\right) d\Omega_R = \left(\underline{\mathbf{H}}^S \hat{\mathbf{U}}^S - \underline{\mathbf{G}}^S \hat{\mathbf{T}}^S\right) \alpha^S \tag{9.19}$$

In this equation, the influence matrices $\underline{\mathbf{H}}^S$ and $\underline{\mathbf{G}}^S$ are those defined in equation (9.16) if functions $\hat{u}_{kj}^d$ and $\hat{t}_{kj}^d$ are approximate within each boundary element by using interpolation functions and nodal values as done for $u_j^S(\mathbf{x})$ and $t_j^S(\mathbf{x})$ in equation (9.15).

Discretizing the boundary, equations for the sheet (including traction equation) can be write in compact form as:

$$\begin{aligned} \underline{\mathbf{H}}_c^S \mathbf{u}_c^S - \underline{\mathbf{G}}_c^S \mathbf{t}_c^S &= \underline{\mathbf{A}}_c^S \alpha^S \\ \underline{\mathbf{I}} \mathbf{u}_d^S + \underline{\mathbf{H}}_d^S \mathbf{u}_c^S &= \underline{\mathbf{A}}_d^S \alpha^S \end{aligned} \tag{9.20}$$

where matrix $\underline{\mathbf{A}}^S$ is given by: $\underline{\mathbf{A}}^S = \underline{\mathbf{H}}^S \hat{\mathbf{U}}^S - \underline{\mathbf{G}}^S \hat{\mathbf{T}}^S$. In similar way, the equations for repair are:

$$\begin{aligned} \underline{\mathbf{H}}_c^R \mathbf{u}_c^R - \underline{\mathbf{G}}_c^R \mathbf{t}_c^R &= \underline{\mathbf{A}}_c^R \alpha^R \\ \underline{\mathbf{I}} \mathbf{u}_d^R + \underline{\mathbf{H}}_d^R \mathbf{u}_c^R &= \underline{\mathbf{A}}_d^R \alpha^R \end{aligned} \tag{9.21}$$

Now, equation (9.10) can be write in matrix form for the sheet and the repair as:

$$\begin{aligned} \mathbf{u}_d^S - \mathbf{u}^R &= \frac{h_A}{G_A} \underline{\mathbf{F}}^S \alpha^S \\ \mathbf{u}^R - \mathbf{u}_d^S &= \frac{h_A}{G_A} \underline{\mathbf{F}}^R \alpha^R \end{aligned} \tag{9.22}$$

Finally, the coupling equations for the sheet and the repair using the DRBEM integration

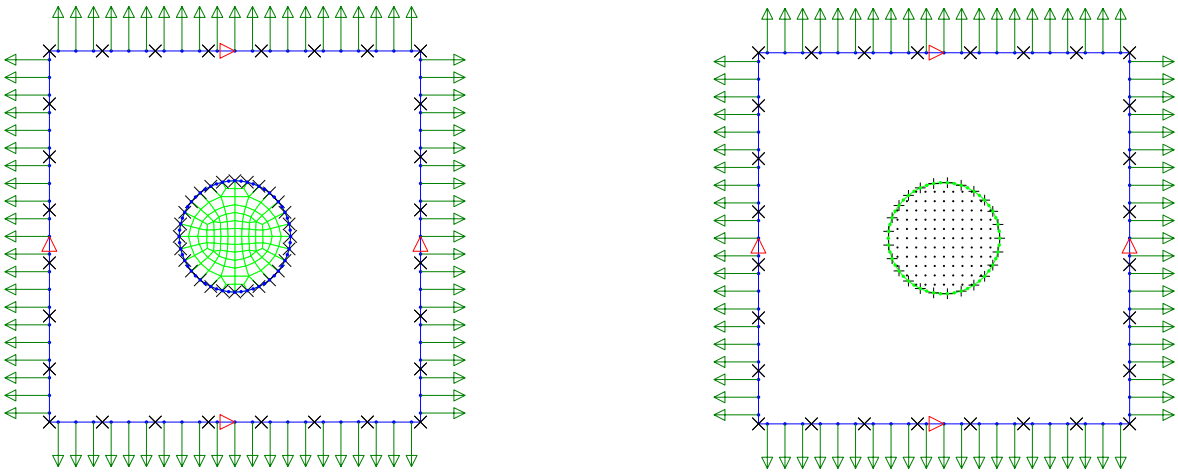

Figure 9.2: Model of uncracked sheet repaired with adhesive isotropic patch. Left: cell model. Right: DRM model

technique are:

$$\begin{bmatrix} \left(\underline{\mathbf{H}} - \underline{\mathbf{AF}}^{-1}\right)^S & \left(\underline{\mathbf{AF}}^{-1}\right)^S \\ \left(\underline{\mathbf{H}} - \underline{\mathbf{AF}}^{-1}\right)^R & \left(\underline{\mathbf{AF}}^{-1}\right)^R \end{bmatrix} \begin{Bmatrix} \mathbf{u}^S \\ \mathbf{u}^R \end{Bmatrix} = \begin{Bmatrix} \underline{\mathbf{G}}^S \mathbf{t}^S \\ \mathbf{0} \end{Bmatrix} \tag{9.23}$$

9.4.3 Coupled DRM and DBEM modeling considerations

If the sheet contains a crack which is overlaid by a patch, the attachment region boundary includes the corresponding region of the crack boundary, which contains nodes with the same coordinates in opposite crack surfaces (see Salgado and Aliabadi, 1998). As a consequence, the direct application of the formulation presented leads to a series of difficulties as:

- Two nodes with the same coordinate produces two identical displacement compatibility equations.

- Each point where displacement compatibility is enforced is used as DRBEM collocation point. This means having coinciding points at crack boundaries, producing DRM coefficient matrix become singular and requires explicit treatment and identical values for the attachment forces at points in opposite crack surfaces.

Salgado, 1998 shows that it is not necessary to include the crack boundary in the attachment boundary region, because the contribution of the integration over this boundary to DRM matrix coefficients is equal to zero. In this case the above difficulties are eliminated as the exclusion of the crack boundaries from the attachment boundary, meaning that neither displacement compatibility nor DRM collocations points will be created at the crack boundary. The absence of those points can be compensated by placing internal points in the vicinity of the crack boundaries. Same considerations applies when cell integration method is used.

9.5 Numerical examples

9.5.1 Circular composite patch over uncracked square sheet

A square sheet with edge of 200mm is subjected to constant tension of $\sigma_0 = 1$ GPa in the direction of the y-axis. The sheet has a thickness of 1.5mm. Sheet have a Young modulus of $70GPa$ and Poisson modulus of 0.3. A circular isotropic patch of radius of 30 mm thickness of 1.5 mm is bonded at the center of sheet using an adhesive with 0.15 mm of thickness and shear modulus of G=0.6 GPa.

This problem was analyzed to test the BEM formulation proposed in this chapter, using the cell and the DRBEM methodologies proposed. To model the isotropic repair a quase-isotropic formulation was used with $E_1 = 70GPa$, $E_2 = 70.0001GPa$, $G_{12} = 26.92GPa$ and $v_{12} = 0.3$. Figure 9.2 shows the cell and the DRBEM model used. Figure 9.3 shows the shear stress distribution map at the adhesive layer. This graphic shows that shear stress is zero at center of repair area and maximum at repair border as expected. Figure 9.4 shows a convergence analysis for normalized shear stress (τ/σ_0) as function of normalized distance y/R along y-axis. Both cell and DRM methods shows a rapid convergence to analytical

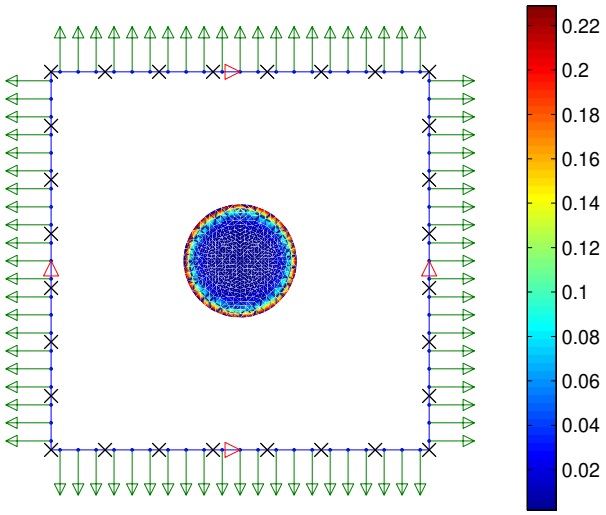

Figure 9.3: Normalized shear stress map at adhesive layer for quase-isotropic patch solution given by Rose (see previous chapter).

9.5.2 Circular composite patch over cracked square sheet

A square sheet whose edge length is 200 mm is subjected to a uniform constant tension of 1 GPa in the direction of the y-axis. A central crack of length $2a = 30$ mm in the sheet is considered. The sheet has a thickness of 1.5 mm. A circular anisotropic repair of radius equal to 30 mm and thickness of 1.5 mm is bonded at the center of the sheet using an adhesive with 0.15 mm of thickness and shear modulus $G = 0.6$ GPa. Properties of the sheet and the patch are given in Table 9.1.

The problem was analyzed using the method of cells and the DRBEM. In both cases, the mesh comprises of 28 discontinuous quadratic elements on the edge of the plate and on the edge of the repair. As shown in Figure 9.5, quadratic continuum cells with nine nodes were used to discretize the load transfer domain between the sheet and the patch except in crack's

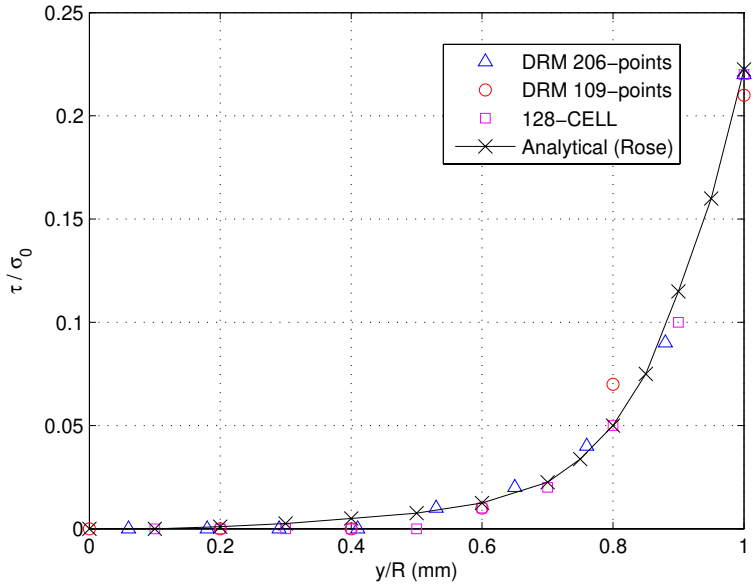

Figure 9.4: Convergence analysis for normalized shear stress (τ/σ_0) as function of normalized distance y/R along y-axis.

Table 9.1: Mechanical properties of the sheet and the composite patch

Sheet	**Patch**
Young modulus (E) = 72400 Mpa	$E_1 = 25000$ MPa
Poissons ratio(v) = 0.3	$E_2 = 208000$ MPa
	$G_{12} = 72400$ MPa
	$\nu_{12} = 0.02$

neighborhood, where constants cells were used. Ten-point Gauss quadrature rule was used to evaluate the domain's integral at quadratics cells.

DRBEM collocations points have been concentrated near the crack and toward boundary repair. The shear stress distribution in the adhesive layer obtained using the DRBEM is shown in Figure 9.6. As was expected, shear stress gradients appear near crack's border where the difference between sheet and repair displacements is higher. The shear distribution obtained in the model with cells is similar and it's not show here.

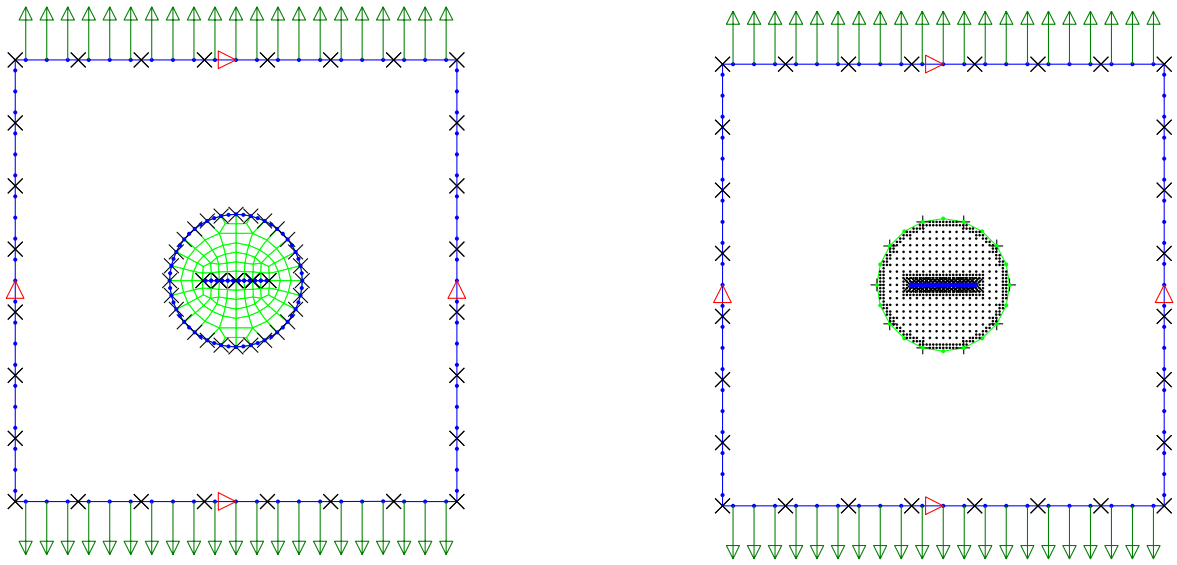

Figure 9.5: Model of cracked sheet repaired with bonded adhesively patch using bi-quadratic interpolation cells. Left: cell model. Right: DRBEM model

The resultant for the shear stress in the adhesive is showed in the Figure 9.7 normalized with respect to the sheet far field stresses (i.e. 1 GPa). This stresses has been obtained using the equation:

$$\tau^* = \frac{1}{\sigma_0}\sqrt{\tau_{zx}^2 + \tau_{zy}^2} \tag{9.24}$$

where σ_0 is the far stresses applied in the y-axis, τ_{zx} and τ_{zy} are shear stresses in the x and y-axis directions. As can be seen in this figure the convergence of the solution is obtained as the number of internal points increases. Further refining in the boundary mesh hasn't significantly affects the results. Obtained results are compared with analytical solution given by Rose Rose and Wang, 2002 for an infinity orthotropic patches bonded to an infinity orthotropic sheet for patch with elliptic (circular) geometry:

$$\tau\left(y\right) = \sigma_0 \Lambda t e^{(-\Lambda|y|)} \tag{9.25}$$

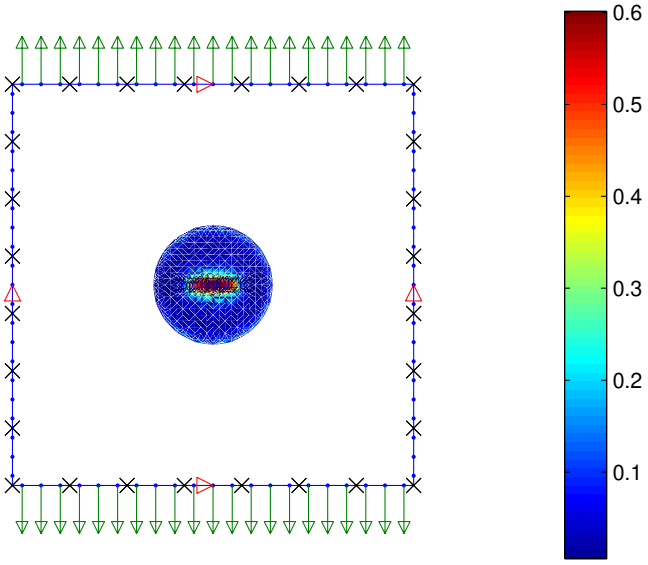

Figure 9.6: Normalized shear stress force in the adhesive

Again, σ_0 is the stress applied in the y-axis (i.e. 1 GPa) and the parameter Λ is given by:

$$\Lambda^2 = (G_A/h_A)\left\{\left(E^S h_S\right)^{-1} + \left(E_y^R h_R\right)^{-1}\right\} \tag{9.26}$$

It can be seen that good agreement was obtained even for relatively coarse internal points grids when the DRBEM were used. Slower convergence to Rose's solution was found with cell method.

Figure 9.8 presents the variation of the stress intensity factor K_I according to the crack length. It is noted the asymptotic behavior that is in agreement with analysis of Rose Rose, 1981, as presented in previous chapter. In this case, the asymptotic value K_∞, predicted by equation 8.15, was 206.6 $MPa.m^{1/2}$. Curves in figure 9.8 tends to this asymptotic value.

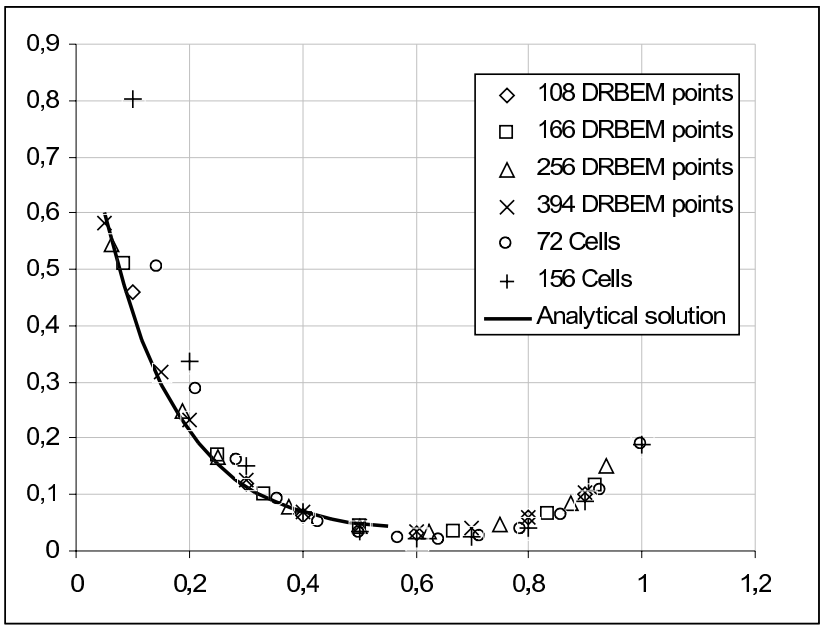

Figure 9.7: Normalized shear stress in the adhesive layer x=0 and $0 \leq y \leq R \leq 1$

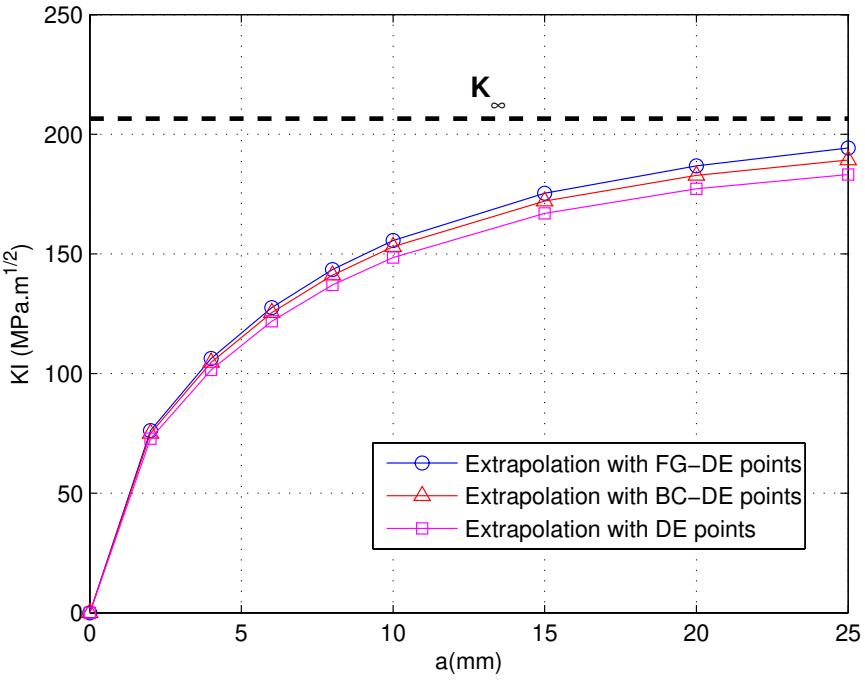

Figure 9.8: Variation of K_I Stress intensity factor with crack length

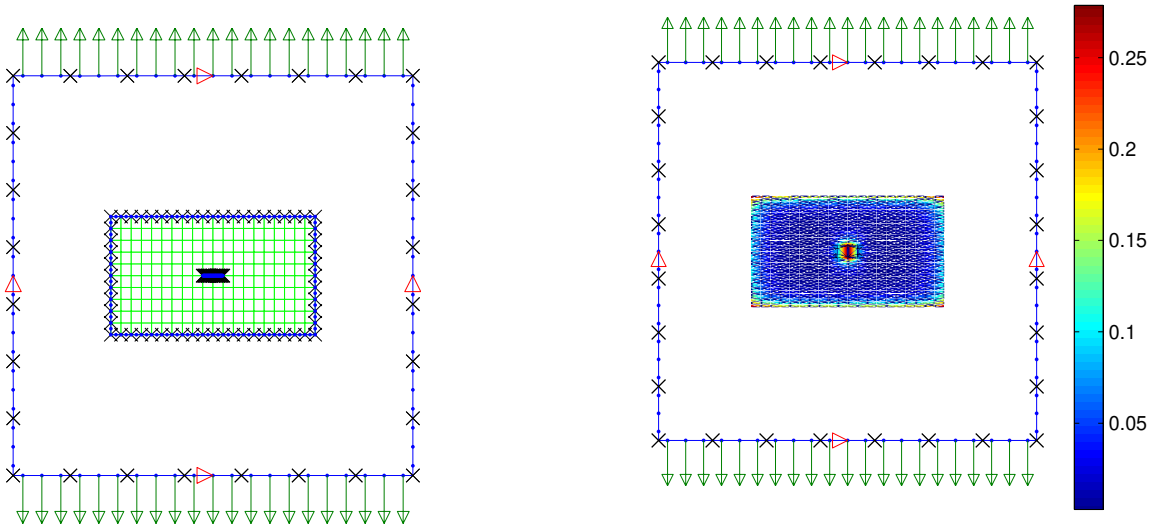

Figure 9.9: BEM model for square sheet with rectangular patch

9.5.3 Rectangular orthotropic patch over square sheet

Consider a thin aluminum sheet with height $H_s =$ of 254mm, width $W_s = 254$ mm, thickness of 5 mm with a central crack of length $a = 13$ mm. repaired with boron-epoxi patch having dimensions: $W_r = 130$ mm; $H_r = 75$ mm. The sheet is subjected to a remote uniaxial tensile load of $\sigma = 70$ MPa, plane stress condition are assumed. The material properties of the plate, patch and adhesive are showed in table 9.2.

Table 9.2: Mechanical properties of the sheet and the composite patch

Sheet	**Patch**
Young modulus $(E) = 72000$ Mpa	$E_1 = 19600$ MPa
Poissons ratio$(v) = 0.33$	$E_2 = 210000$ MPa
	$G_{12} = 5460$ MPa
	$\nu_{12} = 0.3$

The problem was analyzed using the cell method. The mesh comprises of 28 discontinuous quadratic elements on the edge of the plate. A convergence analysis for shear stress in the adhesive layer as function of number of cells and elements at boundary of the repair was performed. Figure 9.9(left) shows the model used.

The shear stress distribution in the adhesive layer obtained is shown in figure 9.9. Again, shear stress gradients appear near crack's border where the difference between sheet and repair displacements is higher. Similar to circular patch, shear stress concentration appears at the patch border and, in this case, at patch corners, has can be seen. The magnitude of shear stress in these corners is similar to those encountered near crack's border.

To compare the behavior of the total shear stress normalized with respect to the sheet far field stresses in the adhesive at $x = 0$ mm, with those encountered in the case of circular anisotropic patch, figure 9.10 was generated. This figure shows that the normalized shear stress variation in direction of y-axis is similar to that case. That is, a high gradients near crack's border and patch border is presented with low values of the shear stress in the adhesive in regions far away from this borders. This behavior is generated by the geometric discontinuity between sheet and repair.

Figure 9.11 presents the variation of the stress intensity factor K_I according to the crack length. Again, is noted the asymptotic behavior that is in agreement with analysis of Belhouari et al., 2004. In this case, the asymptotic value K_∞, predicted by equation 8.15, was 18.66 $MPa.m^{1/2}$. BEM model sub-estimate the asymptotic behavior of K_I as shown in this figure, bringing an asymptotic value of 13.65 $MPa.m^{1/2}$ approximately.

9.6 Special cells

Additionally to the constant cells used in the neighbourhood of the crack, four different types of special discontinuous cells were developed to approximate the displacement field into the cells, trying to capture in a better way the high stress gradient near the crack border. Fig-

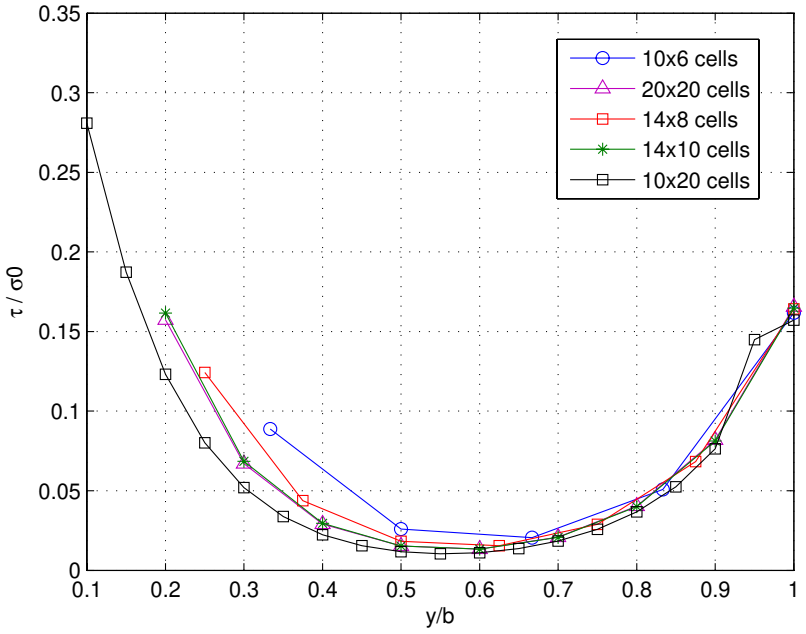

Figure 9.10: Normalized shear stress in the adhesive layer x=0 and $0 \leq y \leq H_R \leq 1$

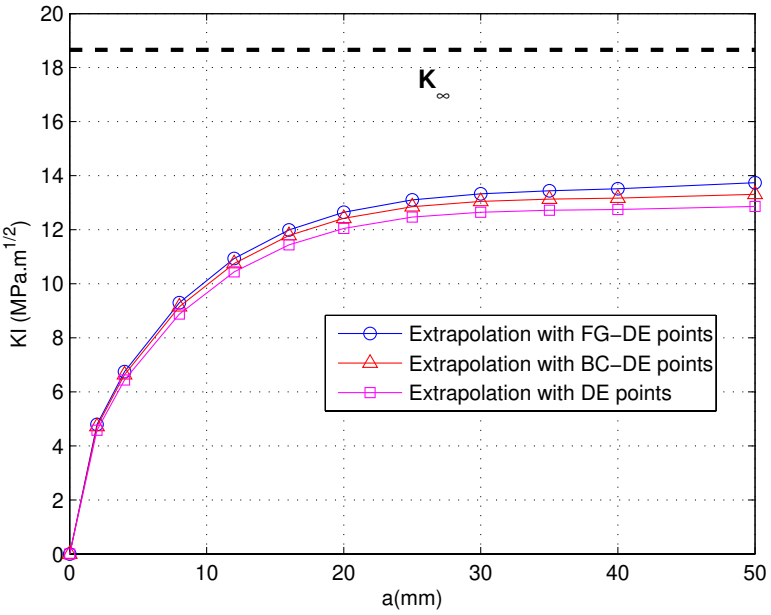

Figure 9.11: Variation of K_I Stress intensity factor with crack length

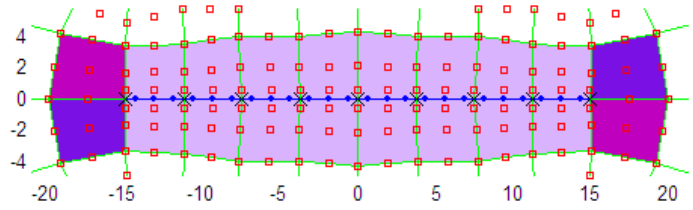

(a)

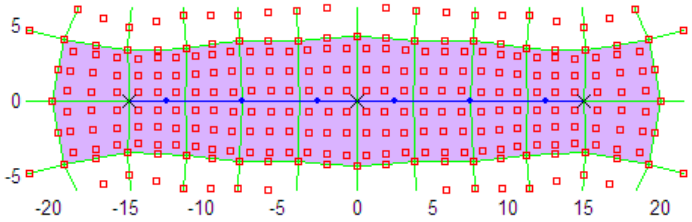

(b)

Figure 9.12: Types of special cells. (a) Semi-discontinuous quadratic cells. (b) Discontinuos quadratic cells

ure 9.12-a shows three different types of special bi-quadratics cells where nodes located on crack borders were dislocated 2/3 away from the crack. Similarly, another type of special discontinuous cells, where all nodes used to describe the displacement field into the cells were moved 2/3 towards interior of the cells were showed in figure 9.12-b.

Unfortunately, the use of those special cells do not improved the results as figure 9.13 shown. This figure compares the normalized shear stress distribution along y-axis obtained using special cells with those results obtained for the circular composite patch over cracked square sheet problem. Little differences between results were found.

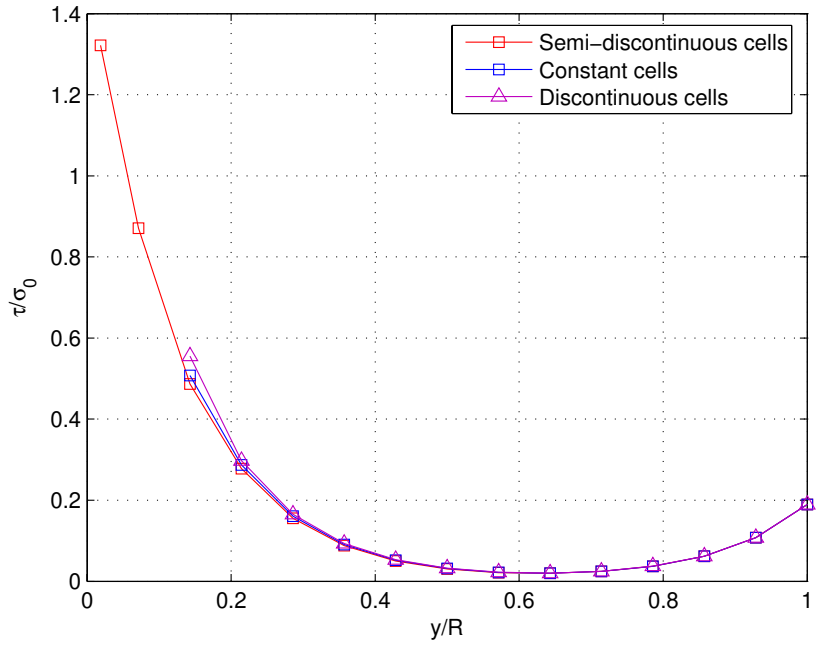

Figure 9.13: Normalized shear stress in the adhesive layer x=0 and $0 \leq y \leq R \leq 1$ for differents types of cells for the circular composite patch over cracked square sheet problem

9.7 Conclusions

A boundary element formulation for modeling cracked sheets repaired with composite patches was developed. The cracked sheet was modeled with the DBEM and the patch was modeled with the BEM. The interaction between the isotropic sheet and the patch was modeled considering shear body forces uniformly distributed on the interaction zone using a linear elastic relationship. The cell domain integration and the dual reciprocity have been used to treat the domain integrals that arise in the formulation due to shear interaction forces. The DRBEM method showed faster convergence to analytical solution than the cell method. It can be concluded that the new formulation can be used with reasonable accuracy to study the mechanical behavior of adhesively bonded repairs, but more research work must be done to explain discrepancy in the stress intensity factors founded.

Chapter 10

Boundary element analysis of cracked plates repaired with bonded anisotropic patches

10.1 Introduction

In this chapter, a boundary integral formulation to describe the mechanical behavior of cracked isotropic thick plates repaired with adhesively bonded composite patch using the Reissner and Kirchhoff plate theories, is presented. To model the isotropic crack plate, the dual boundary element formulation proposed by Dirgantara, 2000 is used. A three parameter boundary integral formulation for anisotropic plates is proposed to model the mechanical response of the composite repair. Integral equations for the problem under consideration are established. Coupling equations based on kinematic compatibility of isotropic plate and anisotropic repair displacements and rotations and equilibrium of forces and moments acting in the adhesive, are showed. In this way a general system of equations for the problem is developed. Numerical examples and preliminary conclusions are presented.

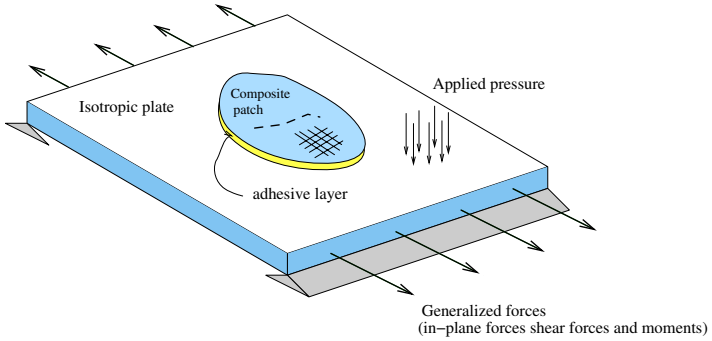

Figure 10.1: Schematic representation of the cracked plate repaired problem

10.2 Boundary integral formulation for isotropic plates

10.2.1 Displacement integral formulation for plane stress

Figure 10.1 shows a schematic representation of the problem. A cracked isotropic plate with arbitrary geometry (but represented here as rectangular ones) is loaded with in-plane forces (membrane forces), bending moments and distributed pressure, is repaired using adhesively bonded composited patch. This work do not consider any kind of forces acting over this patch.

The two dimensional boundary integral equation for displacements at the boundary point $\mathbf{x}' \in \Gamma$ that describes membrane effects can be written as showed in chapter 4:

$$c_{ij}^{P}\left(\mathbf{x}'\right) u_{\beta}\left(\mathbf{x}'\right) = \int_{\Gamma} U_{\alpha\beta}^{P}\left(\mathbf{x}', \mathbf{x}\right) t_{\beta} d\Gamma - \int_{\Gamma} T_{\alpha\beta}^{P}\left(\mathbf{x}', \mathbf{x}\right) u_{\beta} d\Gamma + \frac{1}{h_p} \int_{A} U_{\alpha\beta}^{P}\left(\mathbf{x}', \mathbf{x}\right) f_{\beta} dA \qquad (10.1)$$

where α, $\beta = 1, 2$ and $c_{ij}^{P}(\mathbf{x}')$ is a function of the geometry at the collocation points that can be determinated by considering rigid body movements. The boundary displacements and tractions for the sheet are denoted by u_{α} and $t_{\alpha}(= n_{\beta}\sigma_{\alpha\beta})$, respectively; displacement and traction fundamental solutions for the plane stress condition are $U_{\alpha\beta}^{P}(\mathbf{x}', \mathbf{x})$ and $T_{\alpha\beta}^{P}(\mathbf{x}', \mathbf{x})$ respectively, $f_{\beta}(\mathbf{x})$ denote two-dimensional body forces by unit area over a region A of patch and h_p is the thickness of the plate. In this work no others in-plane body forces will be

considered.

10.2.2 Two-dimensional traction integral formulation

In order to modeling cracked plates, the Dual Boundary Element Method (DBEM) will be used. In this method, the displacement integral formulation is written for source points on one crack surface and the traction integral equation on the other surface. Then, using the stress and strain relationships for plane stress, the traction integral equation for two-dimensional problems in a smooth boundary can be derived as presented in chapter 7:

$$\begin{aligned}\frac{1}{2}t_\alpha\left(\mathbf{x}'\right) &= n_\beta\left(\mathbf{x}'\right)\int_\Gamma U^P_{\alpha\beta\gamma}\left(\mathbf{x}',\mathbf{x}\right)t_\gamma d\Gamma - n_\beta\left(\mathbf{x}'\right)\int_\Gamma T^P_{\alpha\beta\gamma}\left(\mathbf{x}',\mathbf{x}\right)u_\gamma d\Gamma \\ &\quad + n_\beta\left(\mathbf{x}'\right)\frac{1}{h_p}\int_A U^P_{\alpha\beta\gamma}\left(\mathbf{x}',\mathbf{x}\right)f_\beta dA \end{aligned} \tag{10.2}$$

where $n_\beta(\mathbf{x}')$ is the normal to the boundary evaluated at collocation point. $U^P_{\alpha\beta\gamma}(\mathbf{x}',\mathbf{x})$ and $T^P_{\alpha\beta\gamma}(\mathbf{x}',\mathbf{x})$ are the traction fundamental solution for two-dimensional problems.

10.2.3 Displacement integral equation for plate bending

If w_α are defined as rotations in the x_α direction, w_3 is the deflection of the plate along x_3 as shown in figure 10.2, q^P_α and q^P_3 are the distribution of body forces in moment and the out-of-plane body force per unit area, respectively, in the patch area A and p_o is the pressure force applied in the domain of the plate Ω (considered constant in this work); the boundary integrals for the plate bending problem can be obtained as (see chapter 5):

$$\begin{aligned}c^P_{ik}\left(\mathbf{x}'\right)w_k\left(\mathbf{x}'\right) &= \int_\Gamma W^P_{ik}\left(\mathbf{x}',\mathbf{x}\right)p_k d\Gamma - \int_\Gamma P^P_{ik}\left(\mathbf{x}',\mathbf{x}\right)w_k d\Gamma + p_o\int_\Omega W^P_{i3}\left(\mathbf{x}',\mathbf{x}\right)d\Omega \\ &\quad + \int_A W^P_{ik}\left(\mathbf{x}',\mathbf{x}\right)q^P_k dA \end{aligned} \tag{10.3}$$

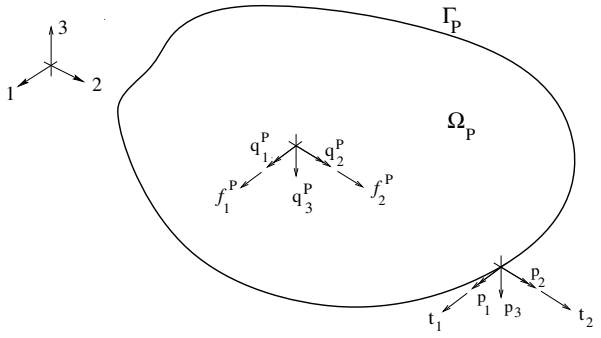

Figure 10.2: Definition of boundary and distributed body forces and moments at isotropic plate

where $k = 1 \ldots 3$. $W^P_{\alpha\beta}(\mathbf{x}', \mathbf{x})$ and $P^P_{\alpha\beta}(\mathbf{x}', \mathbf{x})$ are the fundamental solutions for Reissner's plate model and $p_\alpha = M_{\alpha\beta} n_\beta$, $p_3 = Q_\beta n_\beta$. Constant c^P_{ik} has a similar significance with those at in-plane displacement problem.

10.2.4 Traction integral equation for plate bending

In a similar way, fracture mechanics problems involving plate bending can be modeled using DBEM. In this case, the traction equation can be written as:

$$\begin{aligned} \frac{1}{2} p_i(\mathbf{x}') &= n_\beta(\mathbf{x}') \int_\Gamma W^P_{i\beta k}(\mathbf{x}', \mathbf{x})\, p_k d\Gamma - n_\beta(\mathbf{x}') \int_\Gamma P^P_{i\beta k}(\mathbf{x}', \mathbf{x})\, w_k d\Gamma \\ &\quad + n_\beta(\mathbf{x}')\, p_o \int_\Omega W^P_{i\beta 3}(\mathbf{x}', \mathbf{x})\, d\Omega + n_\beta(\mathbf{x}') \int_A W^P_{i\beta k}(\mathbf{x}', \mathbf{x})\, q^P_k dA \end{aligned} \tag{10.4}$$

where $W^P_{i\beta\gamma}(\mathbf{x}', \mathbf{x})$ and $P^P_{i\beta\gamma}(\mathbf{x}', \mathbf{x})$ are the traction fundamental solution for Reissner's plate, as showed in chapter 7.

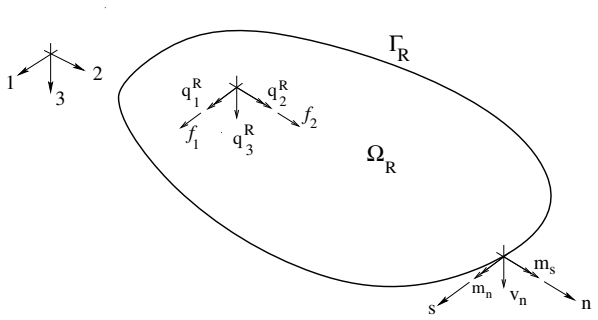

Figure 10.3: Definition of boundary and distributed body forces and moments at repair

10.3 Boundary integral equation for anisotropic repair

10.3.1 Displacement integral formulation for plane stress

Similarly to the isotropic case, the in-plane displacements of a point $\mathbf{x}'$ in the anisotropic patch are given by (see chapter 3):

$$c_{\alpha\beta}^R(\mathbf{x}')\, u_\beta^R + \int_{\Gamma_R} T_{\alpha\beta}^R(\mathbf{x}', \mathbf{x})\, u_\beta^R d\Gamma = \frac{1}{h_R} \int_A U_{\alpha\beta}^R(\mathbf{x}', \mathbf{x})\, f_\beta^R dA \tag{10.5}$$

where $T_{\alpha\beta}^R(\mathbf{x}', \mathbf{x})$ and $U_{\alpha\beta}^R(\mathbf{x}', \mathbf{x})$ are the traction and displacements fundamental solutions for anisotropic plane elasticity problems and h_R represents the repair thickness. Others variables have similar meaning to the isotropic case. In this work, loads acting over the boundary of the repair are not consider. Because of this, the integral term containing traction boundary forces wasn't included into equation 10.5.

10.3.2 Displacement integral formulation for bending plate

In this work, the plate bending response of the repair is modeled using the Kirchhoff's plate theory as presented in chapter 6.

From the generalized Rayleigh-Green identity, if we choose $w^R(\mathbf{x})$ as the deflection of the

plate under consideration, and $W(\mathbf{x}', \mathbf{x})$ as the fundamental solution and making the use of the properties of Dirac δ-function, the following integral representation is obtained (see Shi and Bezine, 1988):

$$c^R D_{22} w^R(\mathbf{x}') = -\int_\Gamma \Big\{ V_n(\mathbf{x}', \mathbf{x})\, w^R(\mathbf{x}) - M_n(\mathbf{x}', \mathbf{x})\, w^R_{,n}(\mathbf{x}) + W_{,n}(\mathbf{x}', \mathbf{x})\, m_n(\mathbf{x}) - W(\mathbf{x}', \mathbf{x})\, v_n(\mathbf{x}) \Big\} d\Gamma + \sum_{i=1}^{m} \left\{ T_n(\mathbf{x}', \mathbf{x})\, w(\mathbf{x}) - W(\mathbf{x}', \mathbf{x})\, t_n(\mathbf{x}) \right\}_i \quad (10.6)$$

where $w_n^R(\mathbf{x})$ is the tangential rotation, $v_n(\mathbf{x})$ and $m_n(\mathbf{x})$ are the shear force and the tangential moment, respectively, and $t_n(\mathbf{x})$ is the normal moment. $V_n(\mathbf{x}', \mathbf{x})$, $M_n(\mathbf{x}', \mathbf{x})$, $W(\mathbf{x}', \mathbf{x})$, $T_n(\mathbf{x}', \mathbf{x})$ and $W_{,n}(\mathbf{x}', \mathbf{x})$ are the fundamental solutions for Kirchhoff plate. The last term at right hand side represents corner effects, where m represents the number of corner points of the boundary.

For a plate bending problem, there always two unknows at any point of the boundary (see figure 10.3). Consequently a second boundary integral equation is obtained by differentiating last equation with respect to point $\mathbf{x}'$ in the direction of the outward unit normal n_0 at collocation point:

$$\frac{1}{2} D_{22} w_{,n_o}(\mathbf{x}') + \int_\Gamma \Big[V_{n,n_o}(\mathbf{x}', \mathbf{x})\, w^R(\mathbf{x})\, d\Gamma - M_{n,n_o}(\mathbf{x}', \mathbf{x})\, w^R_{,n}(\mathbf{x}) + W_{,n_o n}(\mathbf{x}', \mathbf{x})\, m_n(\mathbf{x}) - W_{,n_o}(\mathbf{x}', \mathbf{x})\, v_n(\mathbf{x}) \Big] d\Gamma + \sum_{i=1}^{m} \Big[T_{s,n_o}(\mathbf{x}', \mathbf{x})\, w^R(\mathbf{x}) - W_{,n_o}(\mathbf{x}', \mathbf{x})\, t_s(\mathbf{x}) \Big]_i = 0 \quad (10.7)$$

10.4 Three parameter formulation for Kirchhoff plates

A drawback appears trying to coupling above formulation with Reissner's plate, to model the interaction between plate and repair. In fact, this formulation has two cinematic unknows variables. i.e., w and $w_{,n}$ (deflection and tangential rotation) at every point, whereas Reiss-

ner's plate model has three: w, $w_{,x1}$ and $w_{,x2}$, i.e., deflection and two rotations. In this way, Kirchhoff plate and the Reissner plate models are kinematically incompatibles.

An alternative boundary integral formulation for Kirchhoff plate's model with three unknows at every point can be establish considering the original form of the Betti' theorem for the Kirchhoff plate given in chapter 6.

From the equilibrium of forces and moments, we can write (see chapter 6):

$$\frac{\partial M_{xx}}{\partial x} + \frac{\partial M_{yx}}{\partial y} - Q_x + m_x = 0$$

$$\frac{\partial M_{xy}}{\partial x} + \frac{\partial M_{yy}}{\partial y} - Q_y + m_y = 0$$

$$\frac{\partial Q_x}{\partial x} + \frac{\partial Q_y}{\partial y} - Q_x + q = 0 \tag{10.8}$$

The relation between internal moments and resultants of moments acting in a plane with normal $\vec{n}$ is given by:

$$\left\{ \begin{array}{c} M_x \\ M_y \end{array} \right\} = \left[\begin{array}{cc} M_{xx} & M_{xy} \\ M_{yx} & M_{yy} \end{array} \right] \left\{ \begin{array}{c} n_x \\ n_y \end{array} \right\} \tag{10.9}$$

In a similarly, the relationship between internal shear force and a shear force acting at a plane with normal $\vec{n}$ is:

$$Q_n = Q_x n_x + Q_y n_y \tag{10.10}$$

Using Betti theorem, we can relate two states of stress-deformation of a linear material as:

$$\int_{\Omega} \sigma_{ij} \varepsilon^*_{ij} d\Omega = \int_{\Omega} \sigma^*_{ij} \varepsilon_{ij} d\Omega \tag{10.11}$$

For Kirchhoff plate theory we have:

$$\varepsilon_{xx} = -z\frac{\partial^2 w}{\partial x^2}$$

$$\varepsilon_{yy} = -z\frac{\partial^2 w}{\partial y^2}$$

$$\gamma_{xy} = -2z\frac{\partial^2 w}{\partial x \partial y} \tag{10.12}$$

Replacing these expressions on the left hand side of eqn. 10.11 we have:

$$\int_{\Omega} \sigma_{ij}\varepsilon^*_{ij} d\Omega = -z \int_{\Omega} \left[\sigma_{xx} \left(\frac{\partial^2 w^*}{\partial x^2} \right) + \sigma_{yy} \left(\frac{\partial^2 w^*}{\partial y^2} \right) + 2\tau_{xy} \left(\frac{\partial^2 w^*}{\partial x \partial y} \right) \right] d\Omega \tag{10.13}$$

Considering the resultant of moments:

$$M_{xx} = \int_{-t/2}^{t/2} z\sigma_{xx} dz$$

$$M_{yy} = \int_{-t/2}^{t/2} z\sigma_{yy} dz$$

$$M_{xy} = \int_{-t/2}^{t/2} z\tau_{xy} dz \tag{10.14}$$

Integrating throughout the thickness of the plate equation (10.13), we have:

$$\begin{aligned} \int_{\Omega} \sigma_{ij}\varepsilon^*_{ij} d\Omega &= -\int_{A} \left\{ \left(\frac{\partial^2 w^*}{\partial x^2} \right) \left(\int_{-t/2}^{t/2} z\sigma_{xx} dz \right) + \left(\frac{\partial^2 w^*}{\partial y^2} \right) \left(\int_{-t/2}^{t/2} z\sigma_{yy} dz \right) \right. \\ &+ \left. 2 \left(\frac{\partial^2 w^*}{\partial x \partial y} \right) \left(\int_{-t/2}^{t/2} z\tau_{xy} dz \right) \right\} dA \end{aligned} \tag{10.15}$$

then,

$$\int_{\Omega} \sigma_{ij}\varepsilon^*_{ij} d\Omega = -\int_{A} \left[M_{xx}\left(\frac{\partial^2 w^*}{\partial x^2}\right) + M_{yy}\left(\frac{\partial^2 w^*}{\partial y^2}\right) + 2M_{xy}\left(\frac{\partial^2 w^*}{\partial x \partial y}\right)\right] dA \tag{10.16}$$

The right-hand-side of above equation can be rewritten considering that:

$$\begin{aligned}
M_{xx}\left(\frac{\partial^2 w^*}{\partial x^2}\right) &= \frac{\partial}{\partial x}\left(M_{xx}\frac{\partial w^*}{\partial x}\right) - \frac{\partial M_{xx}}{\partial x}\frac{\partial w^*}{\partial x} \\
M_{yy}\left(\frac{\partial^2 w^*}{\partial y^2}\right) &= \frac{\partial}{\partial y}\left(M_{yy}\frac{\partial w^*}{\partial y}\right) - \frac{\partial M_{yy}}{\partial y}\frac{\partial w^*}{\partial y} \\
2M_{xy}\left(\frac{\partial^2 w^*}{\partial x \partial y}\right) &= \frac{\partial}{\partial y}\left(M_{xy}\frac{\partial w^*}{\partial x}\right) - \frac{\partial M_{xy}}{\partial y}\frac{\partial w^*}{\partial x} + \frac{\partial}{\partial x}\left(M_{xy}\frac{\partial w^*}{\partial y}\right) - \frac{\partial M_{xy}}{\partial x}\frac{\partial w^*}{\partial y}
\end{aligned} \tag{10.17}$$

Replacing into equation (10.16):

$$\begin{aligned}
\int_{\Omega} \sigma_{ij}\varepsilon^*_{ij} d\Omega = \; & - \int_{A} \left[\frac{\partial}{\partial x}\left(M_{xx}\frac{\partial w^*}{\partial x}\right) - \frac{\partial M_{xx}}{\partial x}\frac{\partial w^*}{\partial x} + \frac{\partial}{\partial y}\left(M_{yy}\frac{\partial w^*}{\partial y}\right) - \frac{\partial M_{yy}}{\partial y}\frac{\partial w^*}{\partial y} \right. \\
& \left. + \frac{\partial}{\partial y}\left(M_{xy}\frac{\partial w^*}{\partial x}\right) - \frac{\partial M_{xy}}{\partial y}\frac{\partial w^*}{\partial x} + \frac{\partial}{\partial x}\left(M_{xy}\frac{\partial w^*}{\partial y}\right) - \frac{\partial M_{xy}}{\partial x}\frac{\partial w^*}{\partial y} \right] dA
\end{aligned} \tag{10.18}$$

Now considering the Gauss-Green theorem applied to terms 1, 3, 5 and 7 of the R.H.S. of above equation:

$$\int_{A} \frac{\partial}{\partial x}\left(M_{xx}\frac{\partial w^*}{\partial x}\right) dA = \int_{\Gamma} M_{xx}\frac{\partial w^*}{\partial x} n_x d\Gamma$$

$$\int_{A} \frac{\partial}{\partial y}\left(M_{yy}\frac{\partial w^*}{\partial y}\right) dA = \int_{\Gamma} M_{yy}\frac{\partial w^*}{\partial y} n_y d\Gamma$$

$$\int_{A} \frac{\partial}{\partial y}\left(M_{xy}\frac{\partial w^*}{\partial x}\right) dA = \int_{\Gamma} M_{xy}\frac{\partial w^*}{\partial x} n_y d\Gamma$$

$$\int_A \frac{\partial}{\partial x}\left(M_{xy}\frac{\partial w^*}{\partial y}\right)dA = \int_\Gamma M_{xy}\frac{\partial w^*}{\partial y}n_x d\Gamma$$

Substituting into equation (10.18):

$$\begin{aligned}\int_A \sigma_{ij}\varepsilon^*_{ij}d\Omega = \; & - \int_\Gamma \left[\left(M_{xx}n_x + M_{xy}n_y\right)\frac{\partial w^*}{\partial x} + \left(M_{xy}n_x + M_{yy}n_y\right)\frac{\partial w^*}{\partial y}\right]d\Gamma \\ & + \int_A \left[\left(\frac{\partial M_{xx}}{\partial x} + \frac{\partial M_{xy}}{\partial y}\right)\frac{\partial w^*}{\partial x} + \left(\frac{\partial M_{yy}}{\partial y} + \frac{\partial M_{xy}}{\partial x}\right)\frac{\partial w^*}{\partial y}\right]dA \end{aligned} \quad (10.19)$$

Considering the equations (10.8) and (10.9), the R.H.S. of equation (10.19) can be write as:

$$\begin{aligned}\int_A \sigma_{ij}\varepsilon^*_{ij}d\Omega = & -\int_\Gamma \left(M_x\frac{\partial w^*}{\partial x} + M_y\frac{\partial w^*}{\partial y}\right)d\Gamma + \int_A \left(Q_x\frac{\partial w^*}{\partial x} + Q_y\frac{\partial w^*}{\partial y}\right)dA \\ & - \int_A \left(m_x\frac{\partial w^*}{\partial x} + m_y\frac{\partial w^*}{\partial y}\right)dA \end{aligned} \quad (10.20)$$

The second integral at R.H.S. can be re-written as:

$$\int_A \left(Q_x\frac{\partial w^*}{\partial x} + Q_y\frac{\partial w^*}{\partial y}\right)dA = \int_A \left(\frac{\partial}{\partial x}\left(Q_x w^*\right) + \frac{\partial}{\partial y}\left(Q_y w^*\right)\right)dA - \int_A \left[\left(\frac{\partial Q_x}{\partial x} + \frac{\partial Q_y}{\partial y}\right)w^*\right]dA \quad (10.21)$$

Applying the Gauss-Green theorem to the first integral at R.H.S and considering the third equation at equations (10.8) applied to the second integral at R.H.S., we have:

$$\int_A \left(Q_x\frac{\partial w^*}{\partial x} + Q_y\frac{\partial w^*}{\partial y}\right)dA = \int_\Gamma \left(Q_x n_x + Q_y n_y\right)w^* d\Gamma + \int_A q w^* dA \quad (10.22)$$

Finally, substituting equation (10.10) into above equation and substituting this equation into equation (10.20) we obtain:

$$\int_A \sigma_{ij}\varepsilon^*_{ij}dA = -\int_\Gamma \left(M_x\frac{\partial w^*}{\partial x} + M_y\frac{\partial w^*}{\partial y} + Q_n w^*\right)d\Gamma + \int_A q w^* dA$$

$$-\int_A m_x \frac{\partial w^*}{\partial x} dA - \int_A m_y \frac{\partial w^*}{\partial y} dA \tag{10.23}$$

In a similar way the R.H.S. of equation (10.11) can be written as:

$$\int_A \varepsilon_{ij}\sigma^*_{ij} dA = -\int_\Gamma \left(M^*_x \frac{\partial w}{\partial x} + M^*_y \frac{\partial w}{\partial y} + Q^*_n w \right) d\Gamma + \int_A q^* w dA$$

$$-\int_A m^*_x \frac{\partial w}{\partial x} dA - \int_A m^*_y \frac{\partial w}{\partial y} dA \tag{10.24}$$

Replacing equations (10.23) and (10.24) into equation (10.11) we obtain finally, the Somigliana's identity for the Kirchhoff's plate problem:

$$-\int_\Gamma \left(M_x \frac{\partial w^*}{\partial x} + M_y \frac{\partial w^*}{\partial y} + Q_n w^* \right) d\Gamma + \int_A q w^* dA - \int_A m_x \frac{\partial w^*}{\partial x} dA - \int_A m_y \frac{\partial w^*}{\partial y} dA =$$

$$-\int_\Gamma \left(M^*_x \frac{\partial w}{\partial x} + M^*_y \frac{\partial w}{\partial y} + Q^*_n w \right) d\Gamma + \int_A q^* w dA - \int_A m^*_x \frac{\partial w}{\partial x} dA - \int_A m^*_y \frac{\partial w}{\partial y} dA \tag{10.25}$$

The above equation relates two states of an elastic material. In order to apply this equation to solve bending problems, we need to consider one of states as known and other as the state which stands for the problem which we want to analyze. To obtain a boundary integral equation, the known state is chosen so that the domain's integrals given by the last three integrals at R.H.S. of equation (10.25) vanishes. Using the properties of Dirac delta function to represents q^* and considering $m^*_x = 0$ and $m^*_y = 0$, these integrals are written as:

$$\int_A q^* w dA = \int_A \delta(\mathbf{x}', \mathbf{x}) w dA = w(\mathbf{x}')$$

$$\int_A m^*_x \frac{\partial w}{\partial x} dA = 0$$

$$\int_A m_y^* \frac{\partial w}{\partial y} dA = 0 \tag{10.26}$$

where $\mathbf{x}'$ is the point where the load is applied, known as source point, and $\mathbf{x}$ is the point where the deflection is observed, known as field point. The state corresponding to a linear material under loading of a Dirac delta function is known as fundamental state and the variables of equation (10.25) related to this state (w^*, Q_n^*, M_x^*, M_y^*) are known as fundamental solutions which are computed analytically. Considering the state " $*$ " as the fundamental state, equation (10.25) can be written as:

$$\begin{aligned} cw(\mathbf{x}') &- \int_\Gamma \left(M_x^*(\mathbf{x}', \mathbf{x}) \frac{\partial w}{\partial x} + M_y^*(\mathbf{x}', \mathbf{x}) \frac{\partial w}{\partial y} + Q_n^*(\mathbf{x}', \mathbf{x}) w \right) d\Gamma = \\ &- \int_\Gamma \left(M_x \frac{\partial w^*(\mathbf{x}', \mathbf{x})}{\partial x} + M_y \frac{\partial w^*(\mathbf{x}', \mathbf{x})}{\partial y} + Q_n w^*(\mathbf{x}', \mathbf{x}) \right) d\Gamma \\ &+ \int_A q w^*(\mathbf{x}', \mathbf{x}) dA - \int_A m_x \frac{\partial w^*(\mathbf{x}', \mathbf{x})}{\partial x} dA - \int_A m_y \frac{\partial w^*(\mathbf{x}', \mathbf{x})}{\partial y} dA \end{aligned} \tag{10.27}$$

Alternatively, the boundary integrals at equation (10.27) can be expressed in terms of normal and tangent moments M_n and M_{ns}, using the following relation:

$$\begin{aligned} M_x &= M_n n_1 + M_{ns} s_1 \\ M_y &= M_n n_2 + M_{ns} s_2 \end{aligned} \tag{10.28}$$

where n_i and s_i are the unit-normal and unit-tangent vectors at boundary evaluation point. Replacing into equation (10.27) and simplifying we obtain:

$$cw(\mathbf{x}') - \int_\Gamma \left(M_n^*(\mathbf{x}', \mathbf{x}) \frac{\partial w}{\partial n} + M_{ns}^*(\mathbf{x}', \mathbf{x}) \frac{\partial w}{\partial s} + Q_n^*(\mathbf{x}', \mathbf{x}) w \right) d\Gamma =$$

$$-\int_{\Gamma}\left(M_n\frac{\partial w^*\left(\mathbf{x}',\mathbf{x}\right)}{\partial n}+M_{ns}\frac{\partial w^*\left(\mathbf{x}',\mathbf{x}\right)}{\partial s}+Q_n w^*\left(\mathbf{x}',\mathbf{x}\right)\right)d\Gamma$$

$$+\int_{A} qw^*\left(\mathbf{x}',\mathbf{x}\right)dA-\int_{A} m_x\frac{\partial w^*\left(\mathbf{x}',\mathbf{x}\right)}{\partial x}dA-\int_{A} m_y\frac{\partial w^*\left(\mathbf{x}',\mathbf{x}\right)}{\partial y}dA \tag{10.29}$$

Variables this equation are displacements w, rotations $\partial w/\partial n$, moments M_n and M_{ns}, and loads Q_n. For a given boundary condition, some of these variables are known. In order to have an equal number of equations and unknown variables, it is necessary to write an integral equation corresponding to the derivative of displacement w in relation to a cartesian coordinate system fixed in the source point, i.e., the point where the Dirac delta of the fundamental state is applied. The axis directions of this coordinate system are coincident with normal and tangent to the boundary directions in the source point:

$$c\frac{\partial w}{\partial n_o}\left(\mathbf{x}'\right)-\int_{\Gamma}\left(\frac{\partial M_n^*}{\partial n_o}\left(\mathbf{x}',\mathbf{x}\right)\frac{\partial w}{\partial n}+\frac{\partial M_{ns}^*}{\partial n_o}\left(\mathbf{x}',\mathbf{x}\right)\frac{\partial w}{\partial s}+\frac{\partial Q_n^*}{\partial n_o}\left(\mathbf{x}',\mathbf{x}\right)w\right)d\Gamma=$$

$$-\int_{\Gamma}\left(M_n\frac{\partial}{\partial n_o}\left[\frac{\partial w^*\left(\mathbf{x}',\mathbf{x}\right)}{\partial n}\right]+M_{ns}\frac{\partial}{\partial n_o}\left[\frac{\partial w^*\left(\mathbf{x}',\mathbf{x}\right)}{\partial s}\right]+Q_n\frac{\partial}{\partial n_o}\left[w^*\left(\mathbf{x}',\mathbf{x}\right)\right]\right)d\Gamma$$

$$+\int_{A} q\frac{\partial w^*\left(\mathbf{x}',\mathbf{x}\right)}{\partial n_o}dA-\int_{A} m_x\frac{\partial}{\partial n_o}\left[\frac{\partial w^*\left(\mathbf{x}',\mathbf{x}\right)}{\partial x}\right]dA-\int_{A} m_y\frac{\partial}{\partial n_o}\left[\frac{\partial w^*\left(\mathbf{x}',\mathbf{x}\right)}{\partial y}\right]dA \tag{10.30}$$

and

$$c\frac{\partial w}{\partial s_o}\left(\mathbf{x}'\right)-\int_{\Gamma}\left(\frac{\partial M_n^*}{\partial s_o}\left(\mathbf{x}',\mathbf{x}\right)\frac{\partial w}{\partial n}+\frac{\partial M_{ns}^*}{\partial s_o}\left(\mathbf{x}',\mathbf{x}\right)\frac{\partial w}{\partial s}+\frac{\partial Q_n^*}{\partial s_o}\left(\mathbf{x}',\mathbf{x}\right)w\right)d\Gamma=$$

$$-\int_{\Gamma}\left(M_n\frac{\partial}{\partial s_o}\left[\frac{\partial w^*\left(\mathbf{x}',\mathbf{x}\right)}{\partial n}\right]+M_{ns}\frac{\partial}{\partial s_o}\left[\frac{\partial w^*\left(\mathbf{x}',\mathbf{x}\right)}{\partial s}\right]+Q_n\frac{\partial}{\partial s_o}\left[w^*\left(\mathbf{x}',\mathbf{x}\right)\right]\right)d\Gamma$$

$$+\int_{A} q\frac{\partial w^*\left(\mathbf{x}',\mathbf{x}\right)}{\partial s_o}dA-\int_{A} m_x\frac{\partial}{\partial s_o}\left[\frac{\partial w^*\left(\mathbf{x}',\mathbf{x}\right)}{\partial x}\right]dA-\int_{A} m_y\frac{\partial}{\partial s_o}\left[\frac{\partial w^*\left(\mathbf{x}',\mathbf{x}\right)}{\partial y}\right]dA \tag{10.31}$$

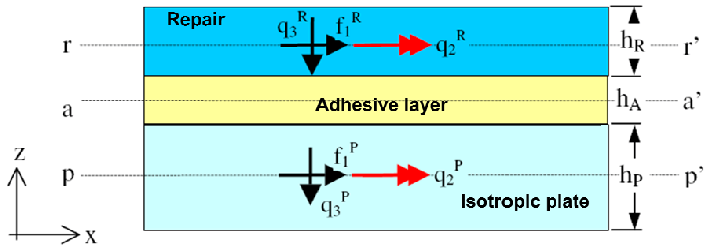

Figure 10.4: Forces and moments at $x_1 - z$ plane for equilibrium equation

Since, neither normal or tangent vectors can be defined at any internal point (as defined for points at the boundary), the "*normal*" direction for internal points will be defined to have the x-axis direction.

Using equations (10.29) through (10.31) we have a formulation kinematically compatible with the Reissner plate model.

10.5 Coupling equations

Isotropic plate equations has fifteen unknowns variables: five displacements (or tractions) at boundary and five unknowns displacements and five interaction body forces at any point in the repair region. In addition, ten unknows appears at repair: five displacements (at boundary and domain) and five interaction body forces (at domain). In this way we have twenty five unknows in the problem.

Boundary integral equations for isotropic plate and the anisotropic repair presented, represents fifteen equations and twenty five unknows. Ten additional equations must be provided. Additional equations can be written if kinematic compatibility between plate's and repair and the equilibrium conditions at adhesive layer, are considered. In this way a total of twenty five equations could be written.

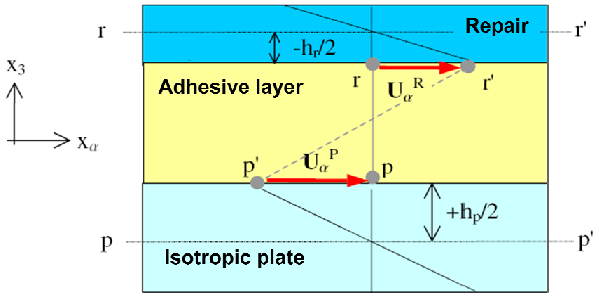

Figure 10.5: Displacements components at adhesive interfaces for shear stress definition

10.5.1 Equilibrium conditions at adhesive layer

The components of forces and moments acting in the $z-x$ plane, the equilibrium of the adhesive layer can be written as (see figure 10.4):

$$\begin{aligned} \sum F_{x_1} &= f_1^P + f_1^R = 0 \\ \sum F_{x_3} &= q_3^P + q_3^R = 0 \\ \sum M_{x_2} &= q_1^P + q_1^R + f_1^R \left(h_A + \frac{h_P + h_R}{2} \right) = 0 \end{aligned} \tag{10.32}$$

Where h_A represents the thickness of the adhesive. In a similar way, equilibrium equations can be written for $x-y$ and $y-z$ planes. In vector form, equations above can be expressed as:

$$\begin{aligned} f_\alpha^P + f_\alpha^R &= 0 \\ q_3^P + q_3^R &= 0 \\ q_\alpha^P + q_\alpha^R + f_\alpha^R \left(h_A + \frac{h_P + h_R}{2} \right) &= 0 \end{aligned} \tag{10.33}$$

10.5.2 Cinematic compatibility equations

The shear force $\tau_{3\alpha}^{A}$, acting at interior of adhesive layer can be written as:

$$\tau_{3\alpha}^{A} = f_{\alpha}^{R} = \mu_A \gamma_{3\alpha} \tag{10.34}$$

where μ_A is the shear modulus of the adhesive and $\gamma_{3\alpha}$ is the shear deformation in the α direction that can be write as (see figure 10.5):

$$\gamma_{3\alpha} = \frac{U_{\alpha}^{R} - U_{\alpha}^{P}}{h_A} \cong \frac{1}{h_A}\left\{\left(u_{\alpha}^{R} - \frac{h_R}{2}w_{\alpha}^{R}\right) - \left(u_{\alpha}^{P} + \frac{h_P}{2}w_{\alpha}^{P}\right)\right\} \tag{10.35}$$

Substituting into equation (10.34) we have:

$$\frac{h_A}{G_A} f_{\alpha}^{R} = \left(u_{\alpha}^{R} - \frac{h_R}{2}w_{\alpha}^{R}\right) - \left(u_{\alpha}^{R} + \frac{h_R}{2}w_{\alpha}^{R}\right) \tag{10.36}$$

Finally, we can consider that deflection and rotation angles at coincident points at plate and repair are related by:

$$\begin{aligned} w_3^P &= w_3^R \\ q_{\alpha}^{P} &= C\left(w_{,\alpha}^{R} - w_{\alpha}^{P}\right) \end{aligned} \tag{10.37}$$

where $C = D(1-\nu)\lambda^2/2$. In this way equations (10.31) through (10.37) represents ten additional equations obtained by considering equilibrium and cinematic compatibility conditions in the adhesive layer.

10.6 Boundary element equations for the plate

10.6.1 In-plane equations

Using the boundary element method as described in chapter 5, the discretized boundary equations for in-plane elasticity (designed as m) for the isotropic plate p, collocations can be written in matrix form as:

$$\begin{bmatrix} {}^{p}\mathbf{H}_c^m & \mathbf{0} \\ {}^{p}\mathbf{H}_d^m & \mathbf{I} \end{bmatrix} \begin{Bmatrix} \mathbf{u}_c^p \\ \mathbf{u}_d^p \end{Bmatrix} = \begin{bmatrix} {}^{p}\mathbf{G}_c^m \\ {}^{p}\mathbf{G}_d^m \end{bmatrix} \{\mathbf{t}^p\} + \begin{bmatrix} {}^{p}\mathbf{B}_c^m \\ {}^{p}\mathbf{B}_d^m \end{bmatrix} \{\mathbf{t}^p\} + \begin{Bmatrix} {}^{p}\mathbf{f}_c^0 \\ {}^{p}\mathbf{f}_d^0 \end{Bmatrix} \tag{10.38}$$

where sub-index c and d refers boundary and domain collocation points respectively. Above equation can be write in compact form as (without considering body forces $\mathbf{f}^0$):

$${}^{P}\mathbf{H}^{M}\mathbf{u}^{P} = {}^{P}\mathbf{G}^{M}\mathbf{t}^{P} + {}^{P}\mathbf{B}^{M}\mathbf{f}^{P} \tag{10.39}$$

Using the cell method, the matrix ${}^{P}\mathbf{B}^{M}$ is given by:

$$\int_{\Omega} U_{ij}^{*} f_i^P d\Omega = \left[\sum_{i=1}^{Ncell} \int_{\Omega cell} U_{ij}^{*} N_{kj} d\Omega_{cell} \right] f_i^P = {}^{P}\mathbf{B}^{M}\mathbf{f}^{P} \quad k = 1 \ldots ND \tag{10.40}$$

where ND and NC are the number of collocation points at domain and boundary of the isotropic plate, respectively.

10.6.2 Bending equations

Bending equations (identify by (b)) for the isotropic plate are given by:

$$\begin{bmatrix} {}^{p}\mathbf{H}_c^b & \mathbf{0} \\ {}^{p}\mathbf{H}_d^b & \mathbf{I} \end{bmatrix} \begin{Bmatrix} \mathbf{w}_c^p \\ \mathbf{w}_d^p \end{Bmatrix} = \begin{bmatrix} {}^{p}\mathbf{G}_c^b \\ {}^{p}\mathbf{G}_d^b \end{bmatrix} \{\mathbf{p}^p\} + \begin{bmatrix} {}^{p}\mathbf{B}_c^b \\ {}^{p}\mathbf{B}_d^b \end{bmatrix} \{\mathbf{q}^p\} + \begin{Bmatrix} {}^{p}\mathbf{q}_c^0 \\ {}^{p}\mathbf{q}_d^0 \end{Bmatrix} \tag{10.41}$$

In compact form this equation can be write as:

$$ {}^{P}\mathbf{H}^{B}\mathbf{u}^{P} = {}^{P}\mathbf{G}^{B}\mathbf{t}^{P} + {}^{P}\mathbf{B}^{B}\mathbf{f}^{P} + \mathbf{q}^{\mathbf{0}} \tag{10.42} $$

where vector $\mathbf{q}^{0}$ represents pressure forces acting on the plate.

10.6.3 Isotropic plate equations

The complete boundary element method equations for the isotropic plate can be write in matrix form, considering equations (10.38) and (10.41) as:

$$ \begin{bmatrix} {}^{p}\mathbf{H}_{c}^{m} & \mathbf{0} & \mathbf{0} & \mathbf{0} \\ {}^{p}\mathbf{H}_{d}^{m} & \mathbf{I} & \mathbf{0} & \mathbf{0} \\ \mathbf{0} & \mathbf{0} & {}^{p}\mathbf{H}_{c}^{b} & \mathbf{0} \\ \mathbf{0} & \mathbf{0} & {}^{p}\mathbf{H}_{d}^{b} & \mathbf{I} \end{bmatrix} \begin{Bmatrix} \mathbf{u}_{c}^{p} \\ \mathbf{u}_{d}^{p} \\ \mathbf{w}_{c}^{p} \\ \mathbf{w}_{d}^{p} \end{Bmatrix} = \begin{bmatrix} {}^{p}\mathbf{G}_{c}^{m} & \mathbf{0} \\ {}^{p}\mathbf{G}_{d}^{m} & \mathbf{0} \\ \mathbf{0} & {}^{p}\mathbf{G}_{c}^{b} \\ \mathbf{0} & {}^{p}\mathbf{G}_{d}^{b} \end{bmatrix} \begin{Bmatrix} \mathbf{t}^{p} \\ \mathbf{p}^{p} \end{Bmatrix} + \begin{bmatrix} {}^{p}\mathbf{B}_{c}^{m} & \mathbf{0} \\ {}^{p}\mathbf{B}_{d}^{m} & \mathbf{0} \\ \mathbf{0} & {}^{p}\mathbf{B}_{c}^{b} \\ \mathbf{0} & {}^{p}\mathbf{B}_{d}^{b} \end{bmatrix} \begin{Bmatrix} \mathbf{f}^{p} \\ \mathbf{q}^{p} \end{Bmatrix} + \begin{Bmatrix} {}^{p}\mathbf{f}_{c}^{0} \\ {}^{p}\mathbf{f}_{d}^{0} \\ {}^{p}\mathbf{q}_{c}^{0} \\ {}^{p}\mathbf{q}_{d}^{0} \end{Bmatrix} \tag{10.43} $$

In compact form, this equation can be written as:

$$ {}^{P}\mathbf{H}\mathbf{x}^{P} = {}^{P}\mathbf{G}\mathbf{y}^{P} + {}^{P}\mathbf{B}\mathbf{z}^{P} + \mathbf{q}^{0P} \tag{10.44} $$

Considering that vector $\mathbf{z}^{P}$ will be an unknown vector always, equation (10.44) can by re-written as:

$$ \begin{bmatrix} {}^{P}\mathbf{H} & -{}^{P}\mathbf{B} \end{bmatrix} \begin{Bmatrix} \mathbf{x}^{P} \\ \mathbf{z}^{P} \end{Bmatrix} = {}^{P}\mathbf{G}\mathbf{y}^{P} + \mathbf{q}^{0P} \tag{10.45} $$

Expanding we have:

$$\begin{bmatrix} {}^{p}\mathbf{H}_c^m & \mathbf{0} & \mathbf{0} & \mathbf{0} & -{}^{p}\mathbf{B}_c^m & \mathbf{0} \\ {}^{p}\mathbf{H}_d^m & \mathbf{I} & \mathbf{0} & \mathbf{0} & -{}^{p}\mathbf{B}_d^m & \mathbf{0} \\ \mathbf{0} & \mathbf{0} & {}^{p}\mathbf{H}_c^b & \mathbf{0} & \mathbf{0} & -{}^{p}\mathbf{B}_c^b \\ \mathbf{0} & \mathbf{0} & {}^{p}\mathbf{H}_d^b & \mathbf{I} & \mathbf{0} & -{}^{p}\mathbf{B}_d^b \end{bmatrix} \begin{Bmatrix} \mathbf{u}_c^p \\ \mathbf{u}_d^p \\ \mathbf{w}_c^p \\ \mathbf{w}_d^p \\ \mathbf{f}^P \\ \mathbf{q}^P \end{Bmatrix} = \begin{bmatrix} {}^{p}\mathbf{G}_c^m & \mathbf{0} \\ {}^{p}\mathbf{G}_d^m & \mathbf{0} \\ \mathbf{0} & {}^{p}\mathbf{G}_c^b \\ \mathbf{0} & {}^{p}\mathbf{G}_d^b \end{bmatrix} \begin{Bmatrix} \mathbf{t}^p \\ \mathbf{p}^p \end{Bmatrix} + \begin{Bmatrix} {}^{p}\mathbf{f}_c^0 \\ {}^{p}\mathbf{f}_d^0 \\ {}^{p}\mathbf{q}_c^0 \\ {}^{p}\mathbf{q}_d^0 \end{Bmatrix} \tag{10.46}$$

10.7 Boundary element equations for the repair

In a similar way as the case of isotropic plate, boundary element equations for the repair are:

$$\begin{bmatrix} {}^{R}\mathbf{H}_c^m & \mathbf{0} & \mathbf{0} & \mathbf{0} & -{}^{R}\mathbf{B}_c^m & \mathbf{0} \\ {}^{R}\mathbf{H}_d^m & \mathbf{I} & \mathbf{0} & \mathbf{0} & -{}^{R}\mathbf{B}_d^m & \mathbf{0} \\ \mathbf{0} & \mathbf{0} & {}^{R}\mathbf{H}_c^b & \mathbf{0} & \mathbf{0} & -{}^{R}\mathbf{B}_c^b \\ \mathbf{0} & \mathbf{0} & {}^{R}\mathbf{H}_d^b & \mathbf{I} & \mathbf{0} & -{}^{R}\mathbf{B}_d^b \end{bmatrix} \begin{Bmatrix} \mathbf{u}_c^R \\ \mathbf{u}_d^R \\ \mathbf{w}_c^R \\ \mathbf{w}_d^R \\ \mathbf{f}^R \\ \mathbf{q}^R \end{Bmatrix} = \begin{Bmatrix} {}^{R}\mathbf{f}_c^0 \\ {}^{R}\mathbf{f}_d^0 \\ {}^{R}\mathbf{q}_c^0 \\ {}^{R}\mathbf{q}_d^0 \end{Bmatrix} \tag{10.47}$$

Considering that all collocation points of the repair are coupled with the domain's collocation points of the plate, the above equation can be written as:

$$\begin{bmatrix} {}^{R}\mathbf{H}^m & \mathbf{0} & -{}^{R}\mathbf{B}^m & \mathbf{0} \\ \mathbf{0} & {}^{R}\mathbf{H}^b & \mathbf{0} & -{}^{R}\mathbf{B}^b \end{bmatrix} \begin{Bmatrix} \mathbf{u}^R \\ \mathbf{w}^R \\ \mathbf{f}^R \\ \mathbf{q}^R \end{Bmatrix} = \begin{Bmatrix} {}^{R}\mathbf{f}^0 \\ {}^{R}\mathbf{q}^0 \end{Bmatrix} \tag{10.48}$$

where,

$$ {}^{R}\mathbf{H}^{m} = \begin{bmatrix} {}^{R}\mathbf{H}_{c}^{m} & \mathbf{0} \\ {}^{R}\mathbf{H}_{d}^{m} & \mathbf{I} \end{bmatrix}; \quad {}^{R}\mathbf{H}^{b} = \begin{bmatrix} {}^{R}\mathbf{H}_{c}^{b} & \mathbf{0} \\ {}^{R}\mathbf{H}_{d}^{b} & \mathbf{I} \end{bmatrix} \tag{10.49} $$

10.8 Equilibrium equations for the adhesive layer

First equation in (10.33) can be written in matrix form as:

$$ \begin{Bmatrix} \mathbf{f}_1^P \\ \mathbf{f}_2^P \\ \vdots \\ \mathbf{f}_{ND}^P \end{Bmatrix} + \begin{Bmatrix} \mathbf{f}_1^R \\ \mathbf{f}_2^R \\ \vdots \\ \mathbf{f}_{ND}^R \end{Bmatrix} = \begin{Bmatrix} \mathbf{0} \\ \mathbf{0} \\ \vdots \\ \mathbf{0} \end{Bmatrix} \Rightarrow \mathbf{I}\mathbf{f}^P + \mathbf{I}\mathbf{f}^R = \mathbf{0} \tag{10.50} $$

Second and third equations in (10.33) can be written in compact form as:

$$ \begin{Bmatrix} \mathbf{q}_1^P \\ \mathbf{q}_2^P \\ \vdots \\ \mathbf{q}_{ND}^P \end{Bmatrix} + \begin{Bmatrix} \mathbf{q}_1^R \\ \mathbf{q}_2^R \\ \vdots \\ \mathbf{q}_{ND}^R \end{Bmatrix} + \mathbf{C}_1 \begin{Bmatrix} \mathbf{f}_1^R \\ \mathbf{f}_2^R \\ \vdots \\ \mathbf{f}_{ND}^R \end{Bmatrix} = \begin{Bmatrix} \mathbf{0} \\ \mathbf{0} \\ \vdots \\ \mathbf{0} \end{Bmatrix} \Rightarrow \mathbf{I}\mathbf{q}^P + \mathbf{I}\mathbf{q}^R + \mathbf{C}_1\mathbf{f}^R = \mathbf{0} \tag{10.51} $$

where,

$$ \mathbf{C}_1 = \left(h_A + \frac{h_P + h_R}{2} \right) \begin{bmatrix} 1 & & & & & & \\ & 1 & & & & & \\ & & 0 & & & & \\ & & 1 & & & & \\ & & & 1 & & & \\ & & & & 0 & & \\ & & & & & \ddots & \end{bmatrix} \tag{10.52} $$

10.9 Kinematic compatibility equations for displacements

Equation (10.36) can be write in matrix form as:

$$\left\{\begin{array}{c}\mathbf{u}_1^R\\ \mathbf{u}_2^R\\ \vdots\\ \mathbf{u}_{ND}^R\end{array}\right\}-\left\{\begin{array}{c}\mathbf{u}_{1d}^P\\ \mathbf{u}_{2d}^P\\ \vdots\\ \mathbf{u}_{(ND)d}^P\end{array}\right\}-\frac{h_R}{2}\mathbf{C}_1^T\left\{\begin{array}{c}\mathbf{w}_1^R\\ \mathbf{w}_2^R\\ \vdots\\ \mathbf{w}_{ND}^R\end{array}\right\}-\frac{h_P}{2}\mathbf{C}_1^T\left\{\begin{array}{c}\mathbf{w}_{1d}^P\\ \mathbf{w}_{2d}^P\\ \vdots\\ \mathbf{w}_{(ND)d}^P\end{array}\right\}=\frac{h_A}{G_A}\left\{\begin{array}{c}\mathbf{f}_1^R\\ \mathbf{f}_2^R\\ \vdots\\ \mathbf{f}_{ND}^R\end{array}\right\} \tag{10.53}$$

or,

$$\mathbf{I}\mathbf{u}^R-\mathbf{I}\mathbf{u}_d^P-\frac{h_R}{2}\mathbf{C}_1^T\mathbf{w}^R-\frac{h_R}{2}\mathbf{C}_1^T\mathbf{w}_d^P-\frac{h_A}{G_A}\mathbf{f}^R=\mathbf{0} \tag{10.54}$$

Finally, equations (10.37) can be written as:

$$\mathbf{C}\left(\mathbf{w}^{\mathbf{R}}-\mathbf{w}_{\mathbf{d}}^{\mathbf{P}}\right)=\mathbf{q}^{\mathbf{P}} \tag{10.55}$$

where, $\mathbf{C}$ is an incidence matrix.

10.10 Plate-repair coupling equations

Substituting equation (10.50) into (10.51) we have:

$$\mathbf{I}\mathbf{q}^P+\mathbf{I}\mathbf{q}^R-\mathbf{C}^1\mathbf{f}^P=\mathbf{0} \tag{10.56}$$

In similar way, replacing equations (10.50) and (10.55) into equation (10.54) we obtain:

$$\mathbf{I}\mathbf{u}^R-\mathbf{I}\mathbf{u}_d^P-\mathbf{C}_2\mathbf{q}^P-\mathbf{C}_1^T\mathbf{w}_d^P+\mathbf{A}\mathbf{f}^P=\mathbf{0} \tag{10.57}$$

where the constant $1/2(h_R + h_P)$ was included into matrix $\mathbf{C}_1^T$, $\mathbf{C}_2 = (h_R/2)\mathbf{C_1}^T\mathbf{C}^{-1}$ and $\mathbf{A} = h_A/G_A\mathbf{I}$. Replacing equations (10.50) and (10.55) into equation (10.48) we obtain:

$$\begin{bmatrix} {}^R\mathbf{H}^m & \mathbf{0} & {}^R\mathbf{B}^m & \mathbf{0} \\ \mathbf{0} & {}^R\mathbf{H}^b & \mathbf{0} & -{}^R\mathbf{B}^b \end{bmatrix} \begin{Bmatrix} \mathbf{u}^R \\ \mathbf{w}_d^P \\ \mathbf{f}^P \\ \mathbf{q}^R \end{Bmatrix} = \begin{Bmatrix} {}^R\mathbf{f}^0 \\ {}^R\mathbf{q}^0 \end{Bmatrix} \tag{10.58}$$

Finally, considering equations (10.46) and (10.56) through (10.58) we obtain the complete equations system for the problem:

$$\begin{bmatrix} {}^p\mathbf{H}_c^m & \mathbf{0} & \mathbf{0} & \mathbf{0} & -{}^p\mathbf{B}_c^m & \mathbf{0} & \mathbf{0} & \mathbf{0} \\ {}^p\mathbf{H}_d^m & \mathbf{I} & \mathbf{0} & \mathbf{0} & -{}^p\mathbf{B}_d^m & \mathbf{0} & \mathbf{0} & \mathbf{0} \\ \mathbf{0} & \mathbf{0} & {}^p\mathbf{H}_c^b & \mathbf{0} & \mathbf{0} & -{}^p\mathbf{B}_c^b & \mathbf{0} & \mathbf{0} \\ \mathbf{0} & \mathbf{0} & {}^p\mathbf{H}_d^b & \mathbf{I} & \mathbf{0} & -{}^p\mathbf{B}_d^b & \mathbf{0} & \mathbf{0} \\ \mathbf{0} & \mathbf{0} & \mathbf{0} & \mathbf{0} & {}^R\mathbf{B}^m & \mathbf{0} & {}^R\mathbf{H}^m & \mathbf{0} \\ \mathbf{0} & \mathbf{0} & \mathbf{0} & {}^R\mathbf{H}^b & \mathbf{0} & \mathbf{0} & \mathbf{0} & -{}^R\mathbf{B}^b \\ \mathbf{0} & \mathbf{0} & \mathbf{0} & \mathbf{0} & -\mathbf{C}_1 & \mathbf{I} & \mathbf{0} & \mathbf{I} \\ \mathbf{0} & -\mathbf{I} & \mathbf{C}_2 & -\mathbf{C}_1^T & \mathbf{A} & \mathbf{0} & \mathbf{I} & \mathbf{0} \end{bmatrix} \begin{Bmatrix} \mathbf{u}_c^p \\ \mathbf{u}_d^p \\ \mathbf{w}_c^p \\ \mathbf{w}_d^p \\ \mathbf{f}^p \\ \mathbf{q}^p \\ \mathbf{u}^R \\ \mathbf{q}^R \end{Bmatrix} = \tag{10.59}$$

$$\begin{bmatrix} {}^p\mathbf{G}_c^m & \mathbf{0} \\ {}^p\mathbf{G}_d^m & \mathbf{0} \\ \mathbf{0} & {}^p\mathbf{G}_c^b \\ \mathbf{0} & {}^p\mathbf{G}_c^b \\ \mathbf{0} & \mathbf{0} \\ \mathbf{0} & \mathbf{0} \\ \mathbf{0} & \mathbf{0} \\ \mathbf{0} & \mathbf{0} \end{bmatrix} \begin{Bmatrix} \mathbf{t}^p \\ \mathbf{p}^p \end{Bmatrix} + \begin{Bmatrix} {}^p\mathbf{f}_c^0 \\ {}^p\mathbf{f}_d^0 \\ {}^p\mathbf{q}_c^0 \\ {}^p\mathbf{q}_d^0 \\ {}^R\mathbf{f}^0 \\ {}^R\mathbf{q}^0 \\ \mathbf{0} \\ \mathbf{0} \end{Bmatrix} \tag{10.60}$$

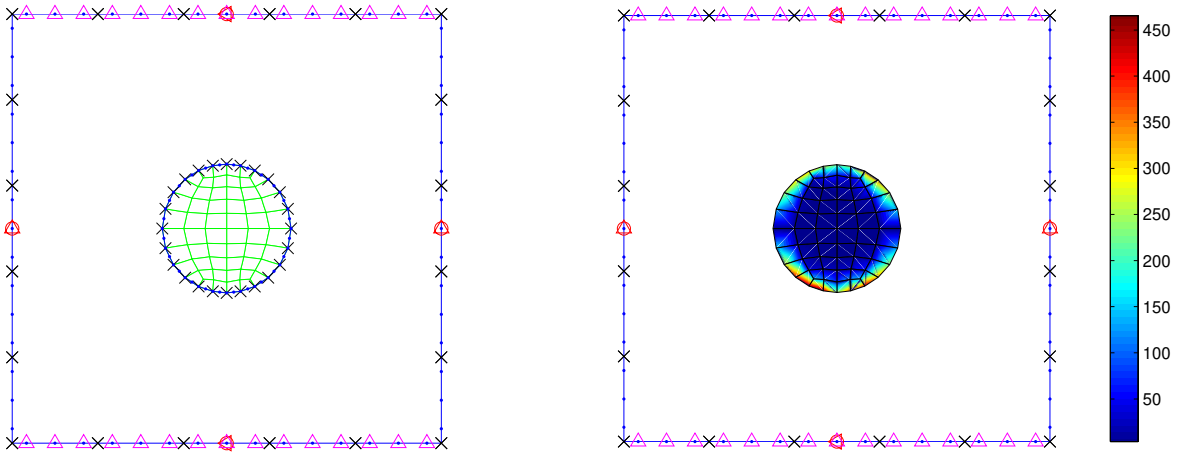

Figure 10.6: Left: BEM model. Right: Shear stress at adhesive layer

10.11 Numerical examples

10.11.1 Plate with adhesively bonded isotropic circular patch

To test the formulation developed here a square isotropic plate with adhesively bonded isotropic circular patch modeled (using the Reissner plate theory) will be analyzed and shear stress distribution in the repair zone will be compared with the theoretical solution given by Rose and Wang, 2002 for isotropic sheet repaired with isotropic repair. The wide of the plate is $90mm$, thickness $1.5mm$ and it is subject to in-plane load σ_0. The material constants are chosen as $E = 70GPa$, $\nu = 0.3$. A circular isotropic patch of radius $R = 30mm$ is bonded to the sheet over the region $A\{x_1^2 + x_2^2\}$. The patch has the same material as the plate with thickness $h_1 = 1.5mm$. The adhesive layer has thickness $h_a = 0.15mm$ and shear modulus $G_a = 0.6GPa$. The boundary of the plate is subdivided into 25 quadratic discontinuous elements and 24 elements at boundary patch (see figure 10.6). 56 continuous and constant bi-quadratic cells has been used. Simply supported conditions are applied to the plate. Figure 10.6 shows the shear stress distribution in the adhesive layer and figure 10.7 presents the normalized shear stress in the adhesive along y-axis obtained compared with analytic

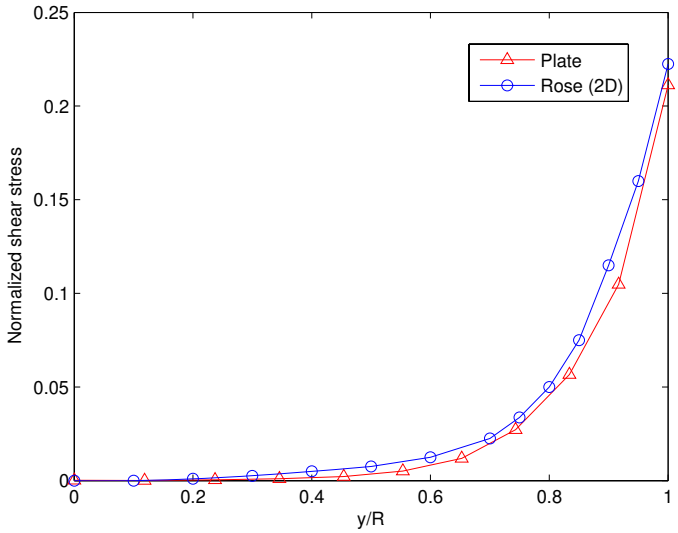

Figure 10.7: Shear stress distribution in the adhesive layer along y-axis

solution given by Rose and Wang, 2002 for the two-dimensional case [1].

10.11.2 Plate with adhesively bonded anisotropic circular patch

The same problem is analyzed but now considering an anisotropic patch. Mechanical properties considered are: $E_1 = 25GPa$, $E_2 = 208GPa$, $G_{12} = 72.4GPa$ and $\nu = 0.02$. Twelve boundary element was used to discretized the plate border and 24 quadratic discontinuous boundary elements in the repair boundary (see figure 10.8). Similar boundary conditions and loads were applied.

Figure 10.8(right) shows the normalized shear stress distribution in the adhesive layer. A similar distribution with that encountered for the isotropic repair is observed. Figure

[1]Since do not exist analytic solution for thick plates repaired with isotropic patch, the shear stress distribution along y-axis in the adhesive layer, was compared with the analytic solution given by Rose for the two-dimensional problem. Furthermore, in this problem the bending effect on the response of the plate is neglectible.

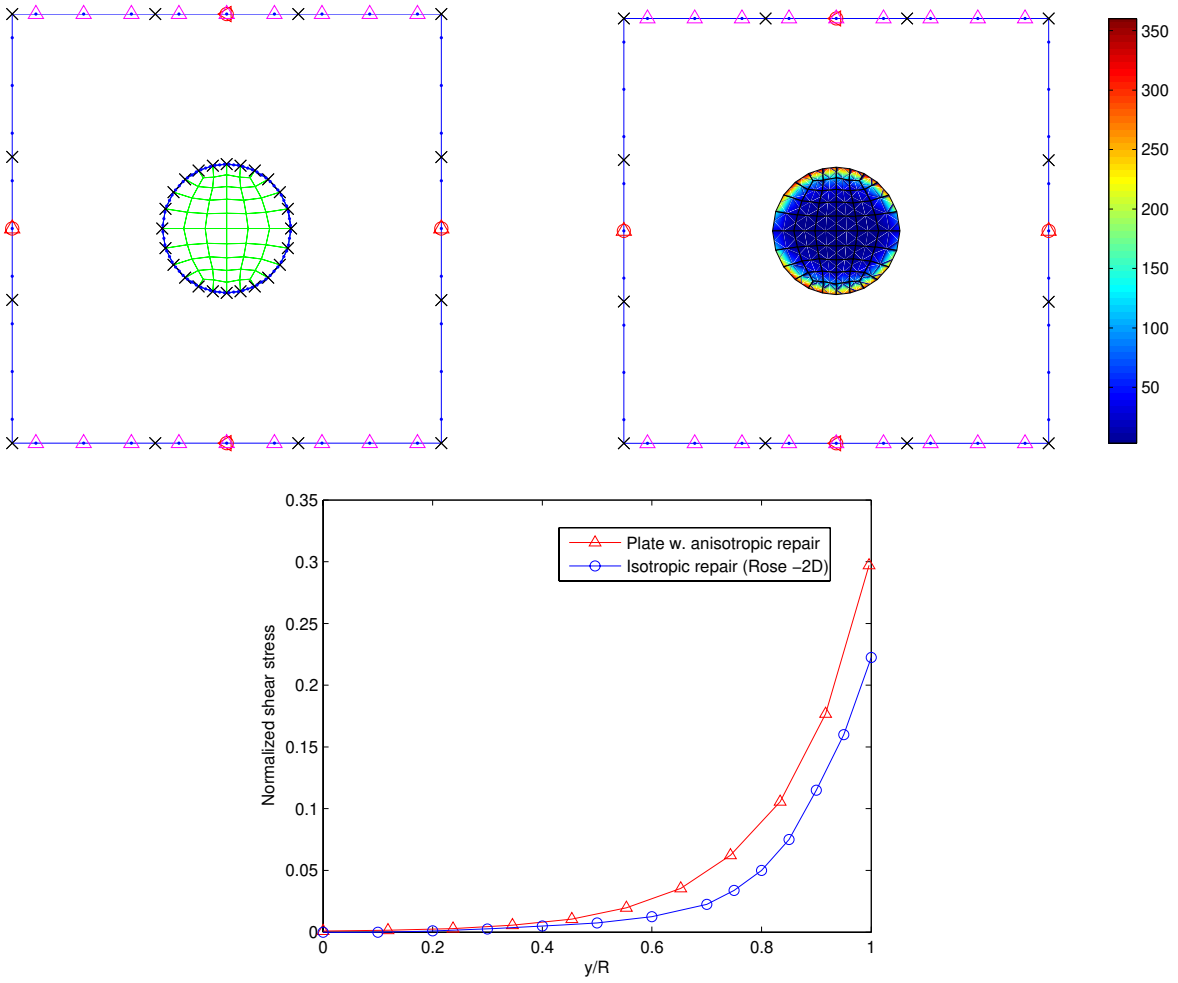

Figure 10.8: Left: DBEM model. Right: Normalized shear stress map in the adhesive Center: Normalized Shear stress in the adhesive layer along y-axis

10.8(center) shows the normalized shear stress in the adhesive along y-axis compared with analytic solution given by Rose and Wang, 2002 for two-dimensional isotropic repair. Since do not exist analytic solution for the case of thick plate repaired with composite patch, the shear stress distribution along y-axis in the adhesive layer, was compared with the analytic solution given by Rose for the two-dimensional isotropic patch problem. In this problem, we can note the effect the bending effect on the shear stress in the adhesive layer.

10.11.3 Cracked plate with bonded anisotropic circular patch

A Square isotropic cracked plate with adhesively bonded anisotropic circular patch is analyzed. The length of the crack is $2a = 15mm$. The wide of the plate is $100mm$, thickness $1.5mm$ and it is subject to in-plane load σ_0, along of $y = \pm 50mm$. The material constants are chosen as $E = 70GPa$, $\nu = 0.3$. A circular orthotropic patch with radius $R = 30mm$ is bonded to the plate. The material properties are: $E_1 = 25GPa$, $E_2 = 208GPa$, $G_{12} = 72.4GPa$ and $\nu = 0.02$, with thickness of $1.5mm$. The adhesive layer has thickness $h_a = 0.15mm$ and shear modulus $G_a = 0.6GPa$.

A similar BEM model used in the example 8.5.2. Seven boundary element was used to discretized the plate border and 24 quadratic discontinuous boundary elements in the repair boundary (see figure 10.9). Plate's border at $y = \pm 50mm$ are simply supported. Figure 10.9(right) shows the shear stress distribution in the adhesive layer. A similar distribution with that encountered for the isotropic repair is observed. Figure 10.9(center) shows the normalized shear stress in the adhesive along y-axis compared with solution obtained for the two-dimensional problem. As can be seen the shear stress in adhesive is lower than those obtained for the two-dimensional problem because the presence of bending effect in the plate. Additional verification is presented in this figure. The anisotropic formulation proposed in this chapter is verified using an quase-isotropic model for the repair and solution is compared with the fully isotropic patch. Good correlation is obtained.

Finally, figure 10.10 shows the K_{RMS} (given by equation (8.30)) as function of crack length. As in two-dimensional problems an asymptotic behavior is founded. The asymptotic analytical value for infinite crack predicted by equation (8.31) is $355.6MPa.m^{1/2}$. A good asymptotic behavior of the K_{RMS} predicted by the BEM model is observed if we consider that equation 8.30 only apply for plates with infinite crack.

10.11.4 Rectangular cracked plate repaired with bonded patch

The boundary element analysis of a rectangular isotropic fracture plate repaired with adhesively bonded anisotropic circular patch is presented. The plate is $248mm \times 118mm$, thickness $h_P = 2.0mm$ and it is subject to in-plane load $\sigma_0 = 79.4MPa$. The material constants are chosen as $E = 72.39GPa$, $\nu = 0.33$. A circular anisotropic patch of radius $R = 25mm$ and thickness $h_R = 3.2mm$ is bonded to the plate (see figure 10.11). The mechanical properties are of patch are: $E_1 = 37.35GPa$, $E_2 = 11.38GPa$, $G_{12} = 5.97GPa$ and $\nu = 0.38$. The adhesive layer has thickness $h_a = 0.1mm$ and shear modulus $G_a = 0.44GPa$. This analysis was performed using a combined boundary element method and finite element method formulation as presented by Sekine et al., 2005, where the cracked plate is modeled using a 3D BEM model and the repair a plate model.

A total of 28 quadratic discontinuous boundary elements were used to discretize the boundary of the isotropic cracked plate. Meshes from 4 to 16 quadratic discontinuous boundary elements were used to discretize the crack faces. Patch domain was discretized using 128 cells and 24 quadratic discontinuous elements has been used. Simply supported conditions were applied to all sides. The resultant shear stress distribution in the adhesive layer obtained is showed in Figure 10.11.

Table 10.1 compares values for the maximum stress intensity factor: $K_{Imax} = K_{Im} + 6/h_P^2 K_I^b$ calculated along plate thickness with those K_I reported in Sekine et al., 2005.

Table 10.1: Stress intensity factors for cracked plate repaired with composite patch

z(mm)	$K_{Imax}(MPam^{1/2})$ **BEM**	$K_I(MPam^{1/2})$**-Sekine**	error
0.40	13.82	12.60	4.32%
0.80	11.56	11.09	4.24%
1.20	9.89	9.52	3.89%
1.60	8.15	7.84	3.95%

10.12 Conclusions

A boundary element method formulation for the analysis of cracked isotropic thick plates repaired with symmetrical laminate composite plates, was developed. The equations for the repair is based on boundary integral formulation considering three parameters, based on the theory of plates of Kirchhoff as a generalization of the integral formulation of thin plates traditionally used. The isotropic model linear proposed for the adhesive was extended to consider shear forces and bending moments acting on it. This way, equations for kinematic coupling for displacements and rotations, as well as a system of equations that describe the equilibrium of forces and moments that act on the adhesive, were established. Domains integrals containing forces and moments in the repair's area are threated with using the cell method. A special type of semi-discontinuous bi-quadratic cells was used in the edge of the repair, used altogether with constant and continuous bi-quadratic cells. In the analysis of problems involving isotropic repairs it was observed that the shear stress in the adhesive are comparable with those in the literature. Results obtained for the problem with anisotropic repair are similar with those encountered in the case of isotropic repair, but needs to be validated yet.

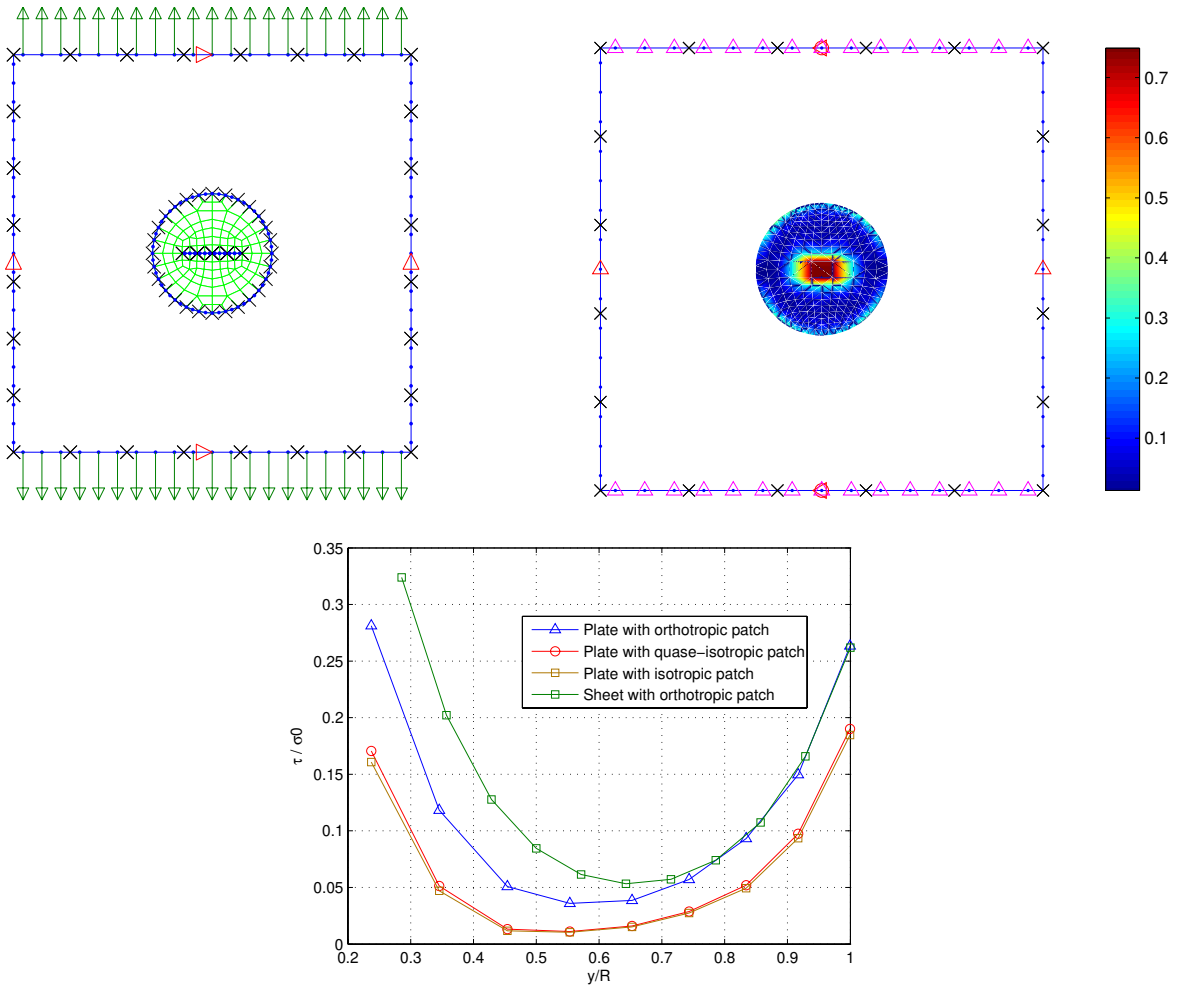

Figure 10.9: Left: DBEM model for cracked plate with anisotropic patch. Right: Normalized shear stress map in the adhesive Center: Normalized Shear stress in the adhesive layer along y-axis

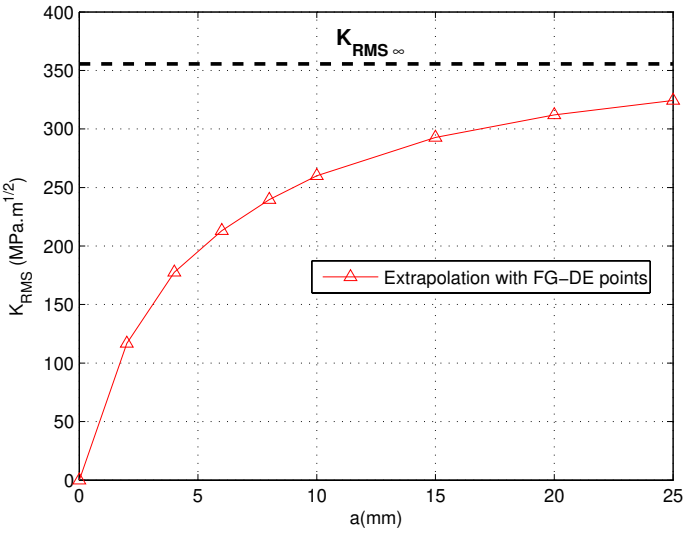

Figure 10.10: K_{RMS} variation for different crack lengths

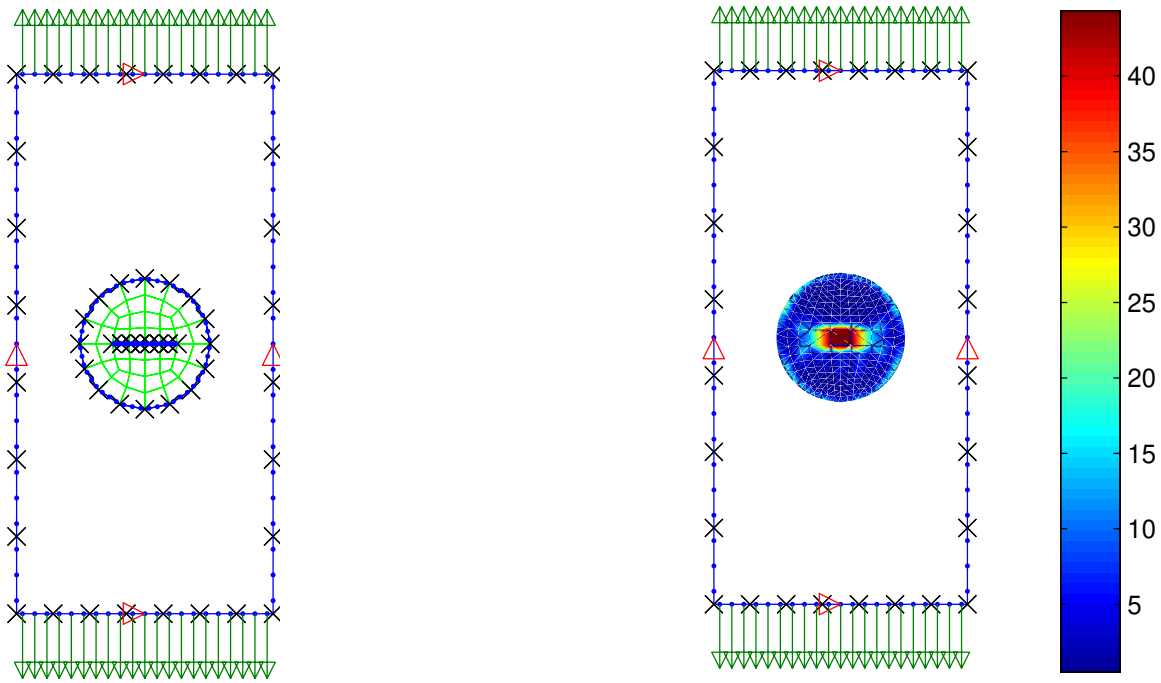

Figure 10.11: Boundary element model for cracked isotropic plate repaired with composite circular patch and shear stress distribution in the adhesive

Chapter 11

Conclusions

11.1 Final Conclusions

This work was developed a boundary element method formulation for the analysis of cracked plates repaired with symmetrical laminate composite materials.

A revision of the theory elasticity applied to bi-dimensional problems involving isotropic and anisotropic materials, as well as the theories of Kichhoff for anisotropic thin plate bending and the theory of Reissner for isotropic thick plates, was presented. For anisotropic materials, was used the theory of symmetrical laminates to obtain the mechanical properties of the plate from the mechanical properties of the laminate components. Also, the five stress intensity factors (two in-plane response and three accounting bending effects) were presented. The application of the extrapolation method for calculate these factors was showed.

The direct boundary element method for bi-dimensional elasticity problems for isotropic and anisotropic materials, was presented. Also, the dual boundary element method for the analysis of fracture mechanics problems in isotropic plane elasticity and thick plate bending. The domains integrals containing in-plane distributed body forces and those containing pres-

sure forces acting on the isotropic plate were transformed to boundary integral ones using the divergence theorem. Singular and hypersingular integrals were treated using rigid body considerations and exact integration, in the case of plane elasticity. For thick plate bending, expansion by Taylor's series for the treatment of strong and hypersingular integrals, along with element subdivision and cubic Telles transformation for strong and weakly singularities were used. Good correlation of the results were obtained, when compared with those reported in the literature. But, the stress intensity factors calculated here do not show satisfactory results in all the cases. More research work must be done to improve this results.

Based on formulations presented, a boundary element method formulation for the analysis of cracked isotropic sheet repaired with symmetrical laminate composite materials, was presented. For this, an isotropic linear elastic response and a shear deformational state in the adhesive is considered. In this way, coupling equations based on compatibility kinematics and forces balance considerations between displacements and the body forces in the repair area. Domain's integrals containing these interaction forces were threated by means of the cell method, using for it constant cells in the fracture neighborhood and continuous bi-quadratic cells for the rest of the region. This way, a general system of equations for the problem was established.

For the analyzed cases comparable results were obtained for shear stress in the adhesive when compared with the theoretical solutions and other numerical results. Differences between results could become from the poor interpolation capacity of the constant cells in the proximity of the crack, due to the high stress gradient that appears in this zone. In some cases, the stress intensity factors obtained differs with those reported in the literature. These differences could be originated in the use of cells, the DRBEM collocations points distribution or by the extrapolation method used.

Finally, a boundary element method formulation for the analysis of cracked isotropic thick plates repaired with symmetrical laminate composite plates, was developed. The equations for the repair is based in an boundary integral formulation considering three parameters, based on the theory of plates of Kirchhoff as a generalization of the integral formulation of thin plates traditionally used. The isotropic model linear proposed for the adhesive it was extended to consider shear forces and bending moments acting on it. This way, equations for kinematic coupling for displacements and rotations, as well as a system of equations that describe the equilibrium of forces and moments that act on the adhesive, were established. Domains integrals containing forces and moments in the repair's area are threated with using the cell method. A special type of semi-discontinuous bi-quadratic cells was used in the edge of the repair, used altogether with constant and continuous bi-quadratic cells. In the analysis of problems involving isotropic repairs it was observed that the shear stress in the adhesive are comparable with those in the literature. Results obtained for the problem with anisotropic repair are similar with those encountered in the case of isotropic repair, including the stress intensity factors calculated. But more research work must be done to improve the formulation proposed in this work.

11.2 Future work

The future work proposed are:

- Boundary element analysis of cracked stiffened panels repaired with adhesively composite patchs.

- Boundary element analysis of cracked assembled plate-structures repaired with adhesively composite patchs.

- Fiber direction optimization of adhesively composite patchs.

- Crack propagation analysis in cracked stiffened panels repaired with adhesively composite patchs.

Referências

Albuquerque, E. L. and Sollero, P. (1998). The boundary element method applied to transient dynamic anisotropic problems. In Kassab, A. J., Brebbia, C. A., e Chopra, M., editors, *Proc. Boundary Element Method XX*, pages 617–624, Orlando - USA.

Albuquerque, E. L., Sollero, P. and Aliabadi, M. H. (1999). The dual boundary element formulation applied to dynamic fracture mechanics in anisotropic materials. In Aliabadi, M. H., editor, *Proc. Boundary Element Techniques*, pages 23–29, London - UK.

Albuquerque, E. L., Sollero, P. and Aliabadi, M. H. (1999). Computation of dynamic stress intensity factors in anisotropic materials using the boundary element method. In Pimenta, P. M., Brasil, R. M. L. R. F., e Almeida, E. S. A., editors, *Proc. XX CILAMCE*, CD-ROM, São Paulo, Brasil.

Albuquerque, E. L. (2001). *Numerical analysis of composite plates using the boundary element method* Pos-doctoral research report, Universidade Estadual de Campinas, Grant number 03/11537-3 Faculdade de Engenharia Mecânica, 2001. In portuguese.

Albuquerque, E. L. (2001). *Análise de problemas dinâmicos em materiais anisotrópicos usando o método dos elementos de contorno.* Campinas, Faculdade de Engenharia Mecânica, Universidade Estadual de Campinas, 164 p., Tese (Doutorado).

Albuquerque, E. L., Sollero, P. and Portilho de Paiva, W. (2007). The radial integration

method applied to dynamic problems of anisotropic plates *Communications in Numerical Methods in Enginnering*, 23: 805-818.

Aliabadi, M. H. (1997). Boundary element formulation in fracture mechanics. *Applied Mechanics Review*, 50(2): 203-210.

Aliabadi, M. H. and Rooke, D. P. (1991). *Numerical fracture mechanics*. Computational Mechanical Publications, Southampton, Boston.

Aliabadi, M. H. (2003). *The Boundary Element Method: Applications in Solids and Structures*. John Wiley and Sons, New York.

Belhouari, M., Bouiadjra, B., Megueni, A., Kaddouri, K. (2004). Comparison of double and single repairs to symmetric composite structures: a numerical analysis. *Composite Structures*, 65: 47-53.

Brebbia, C. A. and Dominguez, J. (1989). *Boundary Element - An Introductory Course.* Computational Mechanics Publications, Southamptom, Boston, second edition.

Dirgantara, T. and Aliabadi, M. H. (2001). Dual boundary element formulation for fracture mechanics analysis of shear deformable shells. *International Journal of Solid and Structures*, 38: 7769-7800.

Dirgantara, T. and Aliabadi, M. H. (1999). A new boundary element formulation for shear deformable shells analysis. *International Journal for Numerical Methods In Engineering*, 45: 1257-1275.

Dirgantara, T. (2002). *Boundary Element Analysis of Cracks in Shear Deformable Plates and Shells*. Topics in Engineering, WIT Press, Southampton, Boston, Vol. 43.

El-Zafrany, A., Fadhil, S. and Debbih, M. (1995). An efficient approach for boundary element. Boundary analysis of thin and thick plates. *Computers and Structures*, 56(4): 565-576.

Erdogan, F. and Arin, K. (1972). A sandwich plate with a part-through and debonding crack. *Engineering Fracture Mechanics*, 4: 449-458.

Gibson, R. (1992). *Principles of composite material mechanics* McGraw-Hill, second edition, New York.

Jones R. and Callinan, R. J. (1977). On the use of special crack tip elements in cracked elastic sheets. *International Journal of Fracture*, 3(1): 51-64.

Jones R. and Callinan, R. J. (1979). Finite element analysis of patched cracks. *Journal of Structural Mechanics*, 7(2): 107-130.

Jones R. and Callinan, R. J. (1981). A design study in crack patching. *Fibre Science and Technology*, 14: 99-111.

Kane, J. A. (1994). *Boundary Element Analysis in Engineering Continuum Mechanics*. Prentice Hall, New Jersey.

Kamiya, N. and Sawaki, N. (1988). The plate bending analysis by the dual reciprocity boundary elements. *Engineering Analysis with Boundary Elements*, 5(1): 36-40.

Kirchhoff, G. (1850). On the equilibrium and motion of an elastic plate. *J. Math.*, 40: 5158.

Lekhnitskii, S. G. (1968). Anisotropic plates. *Gordon and Breach*, New York.

Lourenço F. A. (2000). *Analise de reparos de trincas através do metodo dos elementos de contorno*. Campinas, Faculdade de Engenharia Mecânica, Universidade Estadual de Campinas, 157 p., Tese (Maestrado).

Lourenço F. A., Aguirre, F., Albuquerque, E. L. and Sollero, P. (2003). Boundary element analysis of panels reinforced by adhesives plates. *Proc. COBEM 2003*, CD-ROM, São Paulo.

Lakshminarayana, H. V. and Murthy, S. S. (1984). A shear-flexible triangular finite element model for laminated composite plates. Int. J. for Numerical Methods in Engineering, 20: 591623.

Mitchell, R. A., Wooley, R. M., Chwiruth, D. J. (1975). Analysis of composite reinforced cutouts and cracks *AIAA Journal*, 13(6): 744-749.

Noor, A. K. and Mathers, M. D. (1975). Shear flexible finite element models of laminated composite plates and shells. *Technical Report TND-8044*, NASA, Houston.

Paiva, J. B. (1987). *Boundary element formulation for plate bending and its aplication in engineering*. São Paulo, Escola de Engenharia de São Carlos, Universidade de São Paulo, 203p., Tese (Doutorado).

Palermo, L., Rachid, M. and Venturini, W. S. (1992). Analysis of thin walled structures using the boundary element method. *Engn. Anal. with Boundary Elements*, 9: 359-363.

Patridge, P. W., Brebbia, C. A. and Wrobel, L. C. (1992). *The Dual Reciprocity Boundary Element Method*. Computational Mechanics Publications - Elsevier, Southampton, Boston.

Portilho, W. (2005). Análise numérica de problemas dinâmicos em materiais compósitos sujeitos a flexão usando métodos de elementos de contorno. Campinas, Faculdade de Engenharia Mecânica, Universidade Estadual de Campinas, 154 p., Tese (Doutorado).

Portilho, W., Sollero P. and Albuquerque, E. L. (2003). Treatment of hypersingularities in boundary element anisotropic plate bending problems *Latin American Journal of Solids and Structures*, 1(1): 49-73.

Portela, A. and Albuquerque, E. L. (1992). The dual boundary element method: effective implementation for crack problems *International Journal for Numerical Methods in Engineering*, 33: 1269-1287.

Rashed, F., Aliabadi, M. H. and Brebbia, C. A (1998). Hypersingular boundary element formulation for Reissner plates. *International Journal of Solids and Structures*, 35(18): 2229-2249.

Rashed, Y. F. (1999). *Boundary Element Formulation for thick plates*. Topics in Engineering Vol. 35, W.I.T. Publications Inc.

Ratawani, M. N. (1979). Analysis of cracked adhesivelly bonded laminate structures. *AIAA Journal*, 17: 988-994.

Reissner, E. (1947). On bending of elastic plates. *Quarterly of applied mathematics*, 5(1): 55-68.

Rose L. R. F., Wang, CH. (2002). Analytical methods for designing composite repairs. In Baker A, Rose F, Jones R, editors. *Advances in the Bonded Composite Repair of Metallic Aircraft Structure, Vol. I*, Elsevier, Oxford - UK.

Rose, L.R.F. (1981). An application of the inclusion analogy for bonded reinforcements *International Journal of Solids and Structures*, 17: 827-838.

Salgado, N. K. and Aliabadi, M. H. (1998). The boundary element analysis of cracked stiffened sheets, reinforced by adhesively bonded patches *International Journal for Numerical Methods in Engineering*, 42(2): 195-217.

Salgado, N. K. (1998). Boundary element methods for damage tolerance design of aircraft structures *Topics in Enginnering*, Vol. 33, Computational Mechanics Publications, Southampton, Boston.

Salgado, N. K. and Aliabadi, M. H. (1997). Dual reciprocity method for the analysis of adhesively patched sheets. *Communications in Numerical Methods in Engineering*, 13: 397-405.

Samasphyros, G. J. (2003). Two-dimensional finite element analysis of composite patch repairs using shell laminate elements. *Advanced Composites Letters*, 12(2): 57-62.

Sekine, H., Yan, B., Yasuho, T. (2005). Numerical simulation study of fatigue crack growth behaviour of cracked aluminium panels repaired with a FRP composite patch using combined BEM/FEM *Engineering Fracture Mechanics*, 72: 2549-2563.

Schclar, N. A. (1994). *Anisotropic analysis using boundary elements.* Computational Mechanical Publications, Southampton, Boston.

Shi, G. and Bezine, G. (1988). A general boundary integral formulation for the anisotropic plate bending problems. *Journal of Composite Materials*, 22: 694-716, 1988.

Stroud, A. H. and Secrest, D. (1996). *Gaussian Quadrature Formulas*. Prentice Hall Cliffs, Englewood Editors, New Jersey.

Timoshenko, S. and Woinowski-Krieger, S. (1959). *Theory of Plates and shells*. McGraw-Hill, New York.

Telles, J.C.F. (1987). A self adaptative coordinate transformation for efficient numerical evaluation of general boundary element integrals. *International Journal for Numerical Methods in Engineering*, 24: 959-973.

Tarn, J. G. and Shek, K. L. (1991). Analysis of cracked plates with a bonded patch. *Engineering Fracture Mechanics*, 40(6): 1055-1065.

Vander Weeën, F. (1982). Application of the boundary integral equation method to Reissner's plate model. *International Journal for Numerical Methods In Engineering*, 18: 1-10.

Venturini, W. S. (1988). A study of boundary element method and its application on engineering problems. São Paulo, Escola de Engenharia de São Carlos, Universidade de São Paulo, 145p., Tese (Doutorado).

Wen, P. H. (2000). Application of dual reciprocity method to plates and shells. *Engineering Analysis with Boundary Elements*, 24: 583-590.

Wen, P. H. (2000). Plane stress and plate bending coupling in BEM analysis of shallow shells. *International Journal for Numerical Methods In Engineering*, 48: 1107-1125.

Wen, P. H., Aliabadi, M. H., Young, A. (2003). Boundary element analysis of curved cracked panels with adhesively bonded patches. *International Journal for Numerical Methods In Engineering*, 58: 43-61.

Widagdo, D. and Aliabadi, M.H. (2001). Boundary element analysis of cracked panels repaired by mechanically fastened composite patches. *Engineering analysis with boundary elements*, 25(4-5): 339-345.

Wearing, J. L. and Ahmadi-Brooghni, S. Y. (1999). The evaluation of stress intensity factors in plate bending problems using the dual boundary element method. *Engineering Analysis with Boundary Elements*, 23: 3-19.

Young, A. (1987). Influence of tapering on the stresses in repair patches. In Owen D.R.J. and Luxmoore A.R. editors. *Proceddings of the 3rd International conference on numerical methods in fracture mechanics*, 741-752, San Antonio-EUA.

Young, A., Cartwright, D. J, Rooke, D. P. (1988). The boundary element method for analysing repairs paletes on cracked finite sheets. In Owen D.R.J. and Luxmoore A.R. editors. *Proceddings of the 4th International conference on numerical methods in fracture mechanics*, 463-479, San Antonio-EUA.

Young, A., Rooke, D. P. (1992). Analysis of patched and stiffened cracked panels using the boundary element method. *Int. J. Solid Structures*, 29(17): 2201-2216.